DEVELOPMENT OF AN ALGORITHM(S) FOR HUMAN TISSUES CHARACTERIZATION

A Thesis Submitted in Fulfilment of the Requirement for the Award of the Degree of

DOCTOR OF PHILOSOPHY

in

Computer Science and Engineering Department

Submitted By

SHAIFY KANSAL
(Reg. No. 901403009)

Under the Guidance of

Dr. Jhilik Bhattacharya

Associate Professor

Department of Computer Science and Engineering
Thapar Institute of Engineering and Technology, Patiala

Dr. Vishal Srivastava

Associate Professor

Department of Electrical and Instrumentation Engineering
Thapar Institute of Engineering and Technology, Patiala

THAPAR INSTITUTE OF ENGINEERING & TECHNOLOGY PATIALA, PUNJAB-147004, INDIA

MAY 2022

Dedicated

To

My Parents

Shri Tara Chand Kansal & Smt. Rani Kansal

CERTIFICATE

This is to certify that the thesis titled "**DEVELOPMENT OF AN ALGORITHM(S) FOR HUMAN TISSUES CHARACTERIZATION**" being submitted by **Shaify Kansal** to the Department of Computer Science and Engineering, Thapar Institute of Engineering and Technology (Deemed to be University), Patiala for the award of the degree of **Doctor of Philosophy**, is a record of bonafide research work carried out by her under my guidance and supervision and has fulfilled the requirements for the submission of this thesis, which to my knowledge has reached the requisite standard.

The results embodied in the thesis have not been submitted in part or full to any other University or Institute for the award of any degree or diploma.

Verified by:

Dr. Jhilik Bhattacharya
Associate Professor,
Department of Computer Science and Engineering,
Thapar Institute of Engineering & Technology, Patiala

Dr. Vishal Srivastava
Associate Professor,
Department of Electrical and Instrumentation Engineering,
Thapar Institute of Engineering & Technology, Patiala

ACKNOWLEDGEMENT

This study was an elaborate mission and it would have been unachievable without the help and gratitude of many people. I honestly feel short of words to acknowledge all those who helped me directly and indirectly during this mission.

I want to express my deep gratitude to Dr. Jhilik Bhattacharya and Dr. Vishal Srivastava, my research supervisors, for their guidance, enthusiastic encouragement, and useful critiques of this research work. Their guidance helped me in all the time of research and writing of this thesis. I could not have imagined having a better team to mentor my Ph.D. study.

I want to express my sincere gratitude to Dr. Srivastava for accepting me as his student. I deeply thank him for his constant support and for giving me the freedom to explore my intellectual curiosity without objection. His advice and encouragement were always important guiding lights for when I lost my focus. I can only hope that I have been able to absorb some of his magical intuition for doing interesting collaborative research. Sincere thanks must also go to Dr. Jhilik for her continuous support by always willing to answer my many questions. Her motivation and enthusiasm are contagious. I also express my gratitude to Dr. Shivani Goel with whom I joined my doctorate.

I am also thankful to present Chairman of the Doctoral Committee Dr. Shalini Batra, Head, Department of Computer Science and Engineering for the much-needed support throughout the work.

I am very thankful to Dr. Sushma Jain, Associate Professor, Department of Computer Science and Engineering and Dr. Mandeep Singh, Associate Professor, Department of Electrical & Instrumentation Engineering, for being the members of Doctoral Committee and spending their valuable time in reviewing and critically examining the work. I would also thankful to Dr. Prashant Singh Rana, Associate Professor, Department of Computer Science and Engineering to guide me in machine learning concepts.

Numerous faculty members have always been very kind with their words of encouragement. Crossing paths with them while walking on campus has ever brought a smile to my face. I wish to give them my sincerest thanks. The office staff has always been available and ready for the assistance of any kind. The security guards, the hostel staff, and mess staff have not only been extremely diligent with their duties but have often accommodated requests with a smile. They have made my stay at the campus a pleasurable one.

I thank my fellow labmates for not only their stimulating discussions and valuable suggestions; but also for all the fun we shared. I truly appreciate my colleagues, including those from other disciplines, for enriching me by sharing their experiences. We've all been there for one another and have taught ourselves and each other many tools. I know that I could always ask for advice and opinions on any issue that I may be dealing with. I'm thankful to the graduate and post-graduate students at TIET. My life would have been very dull without their fun interactions.

I bow with gratitude for my parents, who are the most precious persons in my life and without whose efforts I would have not achieved this mission. My sister, Dr. Ishu Goel has been my best friend all my life. I love her dearly and thank her for her care and concern. My brother-in-law, Dr. Ashutosh Goel generously gave his time and support to offer insightful comments towards improving my work. I feel honoured in recognizing the love and affection of my husband Mr**.** Varun Goyal and my daughter Anaisha Goyal.
I express my gratitude to all those, with whom I have worked, interacted, and whose thoughts have helped me in furthering my grasp and understanding of the subject.

Last but not least, I bow in reverence to **ALMIGHTY GOD** who has always showered blessings on me at each and every step to complete this thesis.

Shaify Kansal

ABSTRACT

Various imaging technologies have been employed to investigate skin tissues over the years, but their inadequate sensitivity, specificity, and accuracy limit their usage. Optical coherence tomography (OCT) is a promising imaging technique in comparison to other imaging modalities since it is a non-invasive imaging modality with a high resolution that can do cellular level imaging as well as provide depth information. This imaging technique has been widely utilised to examine tissues in the human body, demonstrating its clinical promise. Furthermore, OCT can be regarded a possible tool for identification, however modern high-speed OCT systems capture a large amount of data, making human interpretation a time-consuming and tiresome operation. Computer-aided diagnostic (CAD) systems can support clinicians in diagnosing by rapidly assessing large amounts of data. The goal of this thesis is to create a CAD system that uses OCT for human tissue measurement. The feasibility of fully automated quantitative assessment based on morphological aspects of human tissue, which will become a biomarker for the removal of non-viable skin, is described in this thesis research work.

We developed an automated algorithm for the classification of malignant and benign human skin tissue, using the dermoscopic images. The resulting algorithm gives a prospective approach for skin tissue characterization, which presents tangible findings in normal and melanoma infected skin tissue by statistical means. Our proposed automated procedure entails building a machine learning based classifier by extracting the features of normal and infected skin images, augmented with various classical transformations and Generative Adversarial Network. The resultant model obtained good accuracy by adding the synthetic data.

Further, a robust machine learning approach was utilised to correctly and automatically identify breast cancer tissue. We presented a novel approach combining pre-trained deep convolutional neural network (CNN) inception-V3 with DCGAN and optical coherence tomography (OCT) imaging modality for classification of human breast tissue. The preliminary results demonstrate the feasibility of using deep learning algorithms with OCT images to perform the automated assessment of breast cancer margin. The results obtained from the classifier has better performance metrics for the diagnosis of breast cancer in terms of accuracy, specificity and sensitivity.

In the next part of this thesis, an automated full-field polarization sensitive optical coherence tomography diagnostic system (FF-PS-OCT) was developed which would be more accessible to laboratories as a research tool for the investigation of biological applications. Spatial phase features were extracted for the investigation of breast cancer tissue. A 2D camera was used instead of the photodetector that records the entire en-face image (orthogonal to the

optical axis) in the single shot. A number of optical parameters of the tissue obtained from their phase images is used to differentiate between healthy and malignant tissues with SVM classifier. Results suggest that FF-PS-OCT can be considered as a strong aspirant for robust and automated diagnosis of breast cancer tissue.

In the last part, a new method to detect skin cancer has been developed, which is more accurate than previous methods. The edges are recognised using a canny edge detector after the input PH^2 dataset image is transformed to gray images using gray scale conversion. For edge identification, the canny edge detector employs a multi-stage approach that is smoothed and run through a non-linear kernel-based ICA. SVM and the Naive Bayes classifier were used, which produced accurate results than previous approaches.

TABLE OF CONTENTS

LISTS OF FIGURES

LISTS OF TABLES

LIST OF ACRONYMS

AUC	Area Under the curve
ANN	Artificial Neural Networks
BCC	Basal Cell Carcinoma
BD	Balanced Detector
BS	Beam Splitter
CAD	Computer Aided Diagnosis
CT	Computed Tomography
CNN	Convolutional Neural Network
CCD	Charge Coupled Device
Coll	Collimator
Cir	Circulator
Conv2DT	Conv2DTranspose
DL	Deep Learning
DCNN	Deep Convolutional Neural Networks
DCGAN	Deep Convolutional GAN
DNN	Deep Neural Network
DOI	Diffusive Optical Imaging
fMRI	Functional Magnetic Resonance Imaging
FC	Fiber Coupler
FF-OCT	Full field Optical Coherence Tomography
FF-PS-OCT	Full field Polarization Sensitive OCT
FPR	False Positive Rate
GAN	Generative Adversarial Networks
GPU	Graphical Processing Unit
H&E	Hematoxylin and Eosin
ISIC	International Skin Imaging Collaboration
IDC	Invasive Ductal Carcinoma
kNN	k-Nearest Neighbours
LIBSVM	Library for Support Vector Machines
LED	Light Emitting Diode
LP	Linear Polarizer
NA	Numerical Aperture
OAI	Off-Axis Interferometry
OCT	Optical Coherence Tomography
PC	Phase Contrast
PSI	Phase Shifting Interferometry
PCA	Principle Component Analysis
PZT	Piezo-Electric Transducer
QPI	Quantitative Phase Imaging
QWP	Quarter Wave Plate
RCNN	Region-Based Convolutional Neural Network
RM	Reference Mirror
RI	Refractive Index
ROI	Region of Interest
ROC	Receiver Operating Characteristic
RF	Random Forest
ReLu	Rectified Linear Unit
SCC	Squamous Cell Carcinoma
SD	Standard Deviation

SLD	Super Luminescent Diode
SNR	Signal to Noise Ratio
SVM	Support Vector Machine
SMO	Sequential Minimal Optimization
SS-OCT	Swept Source OCT
SD-OCT	Spectral Domain OCT
SGD	Stochastic Gradient Descent
TL	Transfer Learning
TD-OCT	Time Domain OCT
TPR	True Positive Rate
2-D	Two Dimensional
3-D	Three Dimensional

CHAPTER 1
INTRODUCTION

1.1 INTRODUCTION

The theory of tissues was first proposed in 1801 by Xavier Bichat, a French pathologist and anatomist. He implied that tissues are a basic component of human life systems, and that organs are essentially assemblages of various tissues. A tissue is described in science as a collection of cells that share a common structure and execute a certain function. The term "tissue" comes from the French and meaning "to weave." Muscle tissue (skeletal, smooth, and cardiac muscle tissues), Connective tissue (tendon, bone, fat, and soft padding tissue), Nervous tissue (spinal cord, neurons, and brain), and Epithelial tissue (found on the skin surface and lines the gastrointestinal tract organs) are the four types of tissues in general [1]. Cancer is capable of causing tissue damage. A tumour can occur when a mass of malignant cells becomes large enough. Furthermore, cancer cells can infiltrate neighbouring tissues, break off, and move to other parts of the body, resulting in the creation of new tumours in those locations. Sarcomas are tumours that arise in the soft tissues of the body, such as fat, fibrous tissue (ligaments and tendons), muscles, lymph arteries, and blood vessels. The most common site of cancer formation is the epithelial tissue [2]. Carcinomas are tumours that begin in epithelial tissue and account for up to 90% of all human cancers. The discovery of pathogenic modifications in biological tissues at an early stage is critical for early clinical diagnosis and a reduction in the severity and mortality of many diseases. In terms of early detection, the present standard of treatment falls short for some conditions. Invasive biopsy and histological testing, for example, are the current gold standard for finding neurotic changes early in sickness. Patient pain and tissue obliteration prevent large-area biopsying, decreasing the method's overall sensitivity. Furthermore, the doctor is unable to get an instant information because its a time-consuming and laborious process [3].

One strategy used to manage malignant growth at all stages is multimodal biomedical imaging. Imaging can provide a lot of information about morphology, structure, digestion, and function as a vital component of malignant development medical care. Imaging approaches combined with other perceptual devices, such as fluid analysis and in vitro tissue, might aid in clinical evaluation [4]. Blended imaging technologies can provide useful information for improving therapeutic planning and staging. Imaging is used to locate minimally invasive treatments in order to improve outcomes and reduce side effects. Early disease detection using imaging-

based screening is probably the most important element in lowering the fatality rate of some malignant growths [5]. Imaging is the most important modality for detecting any disease early on, provided that image acquisition does not cause harm to the human body, as image analysis is critical. Numerous imaging modalities, including X-ray, ultrasound, magnetic resonance imaging (MRI), and endoscopy, have been explored for imaging, although they can occasionally cause harm to the human body [6]. Exceptional efforts have been made over many decades to develop imaging equipment for the study of human skin tissue. Imaging modalities are critical for detecting diseases, staging them, diagnosing them, restaging them, and monitoring their response to therapy [7]. It is unique in its ability to collect data on the human body and may be utilised to advance our understanding of neurobiology and human behaviour [7,8]. Numerous existing and innovative imaging modalities are now the focus of active and promising research. This section goes over the many imaging techniques, both invasive and non-invasive, that can be used to identify and characterise tissue. The following is a list of the several imaging techniques that are used to evaluate human skin tissue:

Radiography: In medical imaging, two forms of radiographic images are used: fluoroscopy, which uses a continuous stream of X-rays to provide real-time images of the internal structure, and projection radiography (X-rays), which is used to determine the degree and type of fracture [8]. Another advancement is a conventional X-ray imaging technique that is based on the attenuation coefficient of the sample. Unfortunately, when utilised for tissue imaging, it is unable to generate significant image contrast. Figure 1.1 (a) [9] illustrates an X-ray image, whereas (b) illustrates a chest X-ray and fluoroscopy image [10].

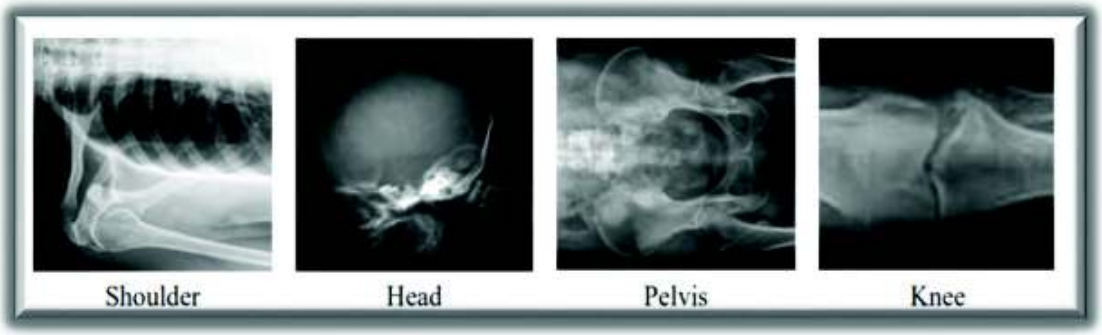

Figure 1.1 (a) Example X-ray images

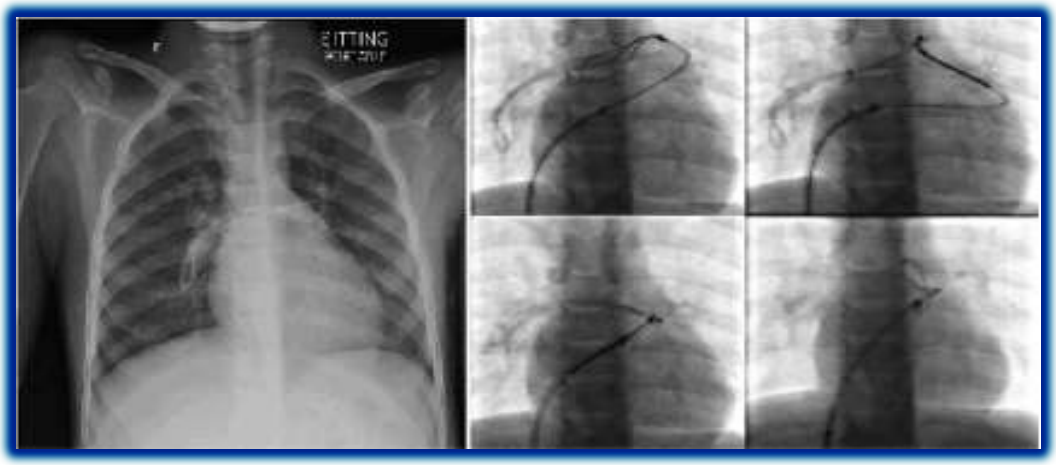

Figure 1.1 (b) Chest X-ray and fluoroscopy image

Computed Tomography Imaging: Computed Tomography (CT) is a form of advanced radiography in which X-rays and a computer are used to create cross-sectional images of the body. It is considered a more prevalent imaging technique than radiography for viewing soft tissues such as the brain, liver and abdominal organs [11]. The brain CT images are shown in figure 1.2 [12]. However, the configuration of skin tissue cannot be determined using CT technology.

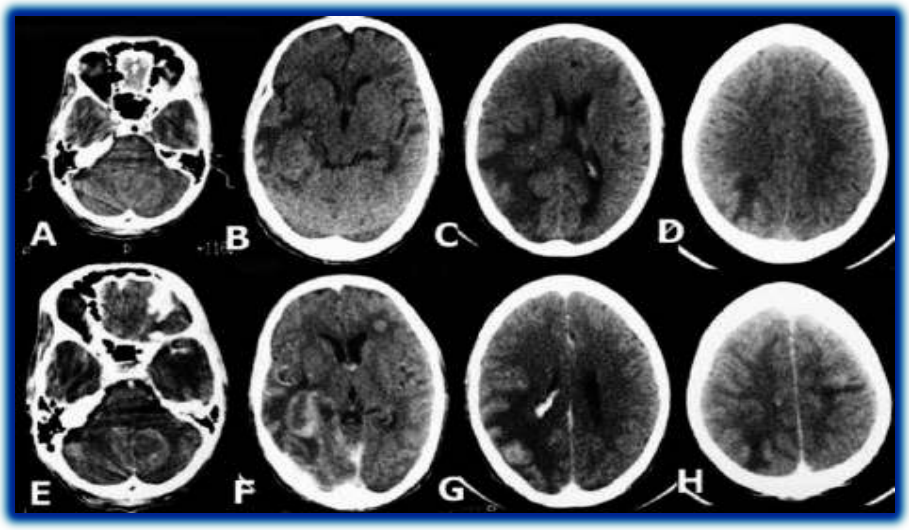

Figure 1.2 CT scan brain images

Magnetic Resonance Imaging (MRI): In MRI, better field quality result in two-layered images with a higher objective (2D). With advancement, it is capable of moulding three-layered (3D) blocks, which are considered to be the equivalent of a single cut. Over atomic imaging, research is being conducted using several differentiation agents in conjunction with MRI. In

tissue imaging, its limited spatial resolution, low responsiveness, and lengthy handling time precluded its use [13,14]. Figure 1.3 [15] illustrates an MRI image.

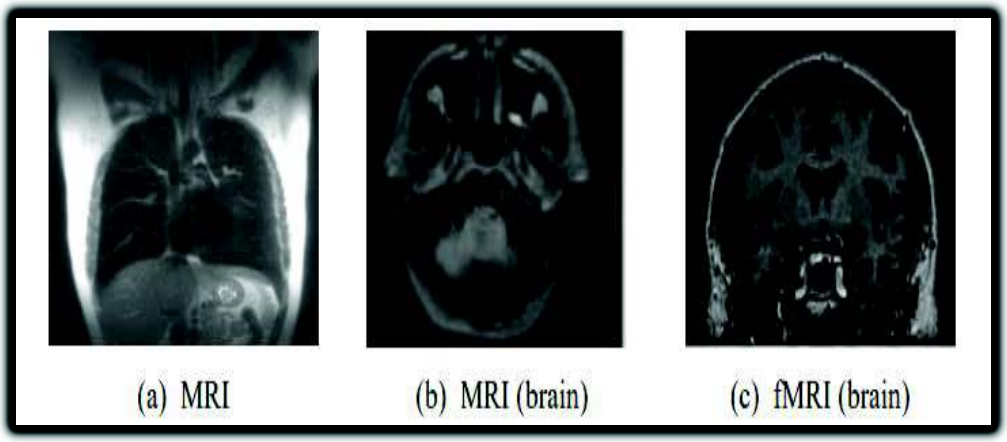

Figure 1.3 Example MRI images

Ultrasound: Ultrasound (US) produces three-dimensional images by utilising high-recurrence sound pulses. When compared to the aforementioned imaging methods, it often provides less physical information but has advantages due to its proclivity to continuously inspect the capability of moving designs without emitting ionising radiation. Due to its ongoing evaluation, it is frequently used for tissue organisation and the development of novel image processing techniques. It requires touch with the skin in order to focus on the morphology of the tissue. Non-contact ultrasonography, on the other hand, is being investigated. The strategy's downside is its somewhat poor contrast for sensitive tissue [16]. However, its application is limited because it is operator-dependent and cannot take a global view of the tissue. Figure 1.4 [17] contains examples of ultrasound pictures.

Figure 1.4 Examples of ultrasound images

Elastography: It is a novel and promising imaging technique since it depicts the elasticity of sensitive tissue. To summarise, this imaging method is advantageous because it enables the

differentiation of atypical tissue from normal tissue in explicit organs [18]. Different elastography approaches have been developed and found to be useful in a variety of areas of therapy monitoring and clinical diagnostics as a result of the use of various imaging modalities such as ultrasound, tactile imaging, and MRI. Due of its low resolution, its utility is limited. The liver elastography images are shown in Figure 1.5 (a) and (b) [19].

(a)

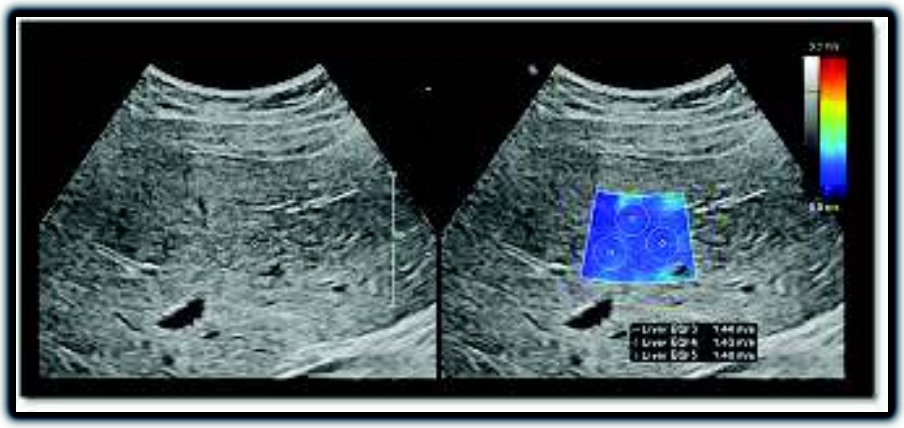

(b)

Figure 1.5 (a), (b) Liver elastography images

Nuclear medicine: Also referred to as molecular therapy and diagnostic imaging due to the fact that it incorporates diagnostic imaging into the treatment of disease. The most significant advancement in nuclear medicine imaging is the ability to deliver anatomical and functional information in a hybrid system. The hybrid system combines MRI's morphological and functional information with PET's physiological data [20]. Nuclear medicine imaging is illustrated in Figure 1.6 [21]. This imaging modality facilitates the application of PET/CT fusion in various fields, such as amyloid imaging oncology.

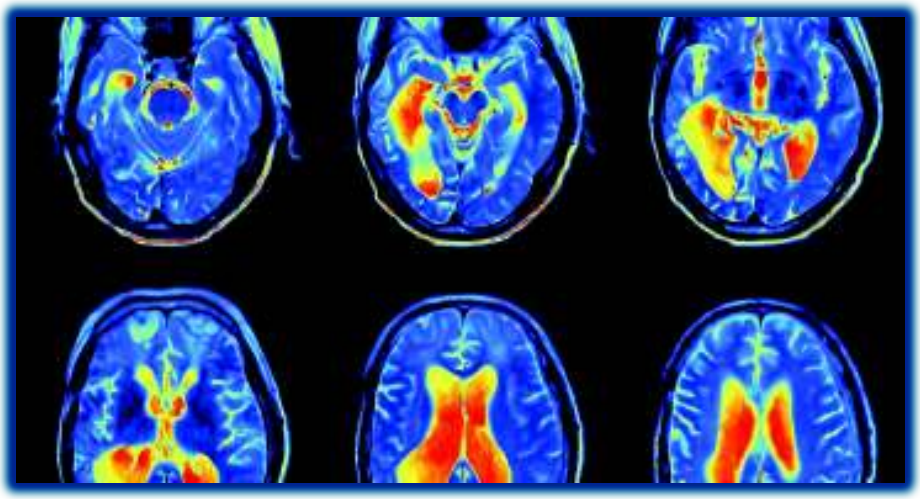

Figure 1.6 Example of Nuclear Medicine Imaging

Photoacoustic Imaging: The photoacoustic effect lies at the heart of today's multimodal biomedical imaging procedures. It combines the advantages of an ultrasonic spatial target with the contrast of optical assimilation for profound imaging. As per ongoing research, this imaging technique can be used in vivo for skin melanoma identification, growth appraisal, blood oxygenation mapping and the functional brain imaging, among other applications [22]. Photoacoustic Imaging for Breast Cancer Management is depicted in Figure 1.7 [23].

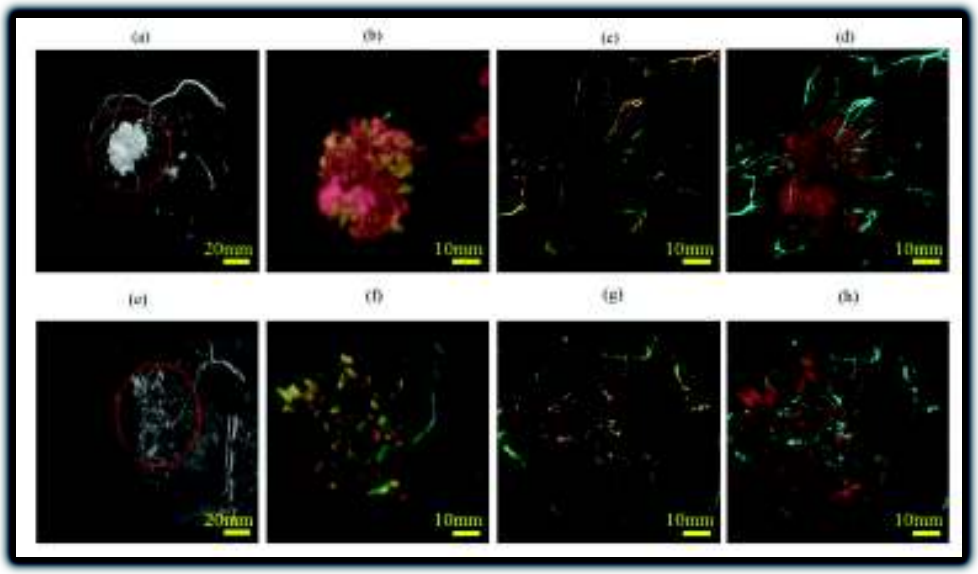

Figure 1.7 Photoacoustic Imaging for management of Breast Cancer

The aforementioned imaging methods either suffer from low resolution, a lengthy data acquisition time, or a limited depth penetration. Historically, imaging techniques was used exclusively for disease detection and painless (non-invasive) mapping of various structures.

Nonetheless, after a paradigm shift, it has been determined that advancements in numerous clinical imaging technologies are necessary to provide meaningful data about organ function, physiology, atomic science, and usable and digesting genetics. Additionally, the high-level processes may be capable of evaluating the organic cycles and condensing the purposeful ingredients into an ideal physical image [24]. Additionally, advanced imaging methods are popular in medical procedures. These advancements in clinical imaging are contingent upon the development of imaging biomarkers for the early detection and treatment of disease, in both functional and molecular imaging. The improvement of optical techniques has facilitated the assessment of optical qualities for tissue imaging; thus, the viability of laser therapy is dependent upon the rate of photon conveyance and dissemination within illuminated tissues. The photodynamic therapy destroys the tissue's optical characteristics, allowing light to be absorbed by the exposed skin [25]. As a result, information on the optical characteristics of tissue plays a significant role in determining its strength. Additionally, a novel optical innovation with regard to tissue dispersion and retention capabilities over a broad frequency range is predicted to be developed for the treatment of obesity and cellulite. It poses fewer risks and discomforts for the user when compared to commonly used drugs and cautious medications [26].

Optical imaging: This imaging technique appears to have significant potential for diagnosing and treating disease. It has a number of advantages over other imaging modalities. To begin, non-ionizing radiation is used to expose the patient to harmful rays, allowing for repeated investigations over time. Second, it is employed as a modality for multimodal imaging [27]. Thirdly, it characterises the biological tissue that will be used to analyse chemicals and functional levels. It is compatible with different imaging modalities and encompasses a wide range of imaging resolutions. The OCT image of a normal fundus is depicted in figure 1.8 [28].

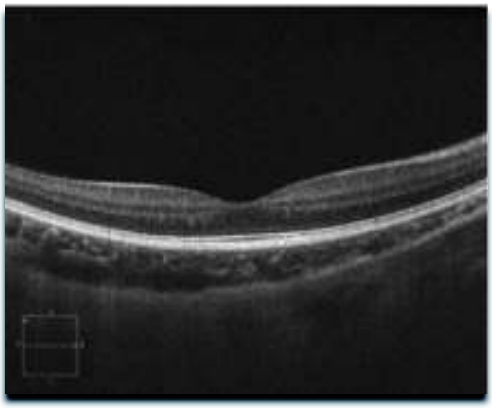

Figure 1.8 OCT image of a normal fundus

Skin Cancer and Breast Cancer are the most common diagnosed cancers among women around the world [29]. The human skin tissue and breast tissue can be affected by cancer.

Skin Cancer - Skin Cancer is a form of cancer that develops in the skin's tissues. Skin cancer comes in a variety of forms. Melanoma is a type of skin cancer that develops in melanocytes (pigment or colour producing skin cells). Basal cell carcinoma is a type of skin cancer that develops in the lower epidermis (the outer layer of the skin). Squamous cell carcinoma is a type of skin cancer that develops in squamous cells (level cells that make up the outer layer of the skin). Seniors with weakened immune systems and body areas that are more exposed to solar radiation are more susceptible to skin cancer [30].

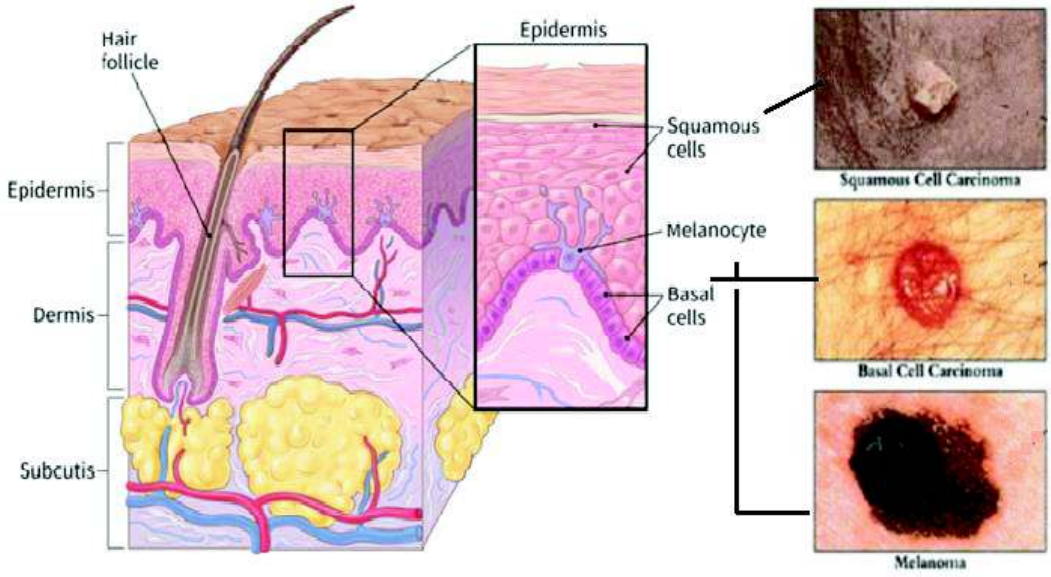

Figure 1.9 Types of skin cells and the corresponding skin cancers

Dermoscopy - Dermoscopy is a non-invasive, painless procedure used to diagnose skin malignancies on a large scale. The viability of dermoscopic assessment in melanocytic tumours, such as melanoma and basal cell carcinoma (BCC), has been established over the last several years. Additionally, dermoscopy was used to analyse non-melanocytic growths. Dermoscopy, alternatively referred to as dermatoscopy, epiluminescence microscopy, or skin surface microscopy, is a non-invasive, in-vivo technique that has historically proved beneficial for evaluating suspicious skin injuries. It can aid in the differentiation of melanocytic sores from dysplastic sores, melanomas, and non-melanoma skin malignant growths such as basal cell carcinoma (BCC) or squamous cell carcinoma (SCC). Additionally, in recent years, dermoscopy has been expanded to include the diagnosis of dermatological conditions such as incendiary dermatosis, pigmentary dermatosis, irresistible dermatosis, and hair, scalp, and nail

problems. As dermoscopy's utility grows, professionals in virtually every field should be familiar with this simple, non-invasive, and high-return demonstrative technique [31].

Breast Cancer Statistics - Cancer is one of the leading causes of death in the globe. Cancer is a disease that, unfortunately, spreads via cells and grows in the body on a regular basis. Cancer is the second biggest cause of mortality worldwide, according to the World Health Organization (WHO), with roughly 9.6 million deaths in 2018 [32]. Cancer comes in numerous forms, including breast cancer, skin cancer, lung cancer, and prostate cancer. Breast cancer is the most prevalent cancer in women, whereas lung cancer is the most common cancer in men, according to the International Agency for Research on Cancer as depicted in figures 1.10 and 1.11 [33] respectively.

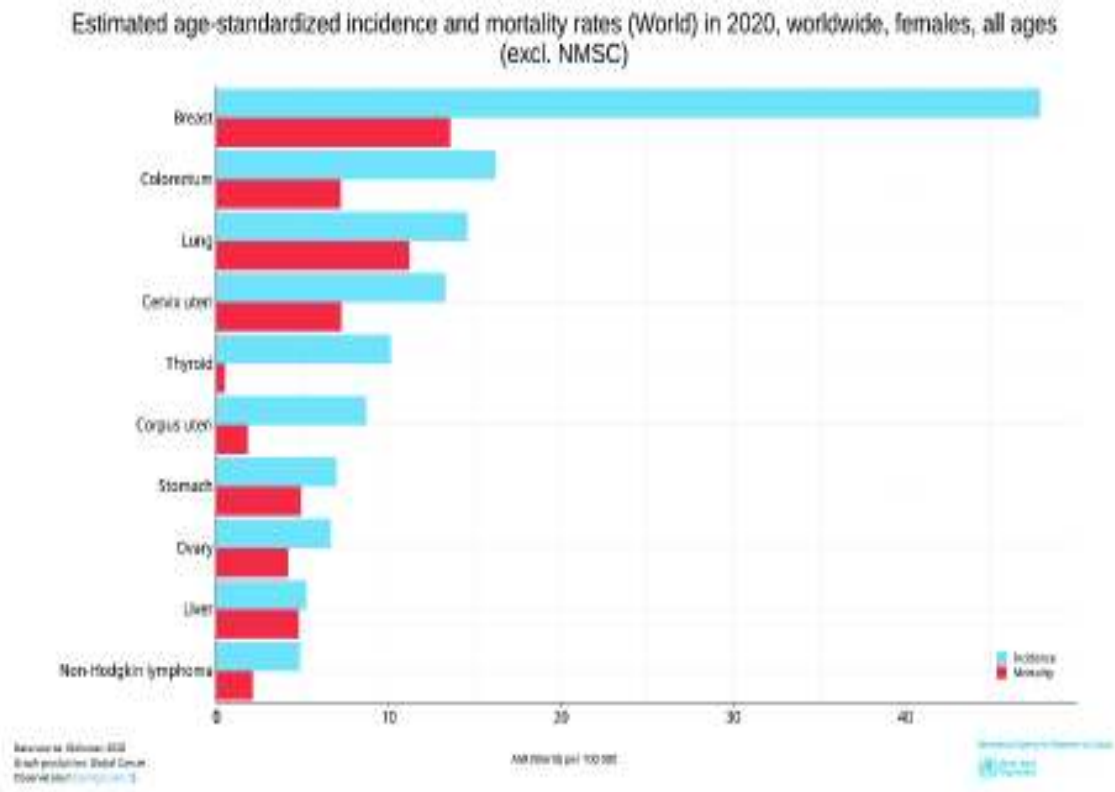

Figure 1.10 Common cancers among women

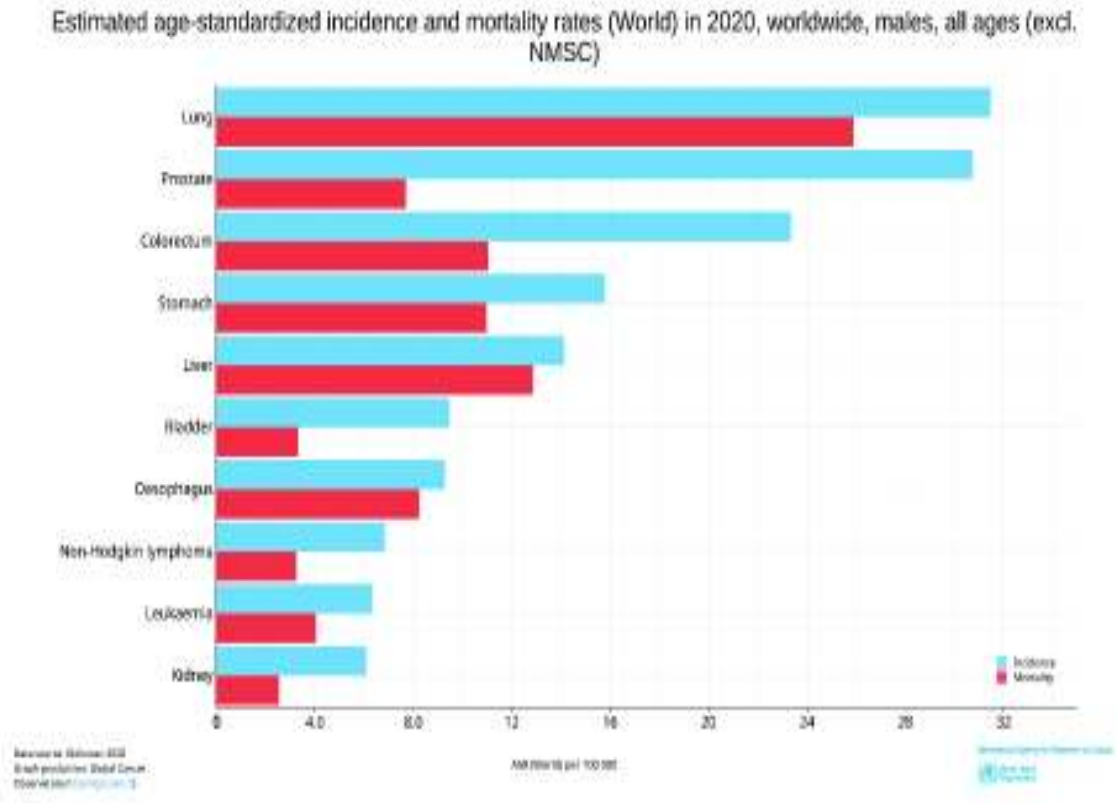

Figure 1.11 Common cancers among men

Morphology of Breast Tissue - Breast tissue is made up of lobules of alveolar glands and ducts, which produce and deliver breast milk to the nipple. The interlobular gap is made up of supportive dense fibrous connective tissue and varied levels of fat between lobules. Connective tissue within lobules is substantially less thick and contains little fat. Breast cancer can start in the ducts or the lobules and may be restricted to these structures at initially, a condition known as in situ disease. On the other hand, in situ disease, can eventually grow into adjacent tissues, resulting in invasive cancer with the potential to spread to other regions of the body through the lymphatic vessels and bloodstream [34]. Tumors also have different quantities of fibrous stroma, which adds to the palpable "stiffness" of the tumour. Lymph nodes are an important part of the lymphatic system that are frequently involved in the metastatic spread of breast cancer. The cortex, paracortex and medulla are functionally and physically separate divisions in lymph nodes. They are enclosed by a stromal capsule that is punctured by afferent channels, allowing lymph fluid to enter sinuses that travel through numerous lymphoid compartments before exiting via an efferent lymphatic stream [35]. Early metastatic malignancy deposits in breast lymph nodes are frequently found in the subcapsular sinus, which is where lymph fluid from adjacent breast tissue enters the lymph node first. Metastatic cells can also extend

throughout the node and multiply to the point where normal lymph node tissue is totally replaced.

Breast Cancer - is a highly malignant disease that affects mostly women. As the subsequent top cause of cancer-related mortality in females, it has remained a significant clinical and economic burden. Mammography tests, which entail collecting X-rays of the breast, are the most often used method for detecting early changes (lesions) in breast tissue. Nonetheless, some types of breast cancer are thought to be mammographically undetected. Even if a woman is not diagnosed with breast cancer, she may be subjected to additional tests and procedures, including surgery [35]. As a result, biological tissue examination is required to determine the appearance of sick cells. In this case, histopathology comes to the rescue because it is the gold standard method for diagnosing and researching tissue disorders. It comprises looking at tissues and/or cells under a microscope. Histopathologists are responsible for diagnosing tissues and assisting clinicians in delivering patient care [36]. However, this form of medical image processing is time-consuming, labor-intensive, costly, and prone to error. Tissue examination also necessitates the use of experienced pathologists. It would be more convenient if a computer-aided application could automatically read the images and give diagnosis and therapy recommendations. In light of these shortcomings, a fresh approach known as optical coherence tomography (OCT) was developed, which offers results in real time and has a resolution of micrometres. OCT is a low-coherence interferometry method that allows for high-resolution, non-contact, non-invasive three-dimensional imaging [37].

Advanced approaches for tendon restoration, such as stem cell therapy, bright field microscopy, and other optical strategies typically employed for studying dyed tissue pieces, had a very good goal when compared to other imaging technologies. Optical technologies allow for the study of tissue architecture and cell morphology. As a result, as histological evaluation processes (for example, the investigation of the minuscule life structures of cells and tissue) are time consuming and escalated care is not possible over a longer timeframe, a more established, non-invasive, high resolution imaging technology is expected to improve the testing of the healing process by observing the effect of stem cells [16] and to detect harmed ligaments. Because of concurrent breakthroughs in numerous domains of technology, OCT has advanced at a faster rate since its inception. Improvements in optical techniques, light sources, data collection methods, and processing methods have all allowed OCT to rapidly extend and penetrate new utility domains, most notably in organic and clinical applications. Currently, video rate verification is done with a near micron critical target and a fast four-dimensional filter. This opens up new opportunities for OCT, since it will explore applications in the field of

cardiovascular medical treatments. OCT is a revolutionary imaging technology that allows for high-resolution (10 m) imaging of organic tissue in the axial direction with a 2 mm imaging range and at a faster rate [38]. Previous research has shown that OCT may be utilised to image critical topographies in a range of domains such as ophthalmology, cardiology, dermatology, and oncology [39]. OCT imaging can be used to characterise diverse tissue structures.

1.2 OPTICAL COHERENCE TOMOGRAPHY

Optical imaging is a developing imaging methodology with colossal potential for ascertainment and treatment of diseases. It offers different benefits over existing imaging modalities. Above all, it utilizes non-ionizing radiation, which diminishes patient openness to unsafe radiations and permits them for rehashed examinations over the long run. Second, it is having the capacity to describe the natural tissues utilized for concentrating on functional and molecular level exercises. Third, it is utilized as a multimodal imaging methodology. It covers a wide reach on the imaging resolution scale and is additionally viable with other imaging procedures [27]. Optical imaging frameworks can be examined under two classes: diffusive optical imaging (DOI) and ballistic imaging framework. DOI is a methodology of imaging in light of close infrared spectroscopy or fluorescence-based strategies. It is called as diffuse optical geology when used to make 2D models and diffuse optical tomography for imaging 3D models. In ballistic imaging framework, light photons drive through the turbid medium along a straight line and called as snake photon when hold some level of intelligence. To make diffraction restricted pictures ballistic scanners and OCT are the pervasive imaging procedures that depend on ballistic photon identification. It achieves axial resolution of the order of 1-10 micro- meters and thus offers critical advantages in terms of axial resolution over other existing imaging modalities (e.g. CT scan, MRI and X-rays) but it is restricted by imaging profundity [40].

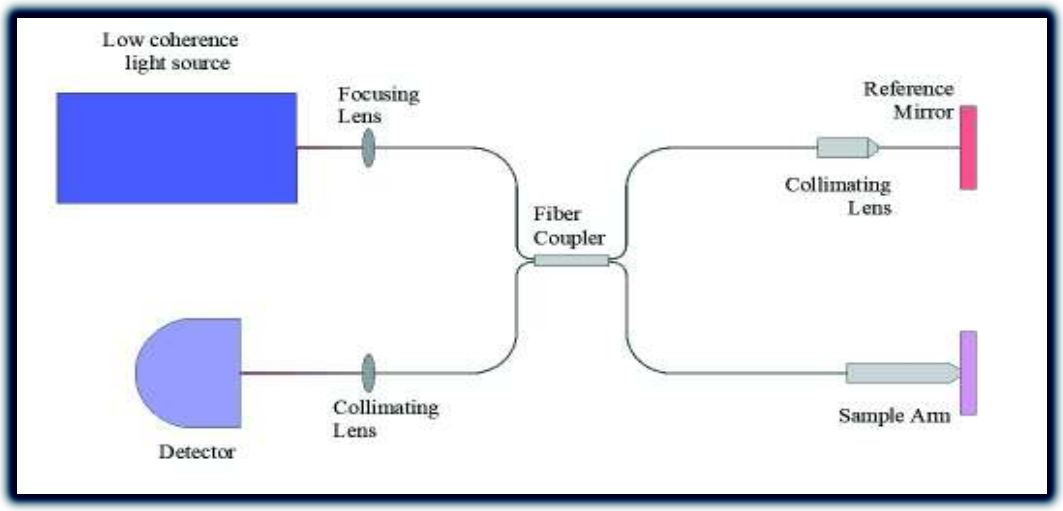

Figure 1.12 Schematic diagram of Optical Coherence Tomography

1.2.1 Reason for involving Optical Coherence Tomography in Biomedical Imaging

The capability of OCT proposes that it will be considered as a critical innovation for biomedical application [41, 42].

1. Compared with traditional ultrasound, OCT can image the example with pivotal goals of 1 to 15 µm, that implies with a request for higher extent. This goal approach, permitting a few cell highlights and compositional morphology to be settled. In OCT based frameworks, imaging should be possible painlessly.

2. It empowers imaging of the tissue structures where biopsy would be dangerous or unimaginable. It additionally diminishes the testing imperfections related with excisional biopsy by giving better inclusion.

3. Real-time imaging and checking are conceivable, which is beyond the realm of possibilities in ordinary biopsy and histopathology. It likewise gives extension to pathology to store videotape of high resolution.

4. OCT can be united with a wide scope of instruments including catheters, endoscopes, laparoscopes, and careful tests allowing the organ system imaging inside the body.

5. A noteworthy concept, for a clinical organized apparatus, OCT is portable and compact.

In any case, manual clarification of OCT images is dreary system and not compelling for examination on gigantic three-layered (three dimensional) volumetric datasets. Accordingly, there is a pressing need of improvement of a robotized algorithm from tissue portrayal utilizing OCT pictures. Quantitative and robotized investigation improvement could subsequently energize the appraisal of a gigantic volume of dataset. Along these lines, computer aided diagnosis (CAD) frameworks utilizing AI in view of image handling of OCT information have been created to build precision, awareness and particularity in tracking down the anomalies in images. Various investigations were finished via prepared specialists to examine the capability of OCT and to arrange the sound and unfortunate tissue both ex-vivo and in-vivo utilizing different elements extricated from OCT images [16, 43].

1.2.2 Applications of OCT

OCT has been extensively used in clinical diagnosis to detect many disorders. OCT is a relatively new imaging modality that is still being developed to determine its best use in current medical applications. OCT has evolved into a useful tool for creating high-resolution cross-sectional images in the biomedical area over the last few decades. The great spatial resolution allows for detailed internal imaging and surface topography examinations of any specimen. OCT, on the other hand, may readily be integrated into catheters and endoscopes and has been developed for intraluminal imaging as opposed to the traditional approaches that utilized fiber couplers for sending and collecting light. OCT is also useful for other biomedical applications, such as developmental biology, cardiology, laryngology, gastrointestinal, pulmonary medicine, dermatology, and dentistry [44]. Their histology data is analysed using OCT, which acts as an optical biopsy for a quick diagnosis during endoscopy. Previously, this could only be accomplished by histological or cytological analysis, which has a significant difficulty in removing tissue samples and preparing them for microscopic study [45]. In most cases, personally examining an image is a time-consuming operation that is highly common in clinical applications. Furthermore, there is invariably a subjective aspect associated with the pathological analysis of a picture that increases the risk of an expert making a mistake. Doctors will benefit much from an automated framework in this way. This research project aims to develop effective diagnostic models for analysing medical picture data using image analysis and machine learning techniques, in order to alleviate the challenges that medical specialists experience while evaluating images.

1.3 CONVOLUTIONAL NEURAL NETWORKS

Artificial intelligence (AI) is becoming increasingly popular, thanks to enhanced processing power, a massive amount of data, and innovative algorithms. It has been used in a variety of industries, including healthcare, industry, and convenient living. In general, AI is divided into three groups. One is a symbolic technique that uses a rule-based search engine to generate answers. The Bayesian theorem-based approach is another option. The other is the deep neural network-based connectionism technique (DNNs). While each technique has advantages and disadvantages, connectionism has recently received a lot of attention as a way to handle complicated problems. Machine learning (ML) is a subset of AI that uses data to identify categories or anticipate future or uncertain conditions with minimal human interaction [46]. Because it is data-driven and can predict from unseen data, ML is characterized as non-symbolic AI. Examples of machine learning challenges include regression, classification, detection, segmentation, and others. In most cases, ML data sets consist solely of training, validation, and test sets. The training data set is used to learn data characteristics, while the validation data set is used to check the learned data characteristics. Finally, the correctness of ML may be verified using the test data set. An artificial neural network (ANN) is a machine learning method that is inspired by the brain and consists of layers with connected nodes (ML). It has hidden layers as well as input and output layers. Machine learning is useful in quantitative phase imaging applications because it allows for the classification and identification of cells and tissues for quick screening and diagnosis. To date, different machine learning algorithms such as neural networks, Naive Bayes (NB) classifier, support vector machines (SVM), decision trees and random forest (RF) classifiers have been developed to create accurate classification systems for a variety of medical images [47]. Convolutional Neural networks (CNNs) fall under deep learning. This means that several aspects of the field make up for all the amazing things within this area. The most important one of these aspects is computer vision. CNN create ease in viewing images to the extent human beings cannot. The perception in imaging-based on machine intelligence is enhanced and involves a multitude of tasks. These tasks range from image and video recognition to image analysis and classification [48]. There is a significant advancement in computer vision and images which means that changes have taken place over the years.

A convolutional neural network (CNN) has recently been highlighted in computer vision for both supervised and unsupervised learning tasks as part of deep learning [49]. CNN has set new records in classic vision tasks [48]. CNN is made up of convolutional, pooling, and fully connected layers. The convolutional layer's principal function is to recognize patterns, lines,

and edges, among other things. Convolutional layers convolve the input array with weight-parameterized convolution kernels in each hidden layer of CNN. Many kernels provide multiple feature images, allowing various vision tasks such as segmentation and classification to be completed successfully. Feature maps are locally sequentially and spatially pooled pooling layers between the convolutional layers. The pooling layer decreases the size of feature maps by transferring the maximum or average value. This method captures image features that are robust to the image's position or form [50]. The maximum pooling procedure is commonly utilized in practice. The importance of max-pooling is that it acts as a noise suppressant. The noisy activations are discarded along with a dimensionality reduction. On the other hand, average pooling is simply meant to reduce dimensionality. The number of pooling and convolutional layers may be increased to capture low levels at an even greater scale [51]. These convolutional and pooling layers are alternated regularly in the CNN architecture. The fully connected layers are attached at the end of the CNN architecture and provide a final decision for classification or regression tasks. A loss is estimated during training by comparing the labelled and projected values. Convolutional layers and up-sampling layers, on the other hand, are added to the end of pooling layers in the segmentation process to rebuild the size of the input image. As a result, training loss is calculated by comparing the annotated mask picture to the reconstructed output image through CNN. The number of parameters for training might reach millions because CNN architecture is made up of multiple layers. This indicates that a large amount of data is required for training purposes in order to obtain acceptable accuracy. The amount of data required is dependent on the task's goal and image qualities. The basic diagram of CNN is as shown in figure 1.11.

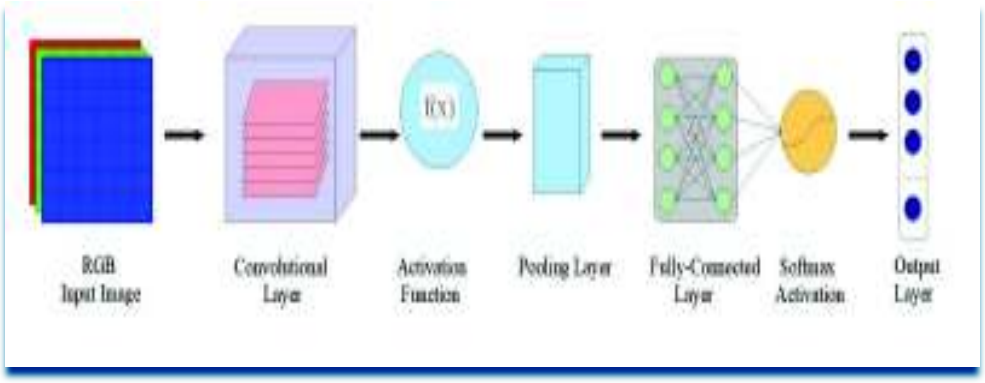

Figure 1.13 An illustration of Convolutional Neural Networks

1.3.1 The Co-relation of CNNs, malignant tissues, and medical images

The identification of malignant issues has been of great concern to doctors and radiologists. The task is considered time-consuming and often tedious. It is generally a challenging task that has required the relevant improvements to flourish in the medical sector. There are, however, computer-aided diagnostics and techniques that help radiologists create a second opinion and give accurate results [52]. Convolutional neural network, the state-of-the-art technique, has had great successes in giving accurate results to radiologists. The detection of abnormalities, identifying their positions and borders, and evaluating their magnitude and severity are all part of image interpretation. The effectiveness of image interpretation is limited by the scarcity of human experts, their exhaustion, costly consultation fees, and rough estimation techniques. Furthermore, the medical anomalies' forms, locations, and structures are highly variable. Even for specialised specialists, this makes diagnosis challenging. As a result, human professionals frequently feel the need for assistance tools to aid in the exact interpretation of medical images. This is why sophisticated image understanding systems exist.

1.4 COMPUTER AIDED DIAGNOSIS APPROACH

In the realm of medical imaging, doctors must deal with images in order to analyse abnormalities in a short amount of time. It is feasible to design a computer-aided diagnostic tool for quantitative and objective analysis that will automatically assist doctors in checking irregularities in any condition [53]. Computer-aided diagnosis (CAD) is a technique for assisting clinicians in making accurate diagnostic judgments based on computer analysis. Pattern recognition, signal processing, computer vision, and machine learning are all covered by CAD systems. Figure 1.12 depicts a generalised CAD system which involves image processing, selecting the region of interest, feature extraction, selection and reduction and finally classification and diagnosis.

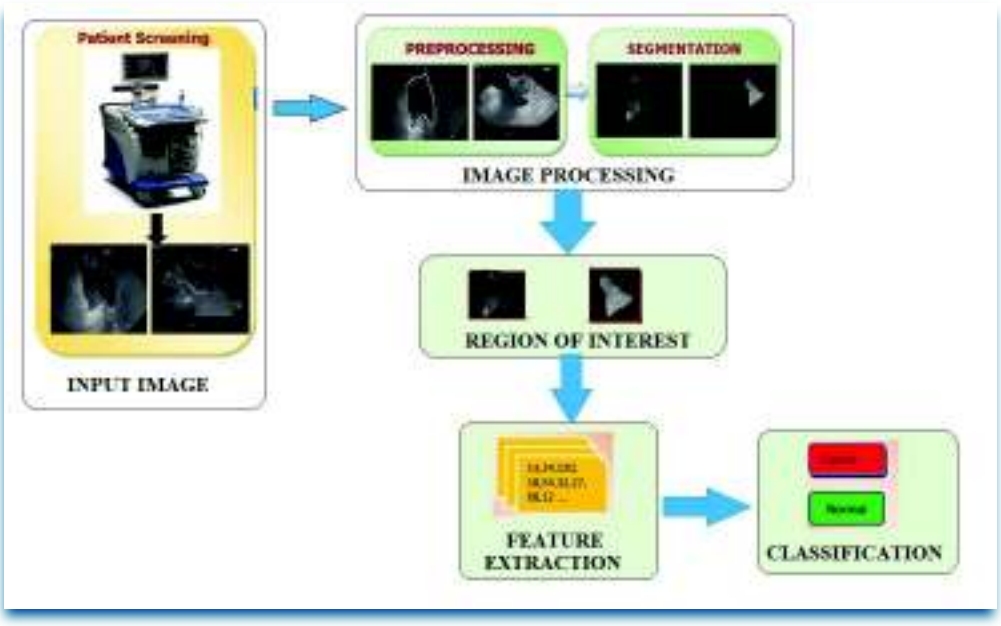

Figure 1.14 General illustration of a CAD system

The quality of an image is increased in image pre-processing by using enhancing, noise reduction, and standardization processes. Because the viability of ongoing improvements such meaning of region of interest (ROI) and feature extraction is based on the quality of the input images, pre-processing is essential. To separate the items of interest from the backdrop, the ROI must be determined. The importance of ROI in medical imaging is defined by I manual or semi-automated approaches that require operator interaction, or (ii) fully automated methods that do not require any manual intervention [54]. Feature extraction refers to the process of identifying and selecting a large number of recognizable and appropriate features from medical images in order to make decisions about a tissue's pathology. Feature extraction is the process of transforming and extracting a large number of useful features from an input dataset. Furthermore, classification is the process of categorizing objects into different groups. In medical imaging, categorization is usually done on a tissue or cells to distinguish between healthy and infected states, as well as different stages of disease [55]. A classifier is usually taught using a training set, which consists of a set of objects that have been labelled by at least one expert.

1.5 DATA AUGMENTATION

Deep learning-based algorithms have lately become more prevalent in artificial intelligence research for medical image processing. While the models created by these algorithms can outperform more typical machine learning approaches in terms of performance, they do require larger datasets for training. To overcome this problem, data augmentation has become a popular strategy for boosting the size of a training dataset, especially in sectors where huge datasets aren't always available, such as when working with medical imaging. Data augmentation tries to generate more data that is used to train the model, and it has been demonstrated to boost performance when tested on a separate dataset that hasn't been seen before. Data augmentation isn't a panacea for all the data challenges. Consider it a free performance boost for the machine learning models, there is still the need of a very large training dataset with enough examples, depending upon the goal application. In some cases, training data may be insufficient for data augmentation to be useful [56]. Before the use of data augmentation in certain circumstances, more data must be collected until a minimal threshold is achieved. Transfer learning can be employed, which involves training an ML model on a large dataset and then fine-tuning its higher layers on the limited data, that are for the target application. Data augmentation is especially handy for supervised learning because extra time will not be used in annotating the new samples as labels are already there. Making copies of existing data and making minor changes to them is one technique to increase the diversity of the training dataset. Rotation, cropping, zooming, shearing and translation are some of the additional changes available. These transformations can also be combined to increase the number of unique training instances in the collection. Geometric modification isn't the only type of data augmentation that may be done [57]. Using noise, adjusting colour settings, and other effects like blur and sharpening filters to repurpose previous training examples as fresh data can also be beneficial. In case of the classical transformations, the information is same in the new images as the old ones. So there is the need of the information enrichment, which is achieved with the help of GANs i.e. Generative Adversarial Networks. GANs are essentially a system of two competing neural network models that compete for the ability to assess, capture, and copy variations within a dataset. GANs comprise of two sections: generators and discriminators. The generator produces images from irregular commotion which are fake in nature and the discriminator, tries to distinguish between the real and the fake images using real examples from a training data set. Both the generator and the discriminator enhance their abilities until the discriminator can no longer distinguish between genuine and synthesized cases [58].

1.6 MOTIVATION

The factors and problems listed below, motivated and inspired us to carry out this research work**:**

a) In the relative methodologies, existent image information goes through various tasks such as zooming, rotation, flipping, editing and translations) to build the quantity of preparing models. There is a need of attention to that such data augmentation procedures that essentially produce very correlated images. They can also generate anatomically incorrect examples, e.g., using rotation. To mitigate the issues identified with the traditional data augmentation approaches, (GANs) have been proposed.

b) Breast cancer is 2nd leading cause of cancer in women worldwide. The feasibility of screening for younger age groups based on X-ray mammography, as dense breast tissue requires accurate interpretations. The false-negative delay in treatment and ultimately worsen the situation that may lead to lower chances of survival. Other imaging methods for cancer detection include ultrasound, X-ray computed tomography, and magnetic resonance imaging, but they are also not very effective when the lesion size is less than ~1 cm. Most cases have been diagnosed in a later stage using these techniques. Histopathology is the standard gold method for cancer detection but has certain drawbacks, such as H&E staining, which requires long processing time and cannot be performed intraoperatively. Hence the development of new techniques is required that can be used intraoperatively.

c) A family of machine learning methods, the accelerated growth of deep learning, has spurred a lot of curiosity in its application to medical imaging issues. Compared to other methods, the DL-based diagnostic architecture has a strong feature learning functionality that can learn hierarchical representations directly from the original sensor data from several hidden layers, and select discriminative features that help accurate breast tissue classification. Training data is an essential factor influencing the efficiency of deep architecture for DL-based approaches. Many deep-neural network algorithms have achieved high performance with sufficient amount of annotated or labelled datasets. But in medical imaging, the labelled data is scared. To achieve generalizable deep learning models, large amounts of data are needed. In order to reduce the annotation burden, researchers apply various augmentation algorithms to produce synthetic images that contain ground truth marks.

1.7 GAPS IN THE RESEARCH

Although a number of research proposals exist in the literature which have addressed various problems in human tissues characterization, but still these proposals lack in many aspects. Based upon the review of literature, following research gaps were identified in the existing solutions:

1. Cancer related tissue abnormalities like angiogenesis, hypermetabolism, and invasion of adjacent normal tissues all exhibit the optical signatures such as polarization, dispersion, and absorption, and therefore detecting them can aid in the early diagnosis.
2. Most of the biological objects and tissues are birefringent or anisotropic in nature, while conventional OCT gives only intensity image. It cannot directly differentiate between different tissues.
3. Point-by-point scanning, for 3D reconstruction of image, atleast three mechanical scan (one depth and two lateral scans) are required. The mechanical scanning system giving rise to motion artefacts due to mechanical jitter and limited repeatability.
4. Currently, large volume of images generated by medical imaging modalities are manually interpreted by persons having expertise for making diagnosis and suggesting treatment. This manual human interpretation process is time-consuming, cumbersome, costly and error-prone. Automated approaches using computer aided programs to read these images, diagnose and suggest treatments can not only help in effective and speedy diagnosis but also do away with the requirement of specialized skills.

Based on the aforementioned problem definitions, the ultimate goal of this research work is the development of an algorithm (s) for human tissues characterization.

1.8 SCOPE AND MAIN OBJECTIVE OF THESIS

This research work majorly focuses on the development of artificial intelligence-based models for the characterization of the biological cells. In view of the previously mentioned issues, the fundamental target of my research work is to find out the health of tissues. We develop an automated algorithm(s) for human tissue characterization. Specifically, the exploration investigates the chance of a CAD system for the classification of human tissues and that could be helpful to the histopathologist.

1.9 OVERVIEW OF THESIS CHAPTERS

The thesis has been organized as given below along with the brief description of what each chapter represents.

Chapter 1: Introduction

This chapter includes the introduction to the tissues, various imaging modalities used and the concept of machine learning. We will conclude this chapter by presenting a brief overview of CAD systems for biomedical sample identification and how effective this technology is in the biomedical industry.

Chapter 2: Classification of melanoma skin cancer images using deep learning

In this chapter, medical images of skin are analysed for classification of melanoma disease. In the proposed work, deep features of residual neural network ResNet50 are used with different classifiers such as SVM, LIBSVM, Neural Network. Data augmentation is done using Generative Adversarial Networks and the results are compared with the basic data augmentation methods such as rotation, translation and shearing. Experiments are done on MED-NODE dataset which consists of 70 melanoma (malignant) images and 100 non-melanoma images.

Chapter 3: Generative adversarial network - Convolutional neural network based breast cancer classification using optical coherence tomography images

This chapter includes the work which focuses on improving classification accuracy for breast cancer tissue, using a CNN (inception-V3), and increasing the training dataset using synthetic OCT images. These synthetic OCT images were generated by a deep convolutional generative adversarial network (DCGAN). The study shows how synthetic images can be exploited by using an inherent intra-sequence variable for GAN-based data augmentation for the purpose of medical imaging.

Chapter 4: Automated full-field polarization sensitive optical coherence tomography diagnostic systems for breast cancer diagnosis

In this chapter, FF-PS-OCT has been demonstrated to be an effective method to monitor tissue morphology changes caused by cancer. A number of optical parameters of the tissue obtained from their phase images is used to differentiate between healthy and malignant tissues with

SVM classifier. The developed automated FF-PS-OCT system and classification algorithm based on machine learning will improve diagnosis and treatment efficiency. It provides a basis for further research into the automated medical diagnosis of breast tumors with spatial phase features.

Chapter 5: Diagnosis of Melanoma Skin Cancer using Machine Learning Approach for Dermoscopic Images

In this chapter, a new system has been proposed in which the canny edge detector is applied on images of PH^2 dataset for edges detection and then these images are smoothened using Gaussian filtration. After the pre-processing operations, the features are extracted using Non-linear kernel ICA and further these features are then classified using Naive Bayes and Support Vector Machines. The proposed work has been analysed with existing techniques in terms of various parameters.

Chapter 6: Conclusions and Future Scope

In this chapter, we summarize the results of the chapters and assess the future scope.

CHAPTER 2

CLASSIFICATION OF MELANOMA SKIN CANCER USING DEEP LEARNING

2.1 INTRODUCTION

Skin covers the entire body and protects it. Being the largest and exterior organ of the body, it is prone to many forms of skin diseases due to different weather conditions. Many of the skin diseases are similar and can be identified only by expert dermatologists in medical area. One of the commonly occurring dangerous skin disease is melanoma. It occurs when there is a rapid growth of cells called melanocytes which produce melanin in skin. The patient suffering from melanoma if may not be able to get a detection in early stage, is likely to get severe skin disorders. The science and engineering can play an important role in early detection of these through analysis using tools and techniques. Dermoscopy is a powerful tool for early identification of melanoma in skin lesions [59]. The availability of medical images (dermoscopic images) helps in easy and accurate diagnosis of skin diseases. The studies in medical images range from image processing, feature extraction, image segmentation, edge detection, image detection and image classification. The binary classification algorithm specifies the result as whether the melanoma is present in the medical image under consideration or not. The multi-class classification algorithm further classifies the type of melanoma as well. The accuracy of detection or classification is the important criteria for judging the success of the algorithm used. The classification can be improved when a large dataset of images can be processed at the same time and with a reasonable speed. This is feasible using deep neural networks (DNNs).

The researchers have applied deep learning for skin disease classification. Deep convolutional neural networks (DCNN) with different number and configuration of layers have been used widely for classification of medical images [60, 61]. Some of the researchers have also combined DCNN with other machine learning algorithms like support vector machine (SVM) for melanoma detection [62]. Another version of convolutional neural network - residual neural network (ResNet) is also used successfully for extracting the features for melanoma classification [63, 64].

2.2 DIAGNOSIS OF SKIN CANCER IMAGES USING MACHINE LEARNING

Most of the early work is based on synthetic analysis of medical images [65]. Other related work is summarized by many researchers [66, 67]. Using deep learning, [62] developed an AlexNet model for classification of melanoma using 2624 dermoscopic images taken from International Skin Imaging Collaboration (ISIC) database. The accuracy achieved was 93.1%. AlexNet was used for feature extraction while SVM was used for classification. An accuracy of 81% was achieved. DCNN was used by [57] for classification of medical images. CNN consisting of 2 layers was applied by [68] in which the model was trained from scratch using 136 images for benign versus nevi malignant melanoma. It was tested on only 34 images from public dataset available publicly from the Department of Dermatology (UMC Groningen). CNN and deep learning for melanoma detection were deployed first in a challenge for skin lesion analysis hosted by the International Symposium on Biomedical Imaging [69, 70]. A CNN ensemble approach was used by [71] and achieved an average accuracy of 79.5% using images from Dermofit Image Library (public). Similarly, [72] used AlexNet and kNN for classification of 399 dermoscopic images as melanomas versus benign nevi. An accuracy of approximately 94% was reported. The authors extracted the representational features. CNN model was trained by [58] with 129,450 clinical images. They used a GoogLeNet Inception v3 model for classification of images in 2 categories: benign nevi versus malignant melanoma and benign seborrheic keratosis versus keratinocyte carcinomas skin cancer. An accuracy of 94% was reported for melanomas in dermoscopic images. Skin lesion classification was done with CNN by [73]. The authors used images from the ImageNet. VGGNet deep learning model was utilized by [74] for classification of medical images as nevi or lentigines versus melanoma using 379 images from ISBI 2016 challenge dataset. An accuracy of 81.33% was achieved. The authors used three configurations of CNN model (network from scratch, pretrained with transfer learning, one with fine-tuning of the weighting parameters). Deep learning was used in [75] to recognize melanoma in skin images. The results were proved to be accurate to a high degree when these were recognized by dermatologists physically.

Residual network is a CNN model proving to be very successful for detection of melanoma. Three ResNets were used in [76] for training by fine-tuning a pre-trained CNN. They classified melanoma versus nevi versus seborrheic keratosis from a dataset of 150 dermoscopic images. The accuracy reported for melanoma was 85.4%. The accuracy of computational methods has also been verified by physical dermatologists. A framework was developed by [64] using multi-channel residual networks. The accuracy of the framework was 82.4% in classifying the medical image as melanoma or seborrheic keratosis skin disease.

2.2 METHODOLOGY

2.2.1 Data Acquisition

MED-NODE dataset [77] is used in this work which consists of a total of 170 images-70 melanoma (malignant) images and 100 non-melanoma images from the digital image archive of the Department of Dermatology of the University Medical Centre Groningen (UMCG) used for the development and testing of the MED-NODE system for skin cancer detection from macroscopic images. Figure 2.1 shows the example of the melanoma and non-melanoma images from the MED-NODE dataset.

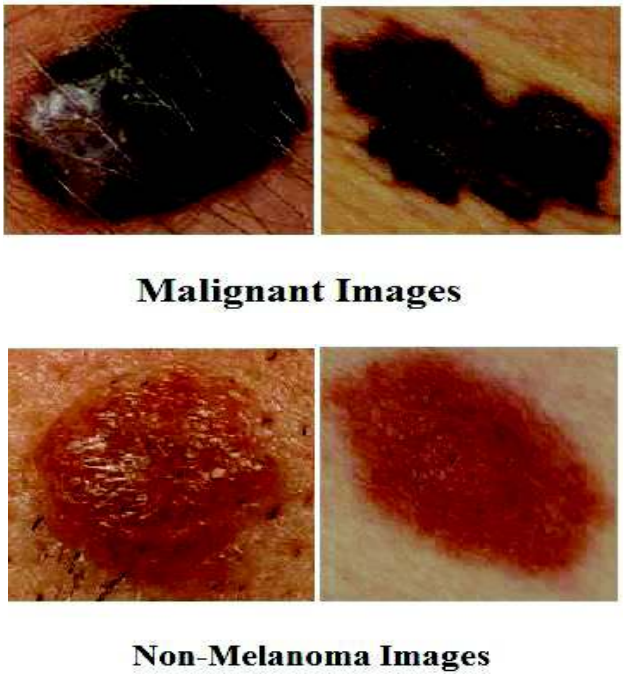

Figure 2.1 Images from the MED-NODE dataset classified as melanoma (malignant) and non-melanoma

2.2.2 Data Augmentation

In the proposed work, the images of the MED-NODE dataset are augmented with the classical transformations such as rotation, translation and shearing. It is done using Generative Adversarial Network (GAN) for the synthesis of medical images. GANs, as presented by [78], right now speak to the cutting edge for generative models. A GAN is a system for evaluating generative models, comprising of two differentiable sub models, which are ordinarily actualized as DNNs: the generator and the discriminator. An outline of an average GAN setup

is showed in figure 3.2 [79]. The generator and the discriminator go up against one another: the generator is prepared to generate images, while the discriminator gets the generated images and is prepared to differentiate between produced images and genuine images.

In GANs, a generative model or something to that affect is tuned to generate new synthetic and additional data, which is identical to the real data. In the proposed work, the images are generated with GAN after the 3000 epochs. The images are quite similar as the original dataset images.

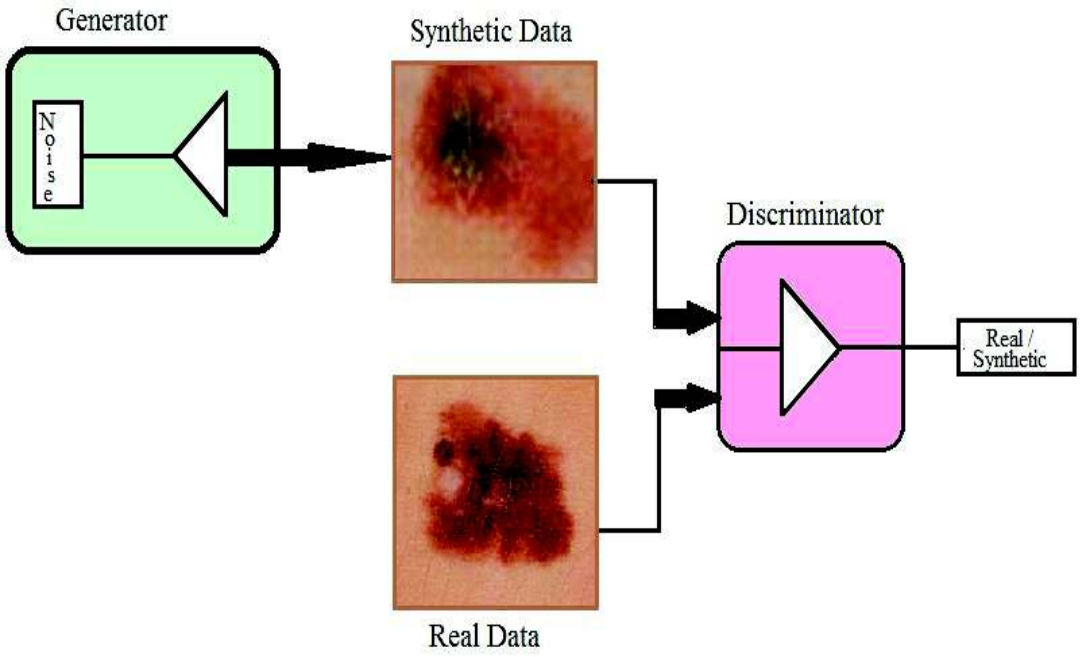

Figure 2.2 Architecture setup of a GAN

2.2.3 Feature Extraction

The pretrained ResNet50 is used for extracting the features in the proposed work. After applying the data augmentation, the images are resized into a size of 224*224 and fed as input to the pretrained ResNet50 model. The extraction of features is done from the higher-level layers of this model. The extracted features are then used for the classification of the melanoma/non-melanoma images. ResNet50 gives the alternate way association between layers, which makes it safe to prepare DNN to gain maximal portrayal power without agonizing over the degradation issue, i.e., learning troubles presented by deep layers. The typical illustration of ResNet50 is described in figure 2.3 [80].

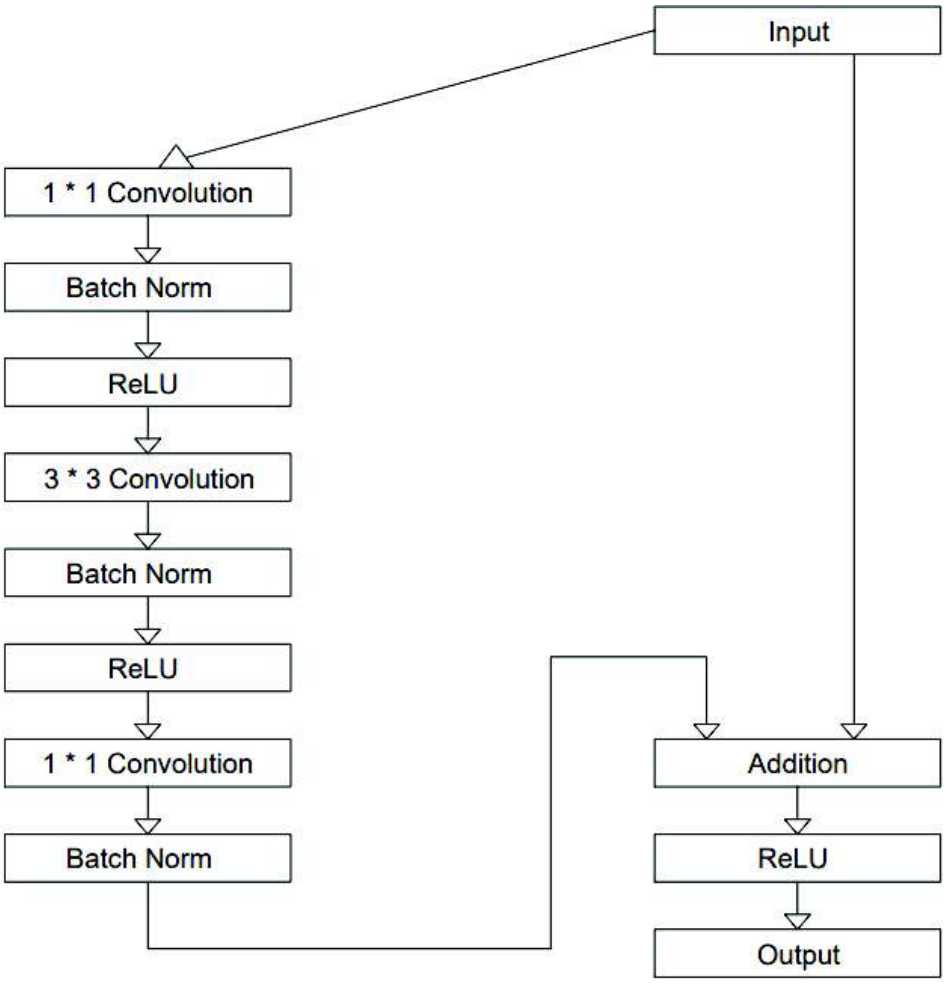

Figure 2.3 The basic residual block of ResNet (50 layers)

2.2.4 Classification Approaches

Various classifiers used for the classification of the skin images are SVM, LIBSVM and NN.

a) Support Vector Machine

SVM is a binary classifier that attempts to separate the classes on the basis of a separating hyperplane. The hyperplane separates the inputs into the two regions. The Gaussian kernel is used in this work for separating the images into two classes by a hyperplane.

b) LIBSVM

LIBSVM is a library for SVM. LIBSVM supports classification and regression by applying Sequential minimal optimization (SMO) algorithm for kernelized SVMs.

c) Neural Networks (NN)

Neural Networks are inspired by the biological neurons and consists of three layers- input layer, hidden layer and output layer. The input layer accepts the feature vectors. The output layer predicts the class – malignant or nevus. The hidden layer performs the computations on the weighted inputs and produces the output via the activation function.

Binary classification is used for images- positive for images with Melanoma and negative for images with non-Melanoma. Accuracy is defined as the proportion of samples correctly classified to total tested samples.

2.3 RESULTS AND DISCUSSION

The experiments are implemented on a system with Intel® Core™ i7-5500U CPU @ 2.40 GHz with 12.0 GB. The software used is MATLAB R2015a.

Table 2.1 compares the accuracy (in percentage) of various classifiers with the ResNet50 feature extraction method and MED-NODE dataset on data augmentation with classical transformations.

Table 2.1 Performance comparison of the proposed methods on data augmentation with classical transformations

METHODS	ACCURACY (%)
ResNet50 + SVM	68
ResNet50 + LIBSVM	62
ResNet50	84
ResNet50 + NN	94

The above table shows the comparisons of the different classification approaches used with ResNet50 and the corresponding accuracy achieved with using different classical data augmentation techniques.

Table 2.2 compares the accuracy (in percentage) of the various classifiers with the ResNet50 and MED-NODE dataset on data augmentation with Cycle Generative Adversarial Network (Cycle GAN).

Table 2.2 Performance comparison of the proposed methods on data augmentation with GAN

METHODS	ACCURACY (%)
ResNet50 + SVM	75
ResNet50 + LIBSVM	78
ResNet50	89
ResNet50 + NN	96

The above table shows the comparisons of the different classifications approaches used with ResNet50 and the corresponding accuracy achieved while using GAN as a data augmentation technique.

The comparison is shown in figure 2.4 and 2.5.

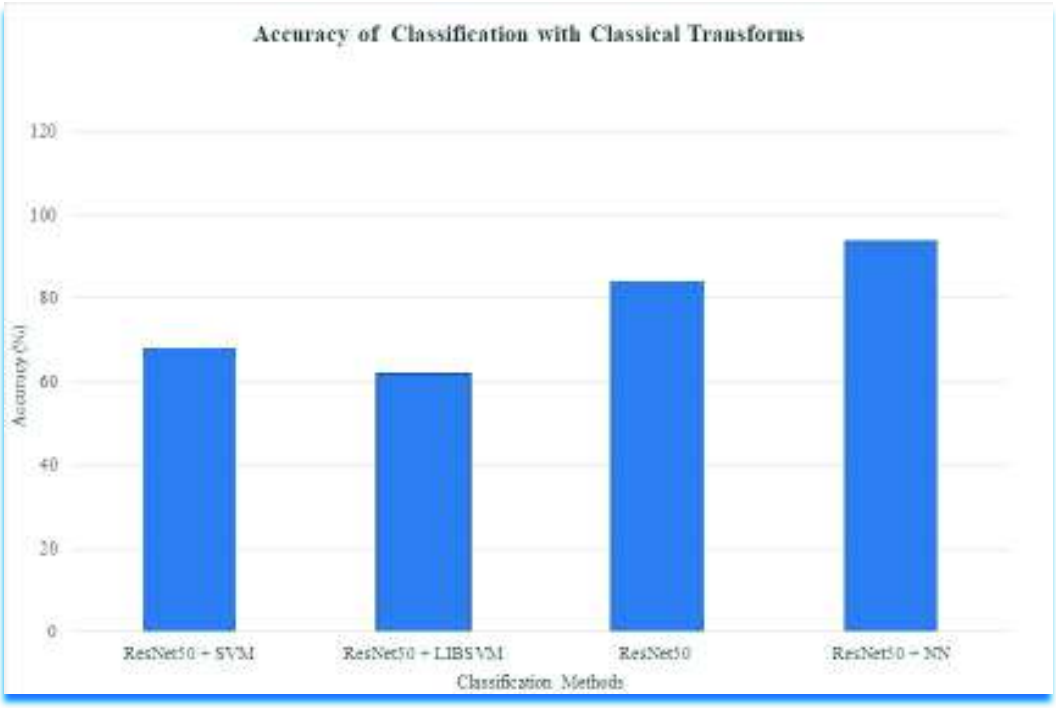

Figure 2.4 Comparison of accuracy of classification with classical transforms.

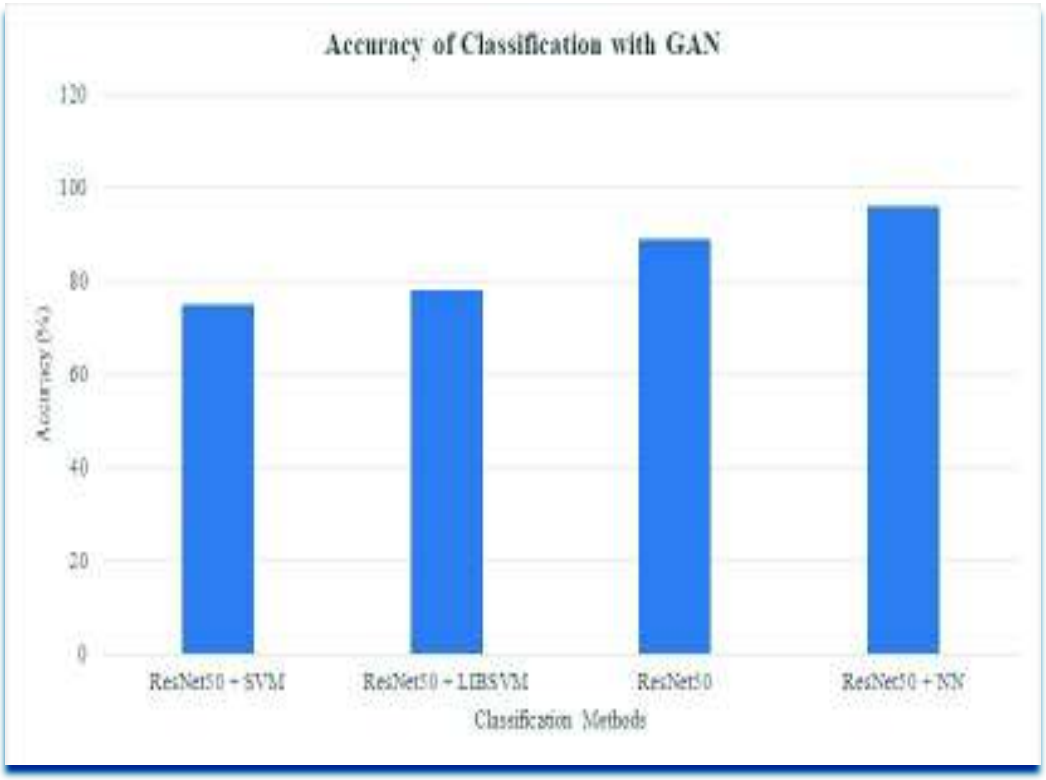

Figure 2.5 Comparison of accuracy of classification with GAN.

Following are the contributions of the proposed work –

a) Data augmentation is done with GAN for the synthesis of the skin cancer images. The results are better as compared to the classical transformations for data augmentation such as rotation, translation and shearing.

b) A deep learning model - The Residual Neural Network (ResNet50) is used in this paper for extracting the features of the image dataset. The output of ResNet50 is used with various classifiers for classifying the melanoma in skin cancer images.

c) The final classification is done using SVM, LIBSVM, Neural Network classifiers.

The results show that the proposed work is efficient than existing studies when classical transformations such as rotation, translation and shearing are used with ResNet50 and NN with 94% accuracy. In the proposed approach, it is proved that the accuracy of all classifiers is improved when data augmentation is done using GAN. The improvement in accuracy with GAN varies from 2% (ResNet50 + NN) to 16% (ResNet50+LIBSVM). The highest accuracy achieved is 96% using the combination of ResNet50 as feature extractor and NN as the machine learning classifier on performing the data augmentation with GAN which is better than existing one [80]. The output of ResNet50 is used with various classifiers for classifying the melanoma in skin cancer images. The combination of ResNet50 as feature extractor and NN as the machine learning classifier is more accurate and fast as compared to ResNet50 alone.

2.4 CONCLUSIONS

In this chapter, an efficient approach is proposed as an integration of ResNet50 for feature extraction, data augmentation of skin cancer images with GAN and classification using NN, SVM and LIBSVM. The experiments are done on the MED-NODE dataset and the images are classified as melanoma and nevus. The highest accuracy achieved is 96% using the combination of ResNet50 and NN as the machine learning classifier on performing the data augmentation with GAN which is better than many existing studies. The work shows an improvement in accuracy of classification (upto 16%) of ResNet50 with the use of augmentation methods like GAN as compared to classical methods for data augmentation.

CHAPTER 3

GAN-CNN BASED BREAST CANCER CLASSIFICATION USING OCT IMAGES

3.1 INTRODUCTION

Medical imaging is a basic component of modern health- care, and plays an important role in the diagnosis and follow-up of cancer following treatment. According to data fromthe GBD (Global Burden of Disease Cancer Collaboration), and the World Health Organization (International Agency for Research on Cancer), the number of cancer patients increased by 28% between 2006 and 2016, and 2.7 million fresh cancer cases are predicted to occur by 2030 [83]. Of the various types of cancer, the most common and deadly cancer in women is breast cancer [84] – [86]. Effective breast cancer diagnosis has therefore become essential. X-ray, MRIand ultrasound are the primary techniques used to diagnose breast cancer, but biopsy is still considered to be the gold standard for a definitive diagnosis [87] [88,89]. Biopsy comprises the extraction of tissue, which is subsequently fixedon a microscopic slide, and stained. These stained histopathology images are of very high resolution, and rich in information. However, histopathological images are assessed by pathologists, and the experience of the individual pathologist plays a very important role in diagnosis due to the complicated geometrical structure and textures of the samples. The major disadvantage of biopsy is that it is a time-consuming affair, and cannot be performed intraoperatively [90, 91]. A non-invasive technique is therefore required, which can be used intraoperatively. Optical coherence tomography (OCT) is an alternative technique, with the capacity to be performed intra-operatively, and its resolution is comparable to that of histopathology. OCT is typically an interferometric technique, capable of visualizing the tissue's microstructure via cross-sectional images. It is a non-contact, non-invasive high-resolution, three-dimensional tomography imaging technique [92, 93], and a potentially excellent resource for real-time patient advice, due to its non-invasive nature, and rapid diagnostic process. However, most OCT image analysis is still reliant onmanual assessment by radiologists or pathologists, which is a tedious and time-consuming job. Manual assessments also lead to inconsistent results, since they are highly dependent on the experience of individual radiologists or pathologists. The development of automatic and reproducible algorithms based on OCT images could therefore prove useful in sup- porting clinicians, by promoting more effective diagnoses, and improving access to medical care and specialist expertise, particularly in circumstances where skilled manpower is limited.

In general, conventional computer aided diagnosis for breast cancer diagnosis is based on machine learning (ML). The performance of ML depends upon the handcraft features extracted. Deep learning, however, is capable of both automatically extracting features, and performing classification tasks [93] – [96]. The convolutional neural network (CNN) is the most popular deep learning method for classification tasks where the information is stored in spatial locations. Recently, the use of CNNs in the field of medical image analysis has increased tremendously, due to its excellent capacity for generalization, and the ready availability of the GPU hardware required for parameter optimization [94] – [97]. The major stumbling block preventing the widespread utilization of deep learning in the field of medical image analysis is that it requires large amounts of annotated/labelled data;in the medical field, it can be very difficult to obtain such labelled data. This issue may be addressed via the application of transferred learning, in which a previously trained net-work transfers its knowledge to subsequent problems [98]. AlexNet, VGG, RCNN and Inception are the most popular types of CNN image classification networks. In order to improve classification accuracy, conventional data augmentation techniques (rotations, flips, color jittering etc.) are generally used to augment the dataset, but more recently, generative models have been used to synthesize a completely new dataset [99]. Data augmentation methods have already been employed to reduce the model's error rate by over 1% on an ILSVRC-2010 dataset [100]. With the development of generalized adversarial networks (GANs), synthesized augmented datasets can easily be generated. GANs have already been used for augmentation purposes, such as creating new trainingimages to improve classification, refining synthetic images, enhancing brain segmentation, and retinal fluid segmentation [101] – [105].

This work focuses on improving classification accuracy for breast cancer tissue, using a CNN (inception-V3), and increasing the training dataset using synthetic OCT images. These synthetic OCT images were generated by a deep convolutionalgenerative adversarial network (DCGAN). This study shows how synthetic images can be exploited by using an inherent intra-sequence variable for GAN-based data augmentation forthe purpose of medical imaging.

3.2 METHODOLOGY

3.2.1 Experimental Setup

For the imaging of normal and cancerous breast tissue, an SS-OCT (OCS1310V1-1300 nm, Thorlabs) imaging system was used. Figure 3.1 shows a schematic diagram of the SS-OCT system, consisting of a light source module (laser), an image module, and a standalone probe.

A swept source, with a wavelength sweeping range from 1250 nm to 1350 nm, BW = 100 nm, and a central wavelength of 1300 nm was used to perform the study. The sample arm has a 5X objective lens (MO, LSM03, Thorlabs, focal size 25.1 mm in air) to image the sample under examination. A dual-balanced photodiode, operating at a 100 KHz A-Scan rate, is used to identify the interference signal.

To obtain the 3D image, the two-dimensional XY galvo scanner scans the probe beam over the sample. The system's axial and lateral resolution measures 12 μm and 16 μm, respectively, in air. The sample is illuminated by a laser with an average output power of 25 mW. The system's sensitivity ranges from 0.5 mm to 4.5 mm in air at 107 dB. It has a higher signal to noise ratio at a greater penetration depth (2.5 mm in tissue) than other conventional OCT systems. The size of the images generated by the system is 250 X125 pixels (B-scan image), and each volume consists of 106 B-scan images. Further details regarding the system can be found in [93].

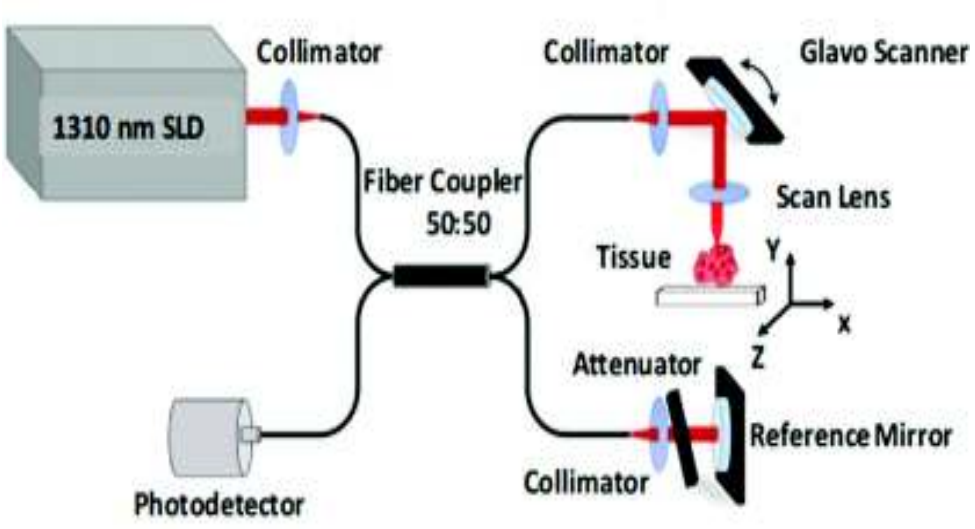

Figure 3.1 Schematic diagram of SS-OCT system.

3.2.2 Sample Preparation

In conducting the study, samples were collected from 22 individuals undergoing biopsy at the All India Institute of Medical Sciences (AIIMS), New Delhi. Ethical clearance for the study was provided by the Indian Technology Institute (IIT), Delhi, and the AIIMS Ethics Committee. In order to con- duct the OCT experiment, the sample tissue was placed in a petri dish. All tissue samples were imaged ex vivo, using the OCT system. The labeling was performed by two pathologists, who analyzed the OCT images and manually separated them

into normal and cancerous tissues. Discrepancies between specialists were rejected, and are not included in the training dataset.

3.2.3 Generation of Synthetic Images

The primary issue in training the CNN to perform more effectively is the absence of an annotated dataset. To improve the performance of the network, we broadened the training dataset by adding the data in two ways: (1) via the classical augmentation technique (flipping, rotation, translation), (2) the addition of synthetic images generated by the GAN.

In classical augmentation techniques, synthetic images can be generated by rotating the images with a random angle between 0◦ to 180◦. Once the images are rotated, they are flipped (left-right and up-down). Further augmented images can be formed by translating and scaling the images, although in our case we ignore the translation and scaling technique of augmentation. The total number of images, having applied the classical augmentation techniques given by equation (4.1) is as given in [106]:

$$N = N_{rotation} \times (1 + N_{flipping}) \qquad (3.1)$$

In general, the classical augmentation technique is used to tune the network and avoid overfitting includes flipping, rotation, and translation. The GAN has the capability to generate new samples, learned from the data distribution [107]. To synthesize the labelled data set, we explored a DCGAN (deep convolutional GAN) model. DCGAN is the modified version of GAN proposed by Ian Goodfellow et al [108]. The model comprises two neural networks: the first, known as a generator, generates fake images, while the second, known as a discriminator, distinguishes between real and fake images. The input to the discriminator is an image, and the output of the discriminator consists of probability data as to whether or not the input image is real. The output of the generator is an image, and its function is to attempt to generate an image that will fool the discriminator; in other words, the generator tries to maximize the probability of the discriminator's finding that the images it receives are from the training set, rather than from the generator. The researchers were also used Wasserstein GAN (WGAN) and WGAN results in stable training and solves the problem of mode collapse and vanishing gradient which we face in DCGAN, but WGAN is slower than DCGAN while training (i.e. it takes longer training time) [102]. Here, the images have been resized to 64 × 64 from 250 × 150 to improve the GAN's performance, since the DCGAN architecture is generally more stable at 64 × 64.

3.3 ARCHITECTURE OF GAN

3.3.1 Generator architecture

The images (64 × 64 × 1) are reshaped into a vector of size 100. The input is fed to the fully-connected layers, consisting of four fractionally stride convolutions, with filter sizes of 256, 128, 64, and 32. Further details are provided in table 4.1. An Adam optimizer is employed, with a learning rate of 0.0002, a batch size of 64, and whose momentum is set to 0.5 and 0.999, respectively. A full description of the architecture may be obtained from [108]. The output of the generator is an image sized at 64x64x1.

∗Conv2DT = Conv2DTranspose (Conv2DTranspose is a convolution process, whose kernel is learned during model training).

Table 3.1 Description of generator architecture layers

Layer (Type)	Output Shape	No. of Parameters
Input (Reshape)	100	0
Dense	(None, 4096)	409600
Batch Normalization	(None, 4096)	16 384
LeakyReLU	(None, 4096)	0
Reshape	(None, 4, 4, 256)	0
Conv2DT	(None, 4, 4, 256)	1638 400
Batch Normalization	(None, 4, 4, 256)	1024
LeakyReLU	(None, 4, 4, 256)	0
Conv2DT∗	(None, 8, 8, 128)	819 200
Batch Normalization	(None, 8, 8, 128)	512
LeakyReLU	(None, 8, 8, 128)	0
Conv2DT	(None, 16, 16, 64)	204 800
Batch Normalization	(None, 16, 16, 64)	256
LeakyReLU	(None, 16, 16, 64)	0
Conv2DT	(None, 32, 32, 32)	51 200

Batch Normalization	(None, 32, 32, 32)	128
LeakyReLU	(None, 32, 32, 32)	0
Conv2DT	(None, 64, 64, 1)	800

3.3.2 Discriminator Architecture

The discriminator network is a conventional CNN, where the input image size is 64x64x1, and the output of the discriminator network discriminates between real and fake images. It comprises four convolutional layers, with a 5 × 5 size filter/kernel, and a fully connected layer. To reduce the spatial dimensions, stride is used, and for the purpose of faster convergence, batch normalization is used in all the layers except input and output. Leaky ReLU is used in all layers except the output, in which a sigmoid function is used to predict probability. In relation to the leaky ReLU, the slope of the leak was set to 0.2. Further details regarding the discriminator architecture are given in table 3.2.

Table 3.2 Description of Discriminator architecture layers.

Layer (type)	Output Shape	No. of Parameters
Conv2D*	(None, 32, 32, 32)	832
Batch Normalization	(None, 32, 32, 32)	128
LeakyReLU	(None, 32, 32, 32)	0
Conv2D	(None, 16, 16, 64)	51200
Batch Normalization	(None, 16, 16, 64)	256
LeakyReLU	(None, 16, 16, 64)	0
Conv2D	(None, 8, 8, 128)	204800
Batch Normalization	(None, 8, 8, 128)	512
LeakyReLU	(None, 8, 8, 128)	0
Conv2D	(None, 4, 4, 256)	819200
Batch Normalization	(None, 4, 4, 256)	1024
LeakyReLU	(None, 4, 4, 256)	0

Flatten	(None, 4096)	0
Dense	(None, 1)	4097

* Conv2D = two dimensional convolution

3.4 CNN ARCHITECTURE FOR THE CLASSIFICATION

Inception-v3 is a very popular CNN, but it is very hard to train the network from scratch, since it requi res a large number of labelled datasets [93]. Transfer learning can be a good solution in such a case. In this process, the parameters of the last layer will be maintained, and extract the last layer of the model, before retraining the last layer of the pre-trained net- work on ImageNet [103,104]. The number of classes in the data- set decides the output node of the last layer. The patch size of the image is 64 x 64 x 1 pixels, resized to 299 x 299 x 3, and with the intensities rescaled between '0′ and '1′. ReLU is used as an activation function in each convolutional layer, while the sigmoid function is used in the softmax layer for the purpose of classification. Prior to feeding any patch/image to the network, a mean value of intensity for all the training patches was subtracted from it. The model was pre-trained on a natural image dataset via ImageNet, and fine-tuned on our training dataset. Further, to train the network, a batch size of 32, and a learning rate of 0.001 for 200 epochs was selected. For optimization purposes, stochastic gradient descent optimization with Nesterov momentum updates was employed. Further details of the network can be found in [108]. Inflating a dataset artificially by means of data augmentation techniques helps to reduce overfitting when training a deep neural network. The developed model output is not evaluated on the 'outside' data- set, but on the ILSVRC-2010 dataset, where data augmentation approaches have already been used to reduce the model error rate by more than 1% [100]. We also used dropout and batch normalization to avoid overfitting.

3.5 RESULTS AND DISCUSSIONS

The patient samples were distributed as follows: 8 out of 12 cancerous patients, and 8 out of 10 normal patient samples were used for training purposes, and the remainder of the sample's dataset was used for testing purposes. Every patient sample comprised 106 B-scan OCT images. All sample images with a mixed response greater than 80% were excluded from the training datasets, as determined with the help of a pathologist. Inceptio-V3, a CNN model, was used for the classification. Initially, the model was trained using only real OCT and classical

augmented images. To further improve the classification accuracy, the training datasets were increased by including synthetic images generated via the DCGAN.

In an attempt to quantitatively assess the realism of the synthetic images, an experienced physician was requested to identify a random selection of 50 real/50 synthesized OCT images as true or synthetic images, which were then shown in a regular sequence for each GAN/sequence, without identifying what was real/synthetic in prior training stages. Figure 4.2 shows the synthetic OCT images generated from the DCGAN which closely resemble genuine OCT images. Even for an experienced physician it proved very difficult to differentiate between the real and synthetic images, particularly in lower resolution, given the absence of finer details. We used the architecture for the DCGAN outlined above. Figure 4.3 shows a flow chart of the classification of breast tissues from the Inception-V3, including real, classically augmented, and synthetic OCT images generated from the DCGAN.

We evaluated the impact of data augmentation using synthetic images on breast tissue classification, relative to the classical data augmentation technique, on the basis of accuracy, sensitivity, and specificity. The model was trained and tested on a Windows 10 system with an Intel (R) Xeon (R) CPU E5- 1620: 0 3.60-GHz processor, a 1 TB HDD, 16 GB RAM, a CUDA-enabled Nvidia GeForce GTX 670: 12GB GPU, and CUDA 9.0 dependencies for GPU acceleration.

Training the inception model for classification using synthetic image-based data augmentation led to improved results, as compared to using classic data augmentation alone. Once the network is trained with real, synthetic, and classical data augmentation-based OCT images, the network is tested on the real OCT test images. Once the model has been developed, there is no need for a specialized pathologist to differentiate between normal and cancerous tissues. The efficiency of the proposed algorithm was reduced if the images included in the training dataset were not identified with the help of a qualified pathologist, or where the data was not cleaned.

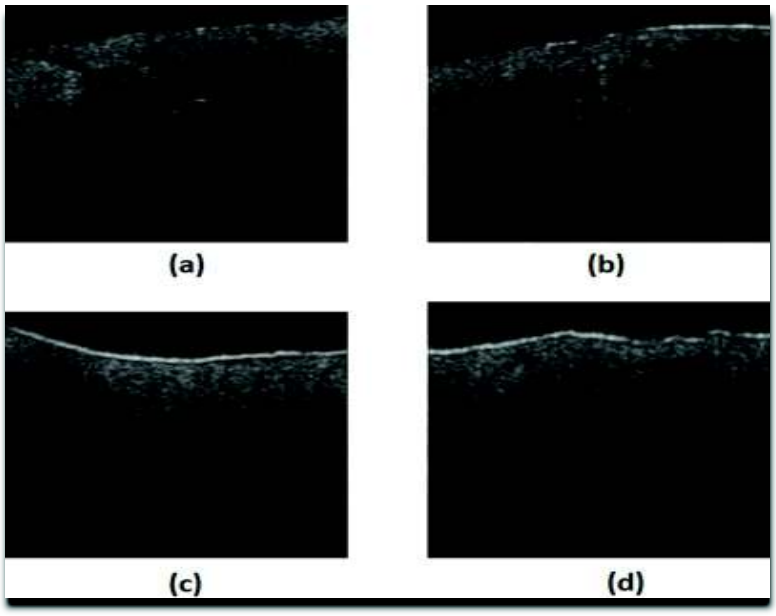

Figure 3.2 (a), (c) Real OCT images, (b), (d) synthetic OCT images of normal and cancerous (ductal carcinoma) breast tissue, respectively.

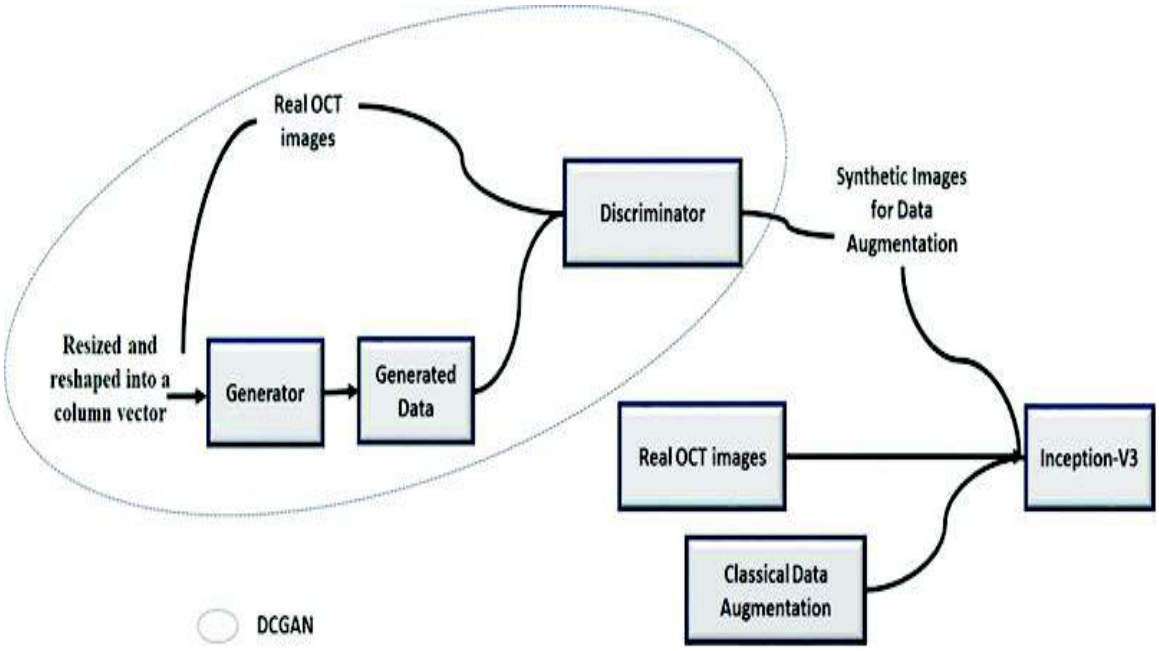

Figure 3.3 Flowchart for classifying breast cancer using OCT images with classical and synthetic data augmentation.

The main focus of this work is on improving the CNN model's performance in classifying breast cancer using OCT images. A small data set was expanded with synthetic OCT images, generated from a GAN, so as to improve network performance. The proposed framework improves the results of classification by incorporating synthesized images, as shown in table 3.3. Classical data augmentation improves the performance of the network by adding data, but beyond an optimal point, adding more data did not improve the results.

To further improve the performance of the network, synthetic images were also used for augmentation purposes. The training accuracy of the network using only classical data augmentation is 94.1%, while incorporating both classical and synthetic data augmentation achieves a result of 95.3%. The network performance achieves 93.6% sensitivity, 90.8% specificity, and 91.7% accuracy based on the testing data- sets shown in table 4.4. In this work, malignant breast tissue samples were extracted from original surgical specimens, and may have provided a clearer depiction of some malignant structures than those typically seen in intact surgical specimens.

Table 3.3 Performance of the network on the training datasets over 200 epochs

	No. of Samples	Accuracy
Without data augmentation	1182	91.1%
With classical data augmentation rotation (0˚, 45˚, 90˚, 135˚,180˚)	5910	92.0%
With both classical and synthetic data augmentation	6400	93.7%

The above table states the performance of the network on the training datasets with and without data augmentation methods with their corresponding number of samples and accuracy achieved.

Table 3.4 Performance of the network on the testing datasets

Augmentation Technique	Accuracy	Sensitivity	Specificity
Classical and Synthetic data Augmentation	91.7%	93.6%	90.8%

The above table states the performance of the network on the testing datasets with the classical and synthetic data augmentation methods.

3.6 CONCLUSIONS

In conclusion, we introduced a framework for the generation of synthetic images to enhance the performance of a networkwith a limited labelled dataset. This technique demonstrates how, by incorporating synthetic images, breast cancer classification using OCT images improved by only 1.7% as com- pared to the traditional technique of data augmentation. To achieve improved results, we implemented an Inception-V3 architecture for the classification of breast cancer tissue. Though the study was done on breast tissue samples using the OCT images. The GAN-CNN based intelligent system was used for the automatic classification of the breast cancer. The future work will cover the detection of breast cancer at different stages. In the next research paper, a new approach will be proposed to detect breast cancer at early stages using OCT images. We believe that this framework could be a potentially useful tool for medical image analysis.

CHAPTER 4

AUTOMATED FULL-FIELD POLARIZATION SENSITIVE OPTICAL COHERENCE TOMOGRAPHY DIAGNOSTIC SYSTEMS FOR BREAST CANCER

4.1 BACKGROUND

The most commonly diagnosed cancer among women worldwide is breast cancer [111,112]. According to WHO the standard method for breast cancer diagnosis is physical examination and X-ray mammography [113]. The feasibility of screening for younger age groups based on X-ray mammography, as dense breast tissue may challenge accurate interpretations [113,114]. The false-negative delay in treatment and ultimately worsen the situation that may lead to lower survival chances. Other imaging methods for cancer detection include ultrasound, X-ray computed tomography, and magnetic resonance imaging, but they are also not very effective when the lesion size is less than ~1 cm [114]. Most cases were diagnosed in a later stage using these techniques. Hence the development of new techniques for early cancer detection is imperative.

Optical coherence tomography (OCT) is a low-coherence interferometry technique with high-resolution, non-contact, non-invasive, three-dimensional imaging [115,116]. The basic principle is similar to ultrasound. The blend of high optical resolution, high-speed, and millimeter image range makes OCT ideal for operating margin measurement [115,118]. Because of its micron-level resolution, OCT can be a potential tool for conducting an "optical biopsy" at a suspicious tissue site [117, 121]. OCT can be incorporated into the biopsy needle used to diagnose cancer, either for better image guidance or for intraoperative cell and tissue microstructure. The handheld OCT sample is being tested in the surgical cavity before resection for the in vivo margin imaging [122, 123]. The typical OCT system uses a point-by-point scan (parallel to optical axes) and results in mechanical jitter and poor reproducibility due to motion artifacts. To avoid point-by-point scanning a photodetector has been replaced by 2D camera that records the entire *en-face* image (orthogonal to the optical axis) in the single shot and system is known as full-field OCT (FF-OCT) [124] – [126]. Different OCT techniques, including FF-OCT for margin assessment [124], and needle based OCT system for biopsy assessment, are also used for breast imaging [119] – [123]. Cancer-related tissue defects, such as angiogenesis, hyper metabolism and invasion of neighboring natural tissues, have optical signatures (polarization, dispersion and absorption) that can detect early cancer [127,128].

Recent studies have shown that breast cancer appears to be more dispersive than healthy tissue, affecting the normal shape of breast adipose and stroma. Nonetheless, solid invasive tumors are hard to differentiate from fibrous stromal tissue islands caused by the lack of specific structures and related refractive indices [129,130]. Intraoperative breast cancer delineation is a major challenge. An effective breast tissue screening technique may reduce the risk of re-excision during operation by specifically identifying positive margins. In this study, a high resolution automated full field polarization sensitive optical coherence tomography (FF-PS-OCT) system was developed to classify healthy and malignant human breast tissue from quantitative phase information of the tissues in *ex vivo*.

4.2 FF-PS-OCT SYSTEM

Polarization-sensitive OCT (PS-OCT) is a functional extension of OCT [131] – [133]. As compared to OCT, PSOCT offers details on the properties of tissue polarization. Anisotropic biological material, such as collagen fibers, is birefringent, causing polarization to change as the light passes through the tissue [134]. PS-OCT has already been used for muscular dystrophy, collagen plaques and skin cancer [135] – [137]. Collagen variability in tumor and stromal tissue may be used as an important source of information for breast cancer imaging. In the past, PS-OCT was used to distinguish between benign fibro adenoma and malignant invasive ductal carcinoma [139]. However, an automated examination of healthy and cancerous breast tissues is rarely performed. Reading, medical images and making a diagnosis or recommendation of treatment, even though it requires highly qualified professionals. Current medical image processing techniques are labor-intensive, time-consuming, costly and error-prone. It would be easier for a computer-aided program to read those images automatically and suggest recommendations for diagnosis and treatment [140] – [142]. Early detection remains the key to successful treatment and the best possible chance of recovery for patients. Most of the studies to screen the cancer are focused on intensity based features [123,141]. We assumed, that phase images that are direct reflection of birefringent generated by PS-OCT with machine learning tool could be used efficiently to evaluate tissue conditions and to classify healthy and malignant tissues. Support vector machine (SVM) model has been used which offers a good alternative to dealing with complex classification problems for diagnostic purposes [143]. SVMs are a type of supervised data interpretation and classification methods used for classification and regression analysis in machine learning. SVM performs a classification based on a model trained from a given training set, by constructing an N-dimensional hyperplane that optimally divides the data into different categories.

4.2.1 System Specification

Figure 4.1 shows the schematic diagram of the FF-PS-OCT system. A near-infrared super luminescent diode (830 nm central wavelength and 40 nm bandwidth) is used as a light source. Before the incident to a non-polarizing beam splitter (BS), the light is linearly polarized by linear polarizer (LP). The beam splitter splits the light into two parts, one part is going toward reference arm and another part is going towards the sample arm. The sample arm light incident on quarter-wave plate oriented at 45^0 which converts linearly polarized light into circularly polarized light. The circularly polarized light illuminates the sample through 60X numerical objective lens and due to anisotropic properties of the sample, the reflected light from the sample achieves an arbitrary (elliptical) polarization state. While the reference light is passing through neutral density filter before the incident on the quarter-wave plate oriented at 22.5^0 and illuminated the reference mirror via 60X numerical objective lens.

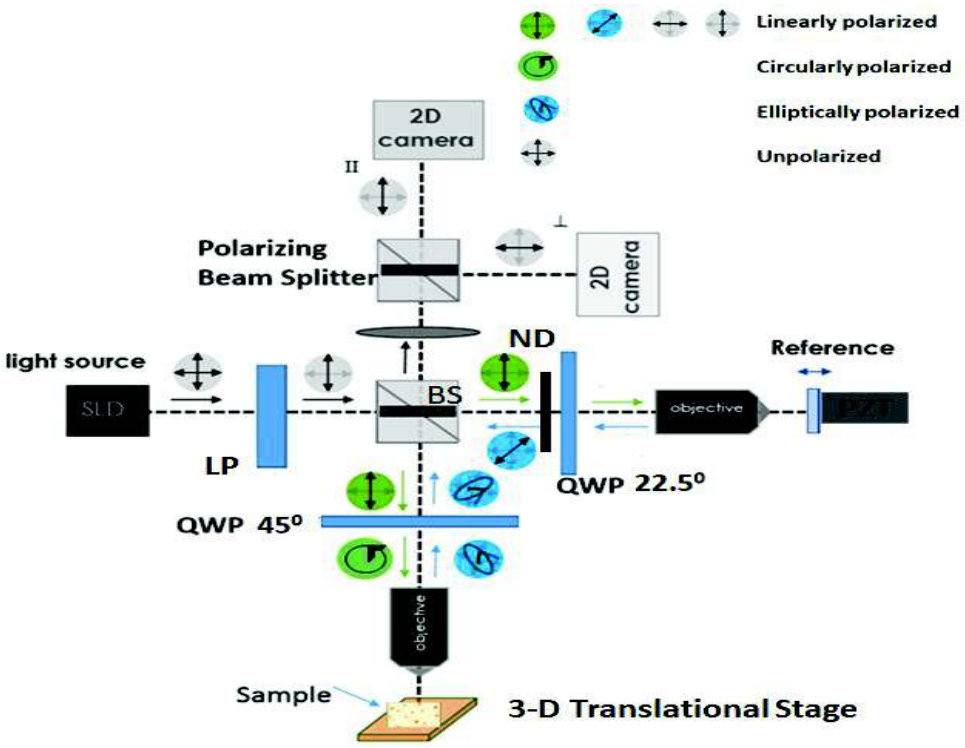

Figure 4.1 The schematic diagram of the FF-PS-OCT system.

The backscattered light from the reference arm and sample interfere at beam splitter BS. Further, the inference signal is transmitted through a polarizing beam splitter. This splits the interference signal into two orthogonal signals, perpendicular and parallel components to the incident polarization which are recorded by two separate charge coupled device (CCD) cameras (30 fps, pixels: 512 x 512, 10-bits). To record the phase shifted interferogram a reference mirror is attached to piezo-electric transducer (PZT). The present system has ~1 μm axial resolution and the lateral resolution is ~0.8 μm in the water as a biological sample majorly consists of water. The imaging depth of developed OCT system is in between 2 to 3 mm and imaging depth was kept constant to acquire data from all the patients.

Birefringent can be an important determinant for quantifying changes in tissue cellular structure and chemical composition. Tissue birefringent is a useful marker for the intrinsic disease [127,128]. It includes the phase information of the sample along with the thickness of the sample. The sample is placed on the 3D stage. The reference mirror is moved with the help of PZT and set of four phase-shifted interferogram were recorded with two CCD cameras. CCD(⊥) records $I_1^{\perp}$, $I_2^{\perp}$, $I_3^{\perp}$, $I_4^{\perp}$ and CCD(∥) records $I_1^{\parallel}$, $I_2^{\parallel}$, $I_3^{\parallel}$, $I_4^{\parallel}$ [133]. The phase map is extracted from the recorded interferogram.

$$\gamma^{\perp}(x,y) = (I_1^{\perp}(x,y) - I_2^{\perp}(x,y))^2 + (I_3^{\perp}(x,y) - I_4^{\perp}(x,y))^2 \quad (4.1)$$

$$\gamma^{\parallel}(x,y) = (I_1^{\parallel}(x,y) - I_2^{\parallel}(x,y))^2 + (I_3^{\parallel}(x,y) - I_4^{\parallel}(x,y))^2 \quad (4.2)$$

$$\gamma^{\perp}(x,y) = k\sin^2\phi(x,y) \; and \; \gamma^{\parallel}(x,y) = k\cos^2\phi\,(x,y) \quad (4.3)$$

$$Phase\ retardation\ \emptyset(x,y) = sqrt\left(\frac{\gamma^{\parallel}(x,y)}{\gamma^{\perp}(x,y)}\right) \quad (4.4)$$

where, (x,y) represent the spatial locations, k is sample reflectivity. Owing to the high numerical objective lens, high spatial resolution can be achieved by compromising the depth of penetration. The axial resolution depends upon the coherence length of the light source. The rate of the phase changes directly reflects the birefringent.

.

4.3 METHODOLOGY

An automated full-field PS-OCT (FF-PS-OCT) system based on SVM for the classification of healthy and malignant breast tissue using phase images information that could be helpful in intraoperative has been developed. The current research aims to be a rapid *ex-vivo* alternative to traditional histology based on H&E that needs staining and long waiting time to be diagnosed. The aim of the developed system is to take a biopsy sample and to quickly diagnose healthy and malignant tissues based on FF-PS-OCT phase images that are comparable in resolution to standard histology methods, and need not be stained.

4.3.1 Data collection

An *ex-vivo* experimental study was conducted in 12 subjects (4 healthy and 8 malignant tissues (cancerous tissues) of freshly excreted breast tissue over an area of 400 µm x 400 µm using the FF-PS-OCT system. Depending on the sampled tissue region, 8-10 images were taken from each subject. With the aid of the pathologist/doctor, the area of interest was selected. The phase images of the healthy and malignant breast tissue are shown in Figure 4.2 (a) and (b), respectively.

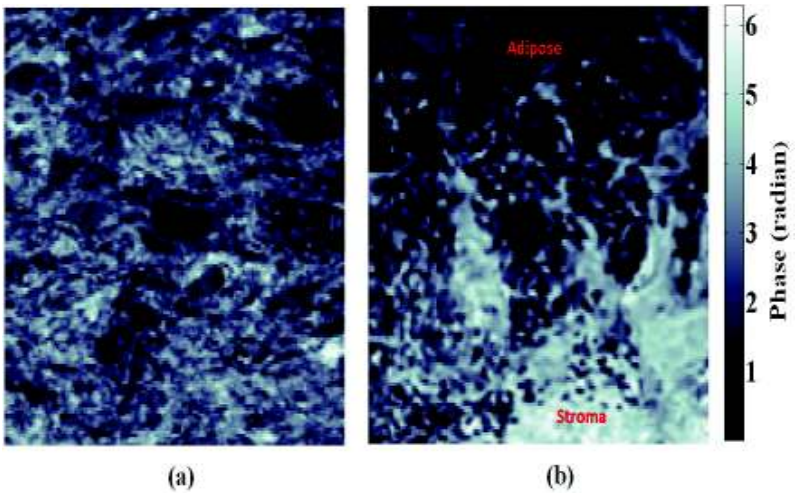

Figure 4.2 (a) Phase image of healthy fibro-adipose tissue and (b) cancer (invasive ductal carcinoma (IDC)) breast tissue.

4.3.2 Feature Extraction

The spatial phase shift distribution induced by a tissue distribution provides information on a set of optical tissue parameters: spatial mean phase, phase entropy, spatial phase standard deviations, spatial phase skewness and the spatial phase kurtosis of the statistical phase shift distribution within the tissue. Equations (5.5) to (5.9) have been used to estimate the respective features.

Spatial Mean Phase (Sφ): describes the mean phase value of the human breast tissue.

$$S_p(x,y) = \Delta\overline{\phi(x,y)} \tag{4.5}$$

where, x, y represents the no. of pixels of the phase image in horizontal and vertical direction.

Spatial Phase Entropy (S_E): describes the randomness of the human breast tissue.

$$S_E(x,y) = \sum_i^N \sum_j^M p(x_i\ y_j)\log_2 p(x_i\ y_j) \tag{4.6}$$

where, p is the probability of each phase value of the phase image, i^{th} and j^{th} are the pixels in the horizontal and vertical direction, N × M is the total no. of pixels.

Spatial Phase Standard Deviation (S_{std}): signifies the variations in the phase values of the human breast tissue.

$$S_{std}(x,y) = \frac{\sqrt{\sum_i^M \sum_j^N \left(\Delta\phi(x_i,y_j) - \overline{\Delta\phi(x,y)}\right)^2}}{n} \tag{4.7}$$

where, n is the number of images, $\Delta\phi(x,y)$ is the change in phase in radian in x and y-direction.

Spatial Phase Skewness (S_{sk}): measures the distribution of the phase values around the mean value and give its shape.

$$S_{sk}(x,y) = \frac{\sqrt{\sum_{i}^{M}\sum_{j}^{N}\left(\Delta\phi(x_i,y_j) - \overline{\Delta\phi(x_i,y_j)}\right)^3}}{S_{std}^3} \qquad (4.8)$$

Spatial Phase Kurtosis (S_{kur}): calculates from the histogram and extent upto the shape of the distribution equals to the normal distribution.

$$S_{kur}(x,y) = \frac{\sqrt{\sum_{i}^{M}\sum_{j}^{N}\left(\Delta\phi(x_i,y_j) - \overline{\Delta\phi(x_i,y_j)}\right)^4}}{S_{std}^4} \qquad (4.9)$$

The average values of all the features for both healthy and malignant breast tissue have been calculated and mentioned in table 4.1.

4.3.3 Machine Learning Classifier

A linear SVM classifier has been evaluated for the ability to distinguish healthy and cancerous types of tissues with spatial phase features derived from phase images of the breast. All features extracted from the field of interest of phase images are mentioned in table 5.1. These features have been used as vector predictors, whereas response variables represent healthy and malignant (precancerous and cancerous) tissue diagnostic outcomes.

4.4 RESULTS AND DISCUSSION

The most of the biological cells/tissues are transparent and so they present a minimal light absorption. Hence, a purely intensity-based method suffers from a low contrast. Phase imaging is based on endogenous refractive index contrast, which is invariant under experiment or instrument variations. Though, conventional OCT gives structural images of biological tissues, but in some cases while distinguishing between healthy and stroma and tumor (such as in case of IDC which have a low scattering) merely on the basis of the intensity image difficulty arises

due to poor contrast. However, these tissues have significant difference in the collagen content and organization. PS-OCT is capable of detecting these changes in the collagen content and enhances contrast over structural OCT images. Due to the highly aligned collagen content of the fibrous stroma, the tissue exhibits birefringence. Thus, the polarisation state of the incident light changes as it passes through tissue, leading to a clear change in the phase retardation. On the other hand, IDC destroys the natural organization of the collagen and results in significant reduction in tissues birefringence. Table 4.1 shows the mean values of all the features extracted from healthy and malignant human breast tissue. Malignant human breast tissue has a higher spatial mean phase value compared to the healthy one as shown in table 5.1, which attributes to the density of the tumor. Although, breast density is the distribution of glandular and fibrous tissues higher density is not unusual and is associated with a higher risk of cancer. The higher value of the entropy may be the tissue inhomogeneity because the entropy determines the complexity or irregularity of the image. The entropy of phase image is higher if the phase distribution of complex textures is not uniform, as shown in table 5.1 that malignant tissue has a higher entropy or randomness in phase as compare to healthy tissue. The standard phase deviation reflects the phase fluctuation in the field of interest. table 5.1 indicates a higher standard deviation value for the cancer cell, which may relate the higher deviation from the mean location of each pixel phase value. Phase kurtosis and skewness indicates smoothness in the phase value of the tissue, which is more prevalent in the healthy tissue compared to cancer. To evaluate all the quantitative phase features, a Tukey–Kramer test is carried out and p-value < 0.05 is considered as statistically significant, as shown in table 4.1. The sample is divided into two parts training and testing, 70% of the data sets were used for train the network while 30% to test the classifier. To asses the statistical significance of the extracted features, a statistical analysis considering a confidence interval of 95% and a hypothesis test were performed. Since the dataset is not normally distributed thus a non-parametric test, i.e., the Mann-Whitney U test has been conducted. The test yields a p-value <0.05 for all the extracted features, indicating a statically significant difference between them.

Table 4.1 Spatial phase features extracted from healthy and cancerous breast tissues with significant p-values.

Normalized Spatial Phase Features	Healthy Breast Tissue	Cancerous Breast Tissue	P-value
S_{φ}	0.33±0.09	0.37+0.11	0.013
S_{std}	0.14±0.5	0.2±0.4	<0.001
S_{E}	7.4±0.6	7.8±0.9	0.011
S_{kur}	2.12±0.5 3	3.01±0. 71	0.001
S_{sk}	0.32±0.01	0.38±0.02	<0.0001

The classifier is tested for sensitivity and specificity. A linear SVM classifier is trained to classify healthy and malignant breast tissue. 5-fold cross-validation is used to test the model robustness, with an average of 92.10 % sensitivity, 89.18% specificity, and with an average of area under curve (AUC) 0.93 for the training data set. 90.90 % sensitivity, 85.0% specificity and AUC 0.90 for testing data set as shown in the figure 4.3.

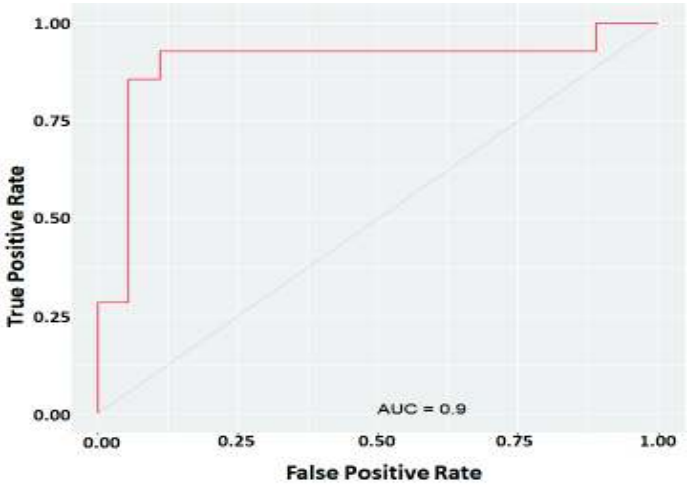

Figure 4.3 Receiver operating characteristic curve for testing data set.

The findings of the training and testing are focused on a small sample pool, and further evidence needs to be obtained.

4.5 CONCLUSIONS

FF-PS-OCT has been demonstrated to be an effective method to monitor tissue morphology changes caused by cancer. A number of optical parameters of the tissue obtained from their phase images is used to differentiate between healthy and malignant tissues with SVM classifier. The developed automated FF-PS-OCT system and classification algorithm based on machine learning will improve diagnosis and treatment efficiency. It provides a basis for further research into the automated medical diagnosis of tumors /cancer with spatial phase features. Future work will include the analysis of large number of freshly-exposed tissue samples and the real-time incorporation of machine learning/deep learning, so that the technology can be transferred from the lab to point of care environment.

CHAPTER 5
DIAGNOSIS OF MELANOMA SKIN CANCER USING MACHINE LEARNING APPROACH FOR DERMOSCOPIC IMAGES

5.1 BACKGROUND

Out of all types of cancers, skin cancer is considered as most spreading cause of death. Diagnosis of these diseases in early stages can cure a person and protect them from death. Malignant melanoma is considered as most harmful type of skin cancer and mutations is triggered by these cancerous cells that form malignant tumors by growth of the cells. The pre-processing, segmentation, feature extraction and classification are main steps of skin detection approaches. Mainly viral infection diseases such as Leprosy, Genetic diseases, melanoma skin cancer are most common types of skin diseases [144]. The motive behind this work is to develop a system that is able to detect skin cancer in early stage so that a person's life can be saved. In this work, a new system has been proposed in which the canny edge detector is applied on images of PH^2 dataset for edges detection and these images are smoothened using Gaussian filtration. After the pre-processing operations the features are extracted using Non-linear kernel ICA and further these features are then classified using Naive Bayes and Support Vector Machines. The proposed work has been analysed with existing techniques in terms of various parameters.

5.2 INTRODUCTION

In scientific community, cancer is considered an unavoidable issue as there is no as such specific treatment that is able to tackle this issue with 100% positive results. Although, various new techniques for its treatment has been innovated from science endeavours. In entire world, skin cancer is considered as most spreading cause of death [145]. If it is diagnosed in early stages, then it can be cured. So, early detection of skin cancer has become important due to increase in statistical foundation of skin cancer. People of various fields get attracted towards the early detection of skin cancer. Malignant melanoma is considered as most harmful type of skin cancer and mutations are triggered by these cancerous cells that form malignant tumors by growth of the cells. The melanocytes produced pigments in epidermis topmost layer are the origin of these skin cancers [146]. The exposure of skin in UV light cause melanoma cancer and most of it look like models, some are bigger in size as compared to models and of brown or black color along with red, blue, pink, white and purple colored skin. Squamous cell

carcinoma, melanoma and basal cell carcinoma are three most popular types of skin cancers and other most unusual types are dermatofibrosarcoma protuberance and merkel cell tumors. As like other types of cancer such as Basal Cell carcinoma, Melanoma and Squamous Cell carcinoma, a skin cancer is considered as one of the major diseases. This has been seen that the chances of sunburns from sun ultra-violet ray's increases in case of skin with lack of melanin. Then the skin cancer is formed by greater extent of sunburn [147] that can be identified by observing the size, texture, shape and color of the skin. The medical diagnosis and treatment comes in existence after the detection of melanoma or skin cancer using image processing techniques that helps in advance prevention of skin cancer.

For evaluation and quantification of findings in dermoscopy, an ABCD rule of dermoscopy is used along with it is used to classify the melanoma from benign lesions. First rule of ABCD is asymmetry that states the lesion slides are different from one another, Irregular or notched comes under border irregularity, C stands for color and color of melanomas is a mixture of white, dark brown, black, blue, light brown and D stands for diameter that means lesions larger than 6 mm is consider as cancerous. But in case of early detection, the size will be less than the 6 mm. Image acquisition, pre-processing, segmentation, feature extraction and classification are some of the steps performed to predict the type of skin cancer by considering various parameters that undergo different evaluations. The skin sore is evaluated using the above given steps and then they are arranged according to dangerous and generous [148]. For analysis of melanoma in early stages a number of researches have worked on all the real parameters so that legitimate treatment can be given to the patient.

5.3 MOTIVATION

Skin cancer is one of the most common cancers in human being that is hard to detect at early stage. Number of people are losing their lives due to skin cancer and its count is getting increased day by day. To save lives, there is a need to detect it as early as possible. There are various manual processes to diagnose it but its very time consuming and expensive. But, now with the advancement in Machine learning it proves to be helpful in various fields [149]. ML is about digesting big volumes of data and learning from that data in how to carry out a particular task, such as to differentiate melanoma and non-melanoma cells. ML in Cancer detection employs a variety of techniques to smartly handle large and complex volumes of information. It also excels at managing large and complex amounts of data. And its use in various areas to engrossed researchers for working on it improves the existing systems and it has been found that acceptable improvement is achieved in various areas of medical by using machine learning

in it. Due to this, its use in early detection of cancerous cells is easy and that's why a SVM, Naive Bayes like machine learning techniques has been introduced in this work.

5.4 RELATED WORK

This section of paper contains review on work done by researchers in skin disease detection using different classifiers. We have considered Support vector machine, K-nearest network, Convolution neural network and deep learning.

5.4.1 Skin cancer detection using different learning techniques

In histopathological images automated detection of cancerous tissue is not an easy task. So, for histopathological images a new pattern recognition method is proposed by Ammara Masood, et al. (2015), that is able to identify cancerous tissues [150]. In their work they have used both autoregressive parameters and intensity, wavelet based statistical features are used for feature selection which are based on differential evolution. This feature selection approach helps in reduction of dimensionality and then for selected features evaluation and images classification a support vector machine is used. The 150 histopathological images are used for training and testing purpose that comparative results give 89.1% of average diagnostic accuracy. Further for segmentation of lesion a K-means clustering is used by Suganya R, (2016) the shape, text and color features are extracted [151]. Various researchers have used number of classifiers for only melanoma or melanocytic skin lesion detection. But in their work Suganya R, have also classify other lesion like Nevus, Seborrheic keratosis, Melanoma and Basal cell carcinoma skin lesions that are classified using SVM. For testing purpose, the Dermweb collected dataset were used out of which a 220 MSLs and 100 No mSLs set of images are used and results show the better accuracy is achieved using it.

A new method has been proposed by F.K. Nezhadian et al. (2017) that is able to diagnose melanoma in early stages [152]. The dermoscopic images are classified into malignant and benign using proposed new algorithm by them. In initial stages colourful and texture components feature extraction and active counter model is used to segment the images. For the first time Farzam Kharaji Nezhadian, et.al, have also used texture based features for disease diagnosis that gives high efficiency. On testing the proposed method using SVM classifier an accuracy of 97% when tested it on international skin imaging collaboration dataset Muhammad Nasir et al. (2017), have done the classification of benign and melanoma skin lesions using a new method [153]. In their new proposed method, they have done pre-processing, lesion segmentation, features extraction, selection and classification. For pre-processing purpose, they have used DullRazor for hair removal and then lesion contrast is enhanced using color and

lesion texture information. The hybrid technique was used for lesion segmentation and then additive law of probability is used to fuse the results. The HOG, texture and color traits are fused after extracting it using serial based method then Boltzman Entropy method is used to select the fused features. In the last SVM is used to classify the selected features and for evaluation purpose a PH^2 dataset is used. The results achieved using proposed method are 97.7% of sensitivity, 97.5% of F-score, 96.7% of specificity and 97.5% of accuracy.

Due to increase in ultraviolet radiation there is rise in melanoma skin cancer and new cases are also being seen in darker skinned communities. It has been seen that if cancer is detected in early stage then there can be more chances of successful treatment on other hand the chances become low in later stages. To get better accuracy in classification of segmented skin lesions there is need of using good approaches for image pre-processing, segmentation and feature extraction. Suleiman Mustafa, et al. (2017), have worked on enhancing the accuracy of visualization for GrabCut segmentation by experimenting the colour space with luminance [154]. On the extracted corner and geometric features, an SVM machine learning technique is employed to produce good results. Suleiman Mustafa et al. (2018) worked on melanoma skin cancer identification utilising a proposed automated approach that was applied to images of affected skin regions [155]. Melanoma is the most serious type of skin cancer, yet like other cancers, it can be cured if caught early. It mostly affects the outside of the body, making it simple for skin specialists to identify by employing digital image processing in computer aided diagnostics. For detection purpose they have used ABCDEs rule. In their process firstly the input image is segmented into lesions of interest appeared to melanoma by GrabCut algorithm and afterward image processing techniques are used to extract geometry, color and shape features. These features were further classified using SVM with a Gaussian radial basis kernel into cancerous malignant and non-cancerous benign models. 200 images are used for evaluation purpose and only 6 features are enough for melanoma detection. Firstly, skin images are pre-processed in method used by Soniya Mane, et al. then image segmentation technique is used to segment the pre-processed lesion part [156]. Further from segmented lesion the unique features are extracted and classified it into normal skin and melanoma skin cancer using SVM. The use of SVM with linear kernel gives optimum accuracy.

5.4.2 Skin cancer detection using Machine Learning classifier

Ms. H. R. Mhaske et al. (2013) [157] employ SVM and a neural network as a classifier for the early diagnosis of Melanoma skin cancer. Image processing plays a vital part in the medical field, and the usage of melanoma skin cancer in humans is a dangerous and critical process.

Melanoma skin cancer can result in a person's death, so it's critical to catch it early. It is treatable and can save a person's life if it is detected in its early stages. Skin cancer is a cancer that affects the skin and is an extremely lethal form of cancer. The SIAscopy and Biopsy are two procedures for diagnosing skin cancer that are both time consuming and uncomfortable. So, Aswin. R. B., et al. (2014) proposed a less time-consuming, uncomfortable, and cost-effective Computer aided skin cancer screening method [158], which employs artificial intelligence and digital image processing. There is no direct touch with the skin in this procedure; instead, dermoscopic images are employed, which are segmented after going through image processing techniques. Further feature extraction techniques are used to extract unique features from images using Fray Level Co-occurrence Matrix and RGB color feature. Further these features are classified using ANN which is optimized by genetic algorithm to improve the classification accuracy. The evaluation of ANN method is done for pigmented and non-pigmented lesion segmentation by Andreea Udrea, et al. (2017) [159]. In their proposed method generative adversarial neural networks are used that is trained on large data set of images taken from smartphone cameras. According to evaluation a 92% of lesions from test set images are identified correctly. As discussed in previous papers there is very fast growth of melanoma skin cancer but people are not much aware about this kind of skin cancer. To have a productive treatment a vital role is played by early detection of melanoma skin tumor. In therapeutic domain an important role is played by image processing. Preeti Shahi, et al. (2018), have worked on gathered dermoscopy image database then perform pre-processing on it and used thresholding for segmentation [160]. Tamura, wavelet and GLCM is used for feature extraction and classified using K-nearest neighbors (KNN), ensemble, SVM and decision trees.

The main focus of Noel B. Linsangan et al. (2018), is to classify the skin cancer using geometric features of skin lesions [161]. The dermoscopy ABCD rule is used to extract the geometry features of skin lesion followed by their border, diameter and asymmetry parameters. For classification purpose they have used shortest, greatest diameter, perimeter, area, irregularity index, circulatory index and equivalent diameter parameters in dataset. The classification of benign melanoma, unknown and malignant melanoma is considered by them. The classification done using KNN gives accuracy of 90%. Due to the complicated structure of lesions, which makes it challenging to visually detect and classify skin lesions [162], Seetharani Murugaiyan Jaisakthi, et al. (2018) offer an automated skin lesion segmentation approach. Pre-processing and segmentation are two steps in their suggested method that can be employed as a pre-lesion classification step. They employ a filtering technique to remove rulers, hair, and light like sounds during pre-processing, and then the GrabCut segmentation algorithm to separate the skin lesions. A colour feature learned from training images, together

with the k-means clustering technique, is utilised to optimise the segment borders. The suggested method is tested using the ISIC 2017 challenge dataset and the PH² dataset, which have Dice coefficient values of 0.8236 and 0.9139, respectively.

5.4.3 Role of deep learning in Skin cancer detection

Pravda Jith Ray, et al. (2015), have worked on enhancing the histopathological images of skin by segmentation and classification [163]. The bilateral filtering and CLAHE algorithm is used by them for image enhancement. Then fuzzy c-means algorithm is used for initial segmentation and final segmentation is performed using local region recursive algorithm. To obtain region ellipticity they have used elliptical descriptor and melanocytes are distinguished from candidate nuclei regions using local pattern characteristics. Mobeen ur Rehman, et al. (2018), have used subsequent application of Convolution Neural Network (CNN) and segmentation on dermoscopy images in groundwork presented by them for skin lesions detection [164]. As a dataset they have used ISIC-2016 images and on the basis of individual channel intensity thresholding a skin lesions images are segmented. Further feature extraction part is done using CNN and classified using ANN classifier. The results of proposed work having accuracy of 98.32% are compared with existing best accuracy of 97%.

For segmentation of automatic skin lesion, a deep learning method is used by Rashika Mishra, et al. (2017), on subset of International Skin Imaging Collaboration (ISIC) Archive dataset that have dermoscopic along with lesion binary masks images provided by IEEE International Symposium on Biomedical Imaging (ISBI) 2017 challenge for Skin Lesion Analysis Towards Melanoma Detection [165]. Their results are compared with the results submitted by other participants that shows an improved results achieved by proposed method in terms of segmentation accuracy. Then Alper ARIK, et al. (2017), have also used deep learning methods for classification of skin lesions for melanoma detection [166]. From study it has been seen that use of deep learning is getting increased due to better results achieved using it in difficult computer vision tasks. So, a new hybrid method is proposed by Mohamed Attia, et al. (2017), in which they have used convolution and recurrent neural networks two most popular deep learning method [167]. 900 images are used for training the proposed method and 375 images are used for testing purpose. ISBI 2016 conference hosted Skin Lesion Analysis Toward Melanoma Detection challenge images are used as dataset. The proposed approach is evaluated that gives 98% of segmentation average accuracy with 93% of Jaccard index.

5.4.4 List of classifiers

This section covers the review on various classifiers used by researchers along with their purpose in improving the task of skin cancer detection.

Table 5.1 List of various classifiers used in skin cancer detection

Name of Classifier	Purpose
Support vector machine (SVM) [150]	For selected features evaluation and images classification
SVM [151]	Classification of lesion like Nevus, Seborrheic keratosis, Melanoma and Basal cell carcinoma skin lesions
SVM [152]	Diagnose melanoma in early stages
SVM with Gaussian radial basis kernel [153]	Classification of benign and melanoma skin lesions
Artificial Neural network optimized using Genetic algorithm [158]	Classification of Fray Level Co-occurrence and RGB color feature
Generative adversarial Neural Network [159]	For pigmented and non-pigmented lesion segmentation
SVM, k-Nearest Neighbors (KNN), decision trees and ensemble [160]	Feature extraction and classification
k-Nearest Neighbors (k-NN) algorithm [161]	The classification of benign melanoma, unknown and malignant melanoma
Fuzzy C-Means algorithm [160]	Initial segmentation and final segmentation
ANN and CNN classifier [164]	Segmentation on dermoscopy images in groundwork and classification
Deep learning method [165]	Classification of skin lesions for melanoma detection

5.5 RESULTS AND DISCUSSION

In this study, we have used two classifiers SVM and Naive Bayes along with non-linear kernel based ICA feature extraction approach and various methods for pre-processing task. This section will give the detail about the implementation and results obtained using proposed approach.

5.5.1 Research Methodology

In this work, a model has been proposed in which various algorithms has been used to improve the results for skin cancer detection. Firstly, the original skin cancer images are taken from PH^2 dataset that consist of 200 dermoscopic images along with corresponding medical annotations that comprised of 80 typical nevi, 80 common nevi and 40 malignant melanomas.

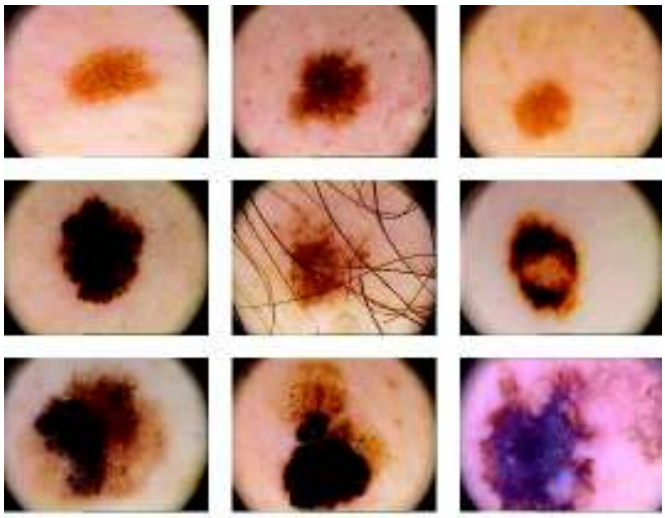

Figure 5.1 Images from PH^2 dataset

For pre-processing of images, it is firstly converted into gray images by gray scale conversion further the edges are detected using canny edge detector. The detection of edges gives more accurate data. The canny edge detector uses multi-stage algorithm for edges detection. For this purpose, it performs five steps in which first is noise reduction, gradient calculation, Non-maximum suppression, Double threshold forwarded with Edge tracking by hysteresis in the end. Furthermore, the output image comes after edges detection is smoothened out.

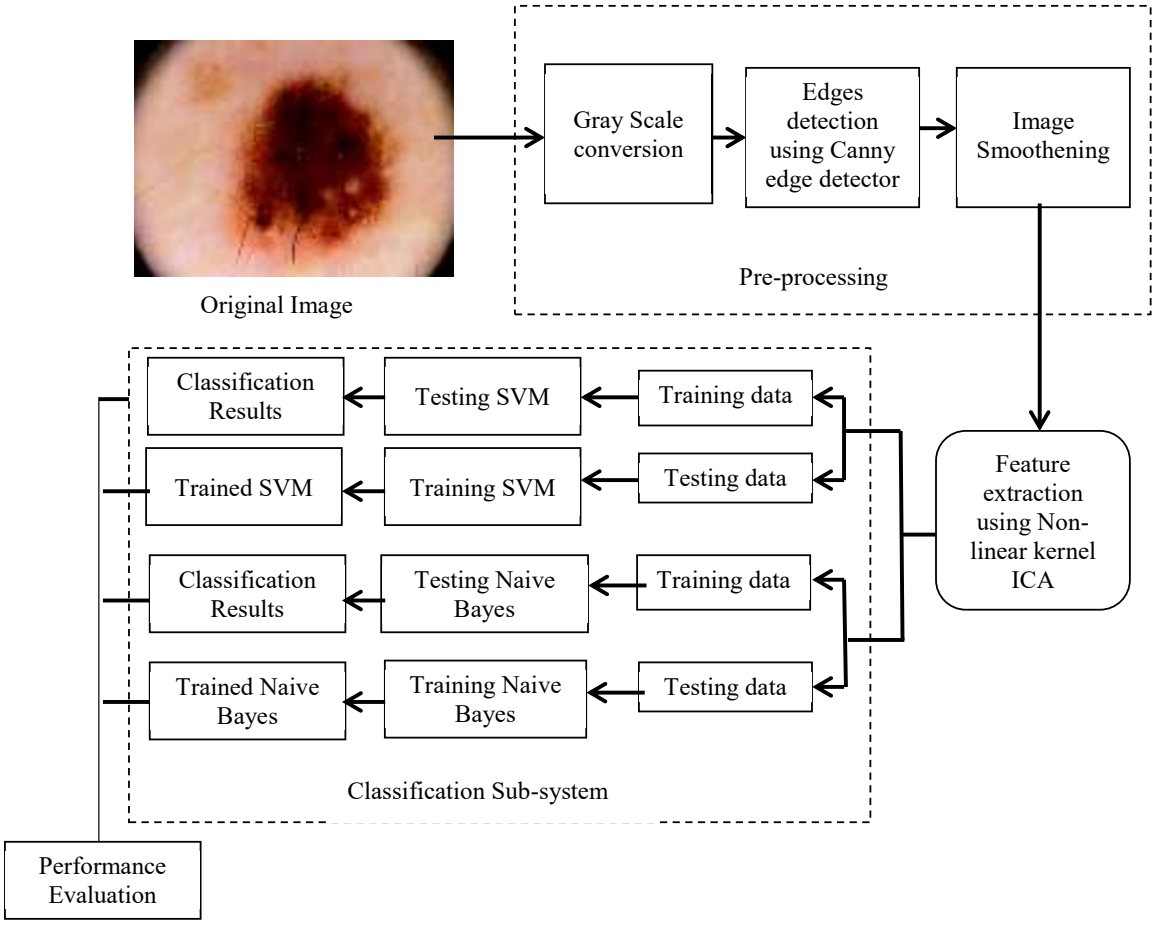

Figure 5.2 Proposed research methodology of skin cancer detection

Once the image is pre-processed by removal of unwanted data, it is passed through Non-linear kernel ICA for feature extraction. Kernel methods are a class of ML that mainly used for handling the non-linear problems that discover nonlinear patterns from the data and retain the computational elegance of matrix algebra [159, 160]. Due to this, it is mainly used in the feature extraction purpose. In this work, we have hybrid it with Independent component analysis (ICA) unsupervised learning that outputs a set of maximal independent component vectors. It takes input data as a mixture of independent components that identify one of them by deleting noisy components from it.

After the extraction part, the extracted features are used to train the system with the input as feature vector in an iterative manner. In this the image guided filter is also use to process the image using image guided filter that helps in detecting the region of interest. It uses content of a second image or guidance image to perform the edge-preserving smoothing on an image that influence the filtering. The guidance image can be an image itself that can be different version of the image or a completely different image. It is different from other image filtering by taking

corresponding spatial neighbourhood statistics of region in the guidance image when calculating the value of the output pixel.

In the end the classification is done using two different classifiers SVM and Naive Bayes separately. The SVM is a supervised ML algorithm that is used by various researchers for the operation of classification or regression [150, 173]. In this, each data item is plotted as a point in n-dimensional space in which the value of each feature is being the value of a particular coordinate. Furthermore, a hyperplane is drawn to differentiate the two classes. Other classifier used in this work is Naive Bayes that is a set of probabilistic classifiers which aim is to categorize the data after being processed and analysed. In this, an assumption is done that the specific feature value is independent from other feature value.

5.5.2 Simulation Outputs

In this work original colour skin image is taken from PH^2 dataset that is further converted into gray colour image. In this firstly the selected images are pre-processed using grayscale conversion and edges detection using canny edge detector the smoothen using Gaussian filtration.

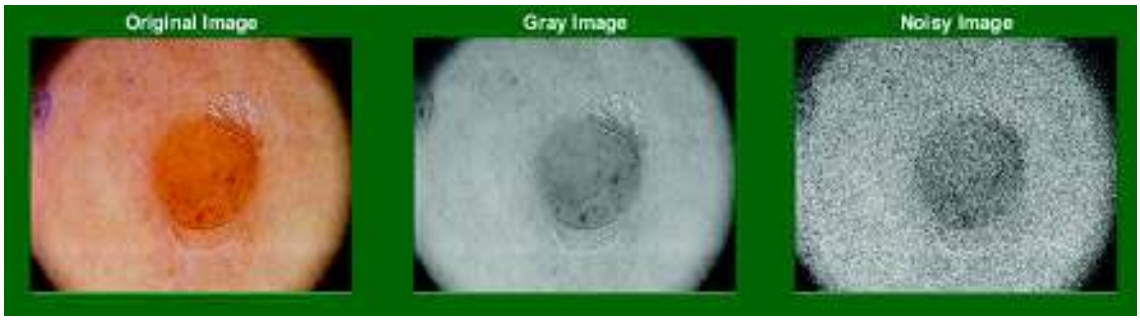

Figure 5.3 Original and pre-processed image

From the pre-processed image the required features are extracted using Non-linear kernel based ICA feature extraction approach. The motive behind using proposed approach is ability to tackle nonlinear algorithms for which it reduces the linear ones in some feature space S, which is related to the original input space in by a possibly nonlinear map *i*.

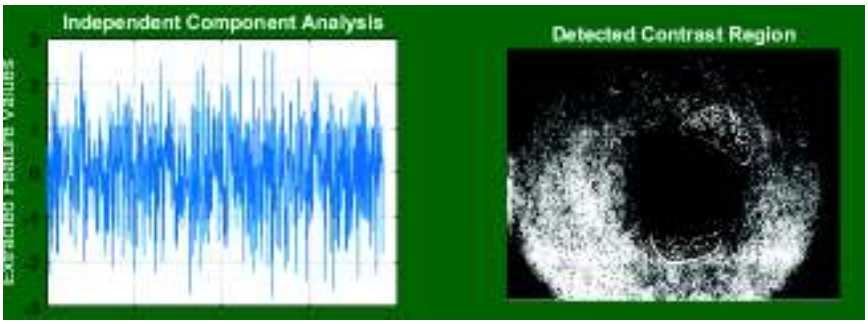

Figure 5.4 Detected contrast region after feature extraction

In this work, two classifiers SVM and Naive Bayes are used to test both of it individually. Classification of data is one of the most frequent decision making tasks performed by various researchers. In this the final decision is made about whether image contains skin cancer or not. Due to it, this step is very critical in decision making and getting the improved results. To make the classification about melanoma from benign lesion is firstly done using SVM. The motive behind using the SVM in this work is its advantage of giving good accuracy, work well in limited datasets and many more. It is mainly work by making hyperplane that define the boundaries for decision for distinguishing the classes.

Table 5.2 Result using Non-linear kernel ICA + SVM

Test Samples	**Accuracy (%)**	**Specificity (%)**	**Sensitivity (%)**
1	92.63	92.21	93.02
2	93.06	93.45	92.05
3	94.10	92.25	94.25
4	96.46	92.36	92.24
5	94.74	93.25	95.51
6	96.30	94.37	91.23
7	92.66	92.30	92.21
8	94.34	93.45	92.19
9	95.65	94.56	93.15
10	94.17	92.35	93.53

11	94.29	92.45	90.42
12	93.27	92.34	92.53
13	92.15	91.09	93.23
14	96.15	90.04	91.64
15	94.27	92.42	91.35
16	90.28	92.62	90.26
17	90.37	90.11	94.46
18	92.46	93.90	92.13
19	90.15	93.82	93.16
20	94.28	92.42	92.19

For testing purpose, we have taken 20 samples. In which 20 different images are taken from PH^2 dataset, then process it individually and given to SVM classifier after being pre-processed and feature extraction using Non-linear kernel based ICA.

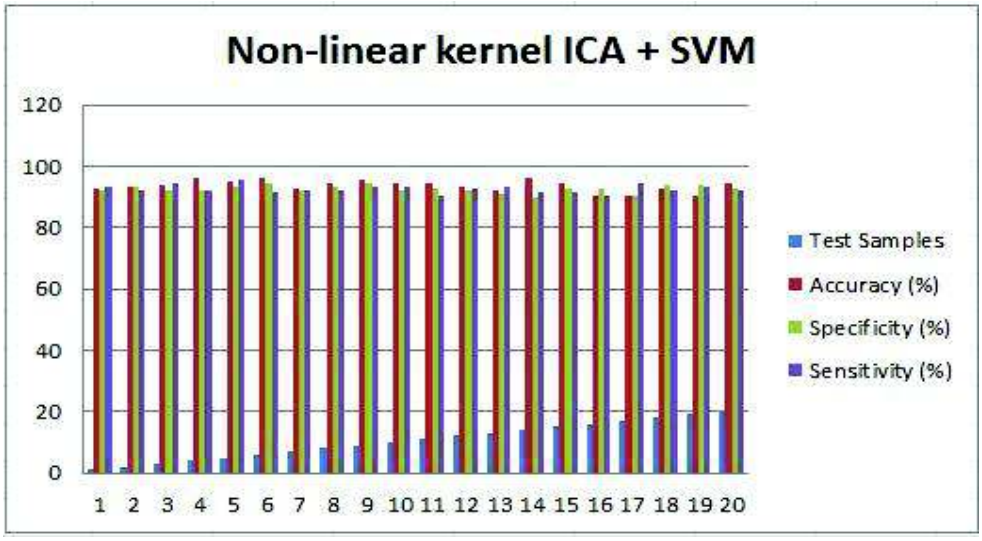

Figure 5.5 Non-linear kernel ICA + SVM results of various samples

The other classifier used for same work is Naive Bayes that is a statistical probabilistic classifier work under assumptions. It is one of the simplest type of supervised learning algorithms that is accurate, fast and reliable out of other algorithms. It is also proved to be best for large datasets in which it gives high accuracy. In this, an assumption has been taken that the effects of particular feature are independent of other features. Due to this assumption a computation gets simplified that is known as class conditional independence.

$$P(h|D) = \frac{P(D|h)(h)}{D} \qquad (5.1)$$

where, the P(h) is the probability of hypothesis being true regardless of data. P(D) is the probability of data regardless of the hypothesis, P(h/D) is the probability of hypothesis h given the data D and P(D/h) is the probability of data D given that hypothesis h was true.

Table 5.3 Results using Non-linear kernel ICA + Naive Bayes

Test Samples	**Accuracy (%)**	**Specificity (%)**	**Sensitivity (%)**
1	97.86	96.13	96.19
2	98.36	98.10	97.91
3	98.60	98.29	97.29
4	97.26	96.43	96.46
5	98.76	97.29	97.59
6	98.60	98.61	97.68
7	97.62	97.48	98.28
8	97.48	97.16	98.10
9	98.46	96.10	96.19
10	97.16	96.49	98.24
11	97.39	96.19	97.80
12	98.46	96.80	98.10
13	97.60	97.19	96.28

14	98.06	98.48	97.49
15	98.16	98.44	96.55
16	97.69	98.28	96.16
17	97.59	97.49	97.48
18	98.62	98.03	96.56
19	98.63	97.34	98.65
20	97.39	98.33	98.20

For testing purpose, we have taken 20 samples. In which 20 different images are taken from PH² dataset, then process it individually and given to Naive Bayes classifier after being pre-processed and feature extraction using Non-linear kernel based ICA.

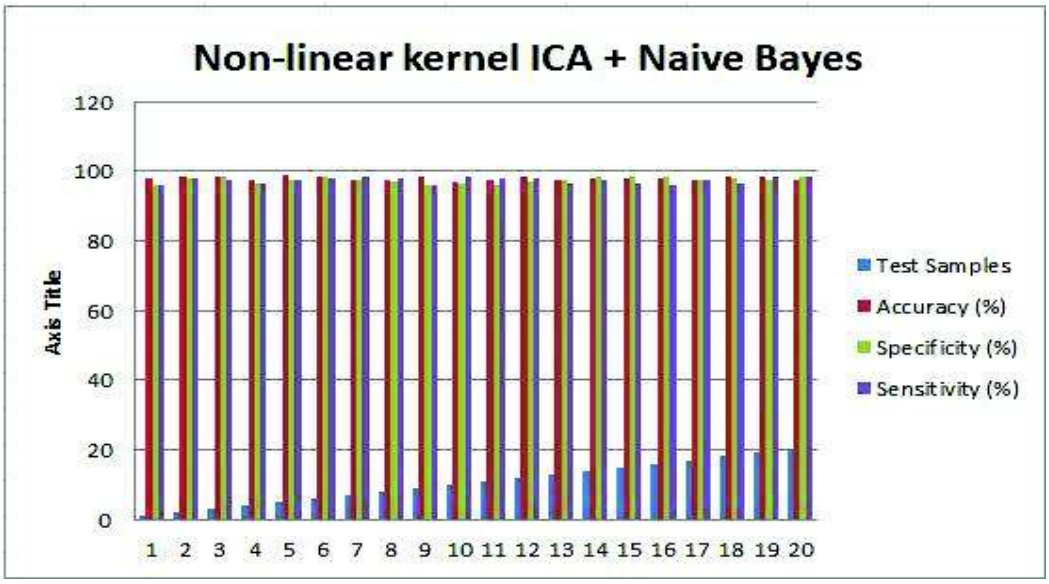

Figure 5.6 Non-linear kernel ICA + Naive Bayes results of various samples

5.6 EXPERIMENTAL RESULTS

The experiment results presented above using SVM and Naive Bayes classifier for various samples in terms of various parameters shows that both algorithms are able to detect skin cancer accurately. In this section, we have compared our best results with other existing algorithms used by different researchers for same work. The results given below shows that the new methods are superior with existing methods.

For performance evaluation purpose, we have firstly computed the confusion matrix name as True positive (TP), True Negative (TN), False positive (FP) and False Negative (FN). These are computed to compute the performance matrix Accuracy, Sensitivity and specificity.

$$Accuracy = \frac{TP+TN}{TP+TN+FP+FN} \quad (5.2)$$

$$Sensitivity = \frac{TP}{TP+FN} \quad (5.3)$$

$$Specificity = \frac{TN}{TN+FP} \quad (5.4)$$

Accuracy defined the ability to differentiate between melanoma and other cases correctly. Sensitivity defined the ability to determine the melanoma skin cancer detected patient correctly. The specificity defines the ability to determine non-melanoma or skin cancer patient correctly.

Table 5.4 Comparative analysis based upon different classification methods

Machine Learning Classifications	**Accuracy**	**Specificity**	**Sensitivity**
SRM [166]	67.66	87.57	10.35
Ostu [167]	65.18	70.64	52.21
SVM Linear Kernel Classifier [168]	90.47	90.90	90
PSO [169]	91.87	99.09	78.26
FCM [170]	93.39	95.17	88.80
JSEG [171]	89.47	97.14	71.08
ASLM [172]	89.66	97.22	80.24
VM with Gaussian radial basis function kernel [174]	96.8	89.3	95.40

Proposed Non-linear kernel ICA+SVM	96.15	94.37	91.23
Proposed Non-linear kernel ICA + Naive Bayes	98.63	98.33	98.20

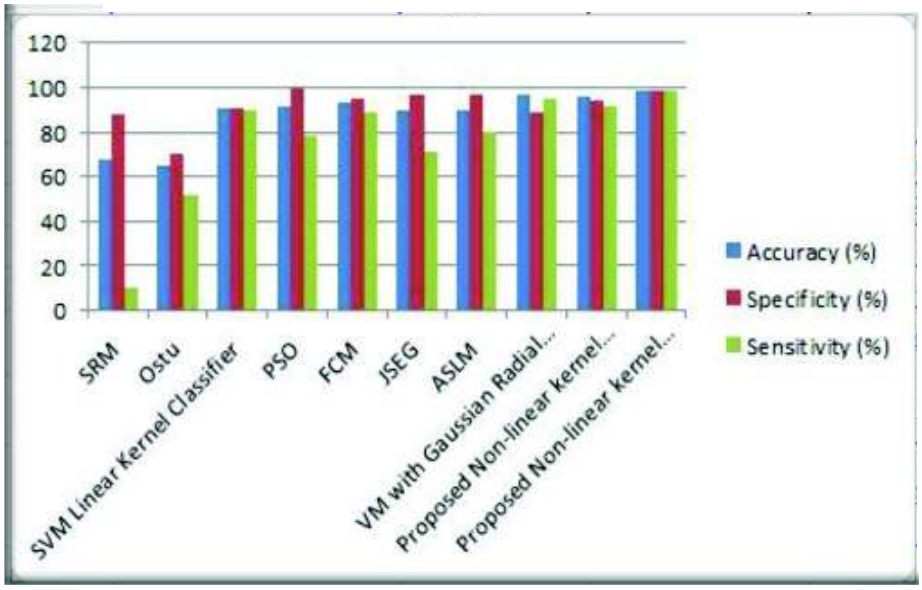

Figure 5.7 Comparative Results based upon different classification

The implementation work has been done in MATLAB software. The table 5.4 and figure 5.7 illustrate the results by various researchers along with results achieved using proposed approach in this work. The comparative results show that the use of proposed method by either using SVM and Naive Bayes gives better results than other existing ones. The classification performance gets improved after performing pre-processing and feature extraction using proposed approach. The accuracy achieved using SVM classifier on proposed approach is 96.15 which even get improved after passing the extracted features through Naive Bayes i.e., 98.63. In terms of specificity and sensitivity, results are 94.33, 98.33 and 91.23, 98.20 respectively for SVM and Naive Bayes classifier.

5.7 CONCLUSIONS

Skin cancer is the most common cause of death throughout the world. It is possible to cure it if it is detected early on. As a result of the growing statistical foundation of skin cancer, early detection has become critical. People from many walks of life are drawn to early detection of skin problems. According to the review, passing images via pre-processing before classification improves the outcomes. As a result, a new strategy to detect skin cancer has been developed in this study, which is more accurate than previous methods. For this project, the edges are recognised using a canny edge detector after the input PH^2 dataset image is transformed to gray images using gray scale conversion. Edge detection provides more precise data. For edge identification, the canny edge detector employs a multi-stage approach that is smoothed and run through a non-linear kernel-based ICA. Melanoma skin cancer is on the rise as a result of increased UV radiation, and new occurrences are now being detected in darker coloured communities. It has been shown that if cancer is found early on, the chances of a successful treatment increase; however, the chances decrease as the cancer progresses. Different researchers employ different classifiers to improve classification accuracy. The SVM and the Naive Bayes classifier were employed, which produced accurate results than previous approaches.

CHAPTER 6

CONCLUSIONS AND FUTURE SCOPE

6.1 CONCLUSIONS

The work presented in this thesis describes the different methods used for the investigation of human tissues (healthy/unhealthy) using dermoscopy and OCT images. The state of the tissue has been characterized by measuring different spatial phase features such as spatial mean phase, spatial phase standard deviation, spatial phase entropy, spatial phase skewness and spatial phase kurtosis. These parameters are very much helpful in the investigation of human breast tissue. In addition, a machine learning based classifier such as SVM and pre-trained models like Inception-V3 and ResNet50 has been used for automatic tissue characterization. The SVM classifier was trained with quantitative phase images-based features for an automated classification between healthy and unhealthy breast tissue in terms of high accuracy, sensitivity and specificity. FF-PS-OCT has been demonstrated to be an effective method to monitor tissue morphology changes caused by cancer.

First, in the suggested work, the medical images of the skin are analyzed for melanoma skin cancer classification. ResNet50, a residual neural network with deep features, is utilized with a variety of classifiers including SVM, LIBSVM, and Neural Network. The outcomes of data augmentation utilizing Generative Adversarial Networks are compared to the results of fundamental data augmentation methods like rotation, translation, and shearing. The integration of ResNet50 for feature extraction, data augmentation of skin cancer images with GAN, and classification using NN, SVM, and LIBSVM is offered as an efficient approach. The studies are carried out on the MED-NODE dataset, with images categorized as melanoma and nevus. On performing data augmentation with GAN, the greatest accuracy achieved was 96 % using a combination of ResNet50 and NN as the machine learning classifier, which is better than many existing research.

In the next part of this thesis, the study was done on breast tissue samples using the OCT images. The GAN-CNN based intelligent system was used for the automatic classification of the breast cancer. The GAN (DCGAN) is utilised in this network to produce synthetic datasets and then use these synthetic datasets to increase the quantity of information in order to improve the CNN's (Inception-V3) classification performance. A small set of OCT images of breast tissue is used to demonstrate our method. Based on the test datasets, the classification performance of our method employing only the classic data increase gave a sensitivity level of

93.6 %, 90.8 % specificity, and 91.7% accuracy. The accuracy of the training datasets increased to 93.7 % from 92.0 % when the synthetic data was added.

Further, in the next part of the thesis, OCT measurements are used to automatically identify malignant breast tissues using robust machine learning. A high-resolution automated full field polarisation sensitive optical coherence tomography (FF-PS-OCT) system was created in this study to distinguish healthy and malignant human breast tissue in ex vivo using quantitative phase information. The FF-PS-OCT technology was used to image 12 breast tissue samples (4 healthy, 8 malignant (cancerous), and distinct phase features were derived from the collected OCT images (106 B-scan images), based on the differences in the optical signatures of the healthy and malignant tissues. With 75 images, a linear support vector model classifier was trained, yielding a sensitivity of 92.10 % and a specificity of 89.18 %. The model was tested with 31 images, yielding a sensitivity of 90.90 % and a specificity of 85.0 %.

In the last part, a new system has been proposed in which the canny edge detector is applied on images of PH^2 dataset for edges detection and these images are smoothened using Gaussian filtration. After the pre-processing operations the features are extracted using Non-linear kernel ICA and further these features are then classified using Naive Bayes and Support Vector Machines. The proposed work has been analysed with existing techniques in terms of various parameters. The comparative results show that the use of proposed method by either using SVM and Naïve Bayes gives better results than other existing ones. The accuracy achieved using SVM classifier on proposed approach is 96.15 which even get improved after passing the extracted features through Naïve Bayes i.e., 98.63. In terms of specificity and sensitivity, results are 94.33, 98.33 and 91.23, 98.20 respectively for SVM and Naïve Bayes classifiers.

6.2 FUTURE SCOPE

The goal of this research is to create a machine learning-based model for automatic tissue analysis and to learn about the factors that influence tissue qualities. This is a significant achievement; as machine learning has grown in popularity in the research community. Computational imaging clearly has a superior role to play in the quantitative characterization of various tissue samples. Because it can analyse data automatically, it is more accurate and faster than manual analysis. Work on the creation of novel methods involving molecular measurements for enhanced tissue characterization can be done in the future. Although our study has significant promise in the medical area, we think that our technique can be used as a criterion for deciding whether or not tissue samples should be diagnosed.

In addition, we plan to use the knowledge gained from my thesis work to categorise various biological and industrial applications. Based on the results, we expect that our proposed method in chapter 2 can be used to examine the severity and different phases of the skin cancer with the large number of samples. It can be useful for other skin cancer studies such as squamous cell carcinoma and basal cell carcinoma including the variation in shape and diameter of skin tissue.

In future, the algorithm developed in chapter 3 can be used with different CNN architectures such as AlexNet, VGGNet and DenseNet etc. in order to measure the performance of the network. This machine learning model of GAN-CNN architecture can detect other tissue abnormalities such as bladder cancer, skin cancer etc. In Chapter 4, the classifier has improved performance measures for breast cancer identification, which will aid in performing a more precise biopsy or intraoperative margin evaluation. For the prediction and classification of normal and malignant cells, our suggested approach does not require any expertise. In clinical pathology labs, assessment of margins of various biological samples can be done and we can identify the area of insalubrious tissue using the CNN model, making it a viable technique for intraoperative applications.

Our recommended classifier, which is based on extracted characteristics from OCT images, will assist clinicians in distinguishing between healthy and diseased tissue and outperforms the previously published OCT image-based classifier. Our proposed method will provide the promising results and will be helpful to the clinician or surgeon to monitor the individual patient's health progress and success of therapy by automatically extracting the hidden image information.

REFERENCES

[1] R. Naga Swetha, "Review on Animal Tissues", *Res. and Rev. J. Zoolog. Sci.*, pp. 101-107, 2016.

[2] L. Hinck and I. Näthke, "Changes in cell and tissue organization in cancer of the breast and colon," *Curr. Opin. Cell Biol.*, vol. 26, pp. 87–95, 2014.

[3] A. Rastogi, "Changing role of histopathology in the diagnosis and management of hepatocellular carcinoma," *World J. Gastroenterol*., vol. 24, no. 35, pp. 4000–4013, 2018.

[4] R. García-Figueiras *et al.*, "How clinical imaging can assess cancer biology," *Insights Imaging*, vol. 10, no. 1, p. 28, 2019.

[5] N.C. Purandare and V. Rangarajan, "Imaging of lung cancer: Implications on staging and management," *Indian J. Radiol. Imaging*, vol. 25, no. 2, pp. 109–120, 2015.

[6] S.N. Kumar, A. Lenin Fred, P. Padmanabhan, B. Gulyas, H. Ajay Kumar, and L.R. Jonisha Miriam, "Deep learning algorithms in medical image processing for cancer diagnosis: Overview, challenges and future," in *Studies in Computational Intelligence*, Singapore: Springer Singapore, 2021, pp. 37–66.

[7] A. P. James and B. V. Dasarathy, "Medical image fusion: A survey of the state of the art," *Inf. Fusion*, vol. 19, pp. 4–19, 2014.

[8] R. M. Kelly, P. Doyle, J. Bennett, P. McKavanagh, P. Donnelly, and P. A. Ball, "Re.: Radiation-reduction strategies in cardiac computed tomographic angiography," *Clin. Radiol*., vol. 66, no. 5, pp. 485–486, 2011.

[9] Alamy Limited, "Own the blank page," *Alamy*. [Online]. Available: https://www.alamy.com/. [Accessed: 18-Apr-2022].

[10] O. Bawazir and E. Banoon, "Efficacy and clinical outcome of the port-a-cath in children: a tertiary care-center experience," *World J. Surg. Oncol*., vol. 18, no. 1, p. 134, 2020.

[11] B. J. Erickson and C. R. Jack Jr, "Correlation of single photon emission CT with MR image data using fiduciary markers," *AJNR Am. J. Neuroradiol*., vol. 14, no. 3, pp. 713–720, 1993.

[12] A. Agrawal, A. Bhake and S. Singhal, "Metastases as the Initial Manifestation of Lung Cancer and Negative Fiberoptic Endobronchial Brush Cytology and Biopsy," *Indian J. of Clin. Practice*, vol. 20, no. 2, pp. 167-169, 2009.

[13] H. Rahbar and S. C. Partridge, "Multiparametric MR imaging of breast cancer," *Magn. Reson. Imaging Clin. N. Am.*, vol. 24, no. 1, pp. 223–238, 2016.

[14] R. Banerjee *et al.*, "Multiparametric magnetic resonance for the non-invasive diagnosis of liver disease," *J. Hepatol*., vol. 60, no. 1, pp. 69–77, 2014.

[15] B. Kim, H. Kim, S. Kim, and Y.-R. Hwang, “A brief review of non-invasive brain imaging technologies and the near-infrared optical bioimaging,” *Appl. Microsc*., vol. 51, no. 1, p. 9, 2021.

[16] P. N. T. Wells and H.-D. Liang, “Medical ultrasound: imaging of soft tissue strain and elasticity,” *J. R. Soc. Interface*, vol. 8, no. 64, pp. 1521–1549, 2011.

[17] A. S. Saad, “Simultaneous speckle reduction and contrast enhancement for ultrasound images: Wavelet versus Laplacian pyramid,” *Pattern Recognit. Image Anal.*, vol. 18, no. 1, pp. 63–70, 2008.

[18] A. Sarvazyan *et al.*, “Overview of elastography- an emerging branch of medical imaging,” *Curr. Medi. Imaging Reviews*., vol. 7, no. 4, pp. 255–282, 2011.

[19] “Elastography - CACTUS lab - UT southwestern, Dallas, TX,” *Utsouthwestern.edu*. [Online]. Available: https://www.utsouthwestern.edu/labs/cactus/clinical/elasto.html. [Accessed: 19-Apr- 2022].

[20] F. Kharfi, “Principles and applications of nuclear medical imaging: A survey on recent developments,” in *Imaging and Radioanalytical Techniques in Interdisciplinary Research - Fundamentals and Cutting Edge Applications*, InTech, 2013.

[21] “Nuclear medicine,” *Regional Medical Imaging | Medical Imaging in Southeast MI*, 24-May-2017. [Online]. Available: https://www.rmipc.net/services/nuclear-medicine. [Accessed: 19-Apr-2022].

[22] W.W. Liu and P.C. Li, “Photoacoustic imaging of cells in a three-dimensional microenvironment,” *J. Biomed. Sci.*, vol. 27, no. 1, p. 3, 2020.

[23] Rao, Bokde, and Sinha, “Photoacoustic imaging for management of breast cancer: A literature review and future perspectives,” *Appl. Sci. (Basel)*, vol. 10, no. 3, p. 767, 2020.

[24] A. Rampun, Z. Chen, P. Malcolm, B. Tiddeman, and R. Zwiggelaar, “Computer-aided diagnosis: detection and localization of prostate cancer within the peripheral zone: Computer-aided diagnosis: detection and localization of prostate cancer within the peripheral zone,” *Int. j. numer. method. biomed. eng.*, vol. 32, no. 5, p. e02745, 2016.

[25] S. Choi, T. Watanabe, T. Suzuki, F. Nin, H. Hibino, and O. Sasaki, “Multifrequency swept common-path en-face OCT for wide-field measurement of interior surface vibrations in thick biological tissues,” *Opt. Express*, vol. 23, no. 16, pp. 21078–21089, 2015.

[26] R. P. Singh-Moon, C. C. Marboe, and C. P. Hendon, “Near-infrared spectroscopy integrated catheter for characterization of myocardial tissues: preliminary demonstrations to radiofrequency ablation therapy for atrial fibrillation,” *Biomed. Opt. Express*, vol. 6, no. 7, pp. 2494–2511, 2015.

[27] A. P. Gibson, J. C. Hebden, and S. R. Arridge, “Recent advances in diffuse optical imaging,” *Phys. Med. Biol.*, vol. 50, no. 4, pp. R1-43, 2005.

[28] Z. Hu, Kellogg Eye Center, Department of Ophthalmology and Visual Sciences, University of Michigan, Ann Arbor, MI, United States of America, Q. Liu, and Y. M. Paulus, “New Frontiers in Retinal Imaging: Hu Z et al. New imaging retina,” *Int. j. ophthalmic res.*, vol. 2, no. 3, pp. 148–158, 2016.

[29] “Breast cancer - statistics,” *Cancer.Net*, 25-Jun-2012. [Online]. Available: https://www.cancer.net/cancer-types/breast-cancer/statistics. [Accessed: 20-Apr-2022].

[30] M. K. Gupta and A. Kaur, “Introduction to skin cancer: A review,” *J. Pharm. Res. Int*., pp. 2275–2281, 2021.

[31] J. Kato, K. Horimoto, S. Sato, T. Minowa, and H. Uhara, “Dermoscopy of melanoma and non-melanoma skin cancers,” *Front. Med. (Lausanne)*, vol. 6, p. 180, 2019.

[32] “Cancer,” *Who.int*. [Online]. Available: https://www.who.int/health-topics/cancer. [Accessed: 20-Apr-2022].

[33] “Cancer today,” *Iarc.fr*. [Online]. Available: https://gco.iarc.fr/today/online-analysis-multi-bars [Accessed: 20-Apr-2022].

[34] A. Anuranjeeta, K. K. Shukla, A. Tiwari, and S. Sharma, “Classification of histopathological images of breast cancerous and non cancerous cells based on morphological features,” *Biomed. Pharmacol. J.*, vol. 10, no. 1, pp. 353–366, 2017.

[35] “Breast Cancer,” *Cleveland Clinic*. [Online]. Available: https://my.clevelandclinic.org/health/diseases/3986-breast-cancer. [Accessed: 20-Apr-2022].

[36] S. Chatterjee, “Artefacts in histopathology,” *J. Oral Maxillofac. Pathol*., vol. 18, no. Suppl 1, pp. S111-6, 2014.

[37] P. H. Tomlins and R. K. Wang, “Theory, developments and applications of optical coherence tomography,” *J. Phys. D Appl. Phys.*, vol. 38, no. 15, pp. 2519–2535, 2005.

[38] M. Carlsson, P. C. Ursell, D. Saloner, and M. Saeed, “Multidetector computed tomography for characterization of calcium deposits in reperfused myocardial infarction,” *Acta Radiol*., vol. 50, no. 4, pp. 396–405, 2009.

[39] A. M. Zysk, F. T. Nguyen, A. L. Oldenburg, D. L. Marks, and S. A. Boppart, “Optical coherence tomography: a review of clinical development from bench to bedside,” *J. Biomed. Opt*., vol. 12, no. 5, p. 051403, 2007.

[40] A. F. Fercher, C. K. Hitzenberger, G. Kamp, and S. Y. El-Zaiat, “Measurement of intraocular distances by backscattering spectral interferometry,” *Opt. Commun.,* vol. 117, no. 1–2, pp. 43–48, 1995.

[41] S. Saxena, S. Sharma, and N. Sharma, “Parallel image processing techniques, benefits and limitations,” *Res. J. Appl. Sci. Eng. Technol*., vol. 12, no. 2, pp. 223–238, 2016.

[42] P. Senthilkumaran, “Optical phase singularities in detection of laser beam collimation,” *Appl. Opt.*, vol. 42, no. 31, pp. 6314–6320, 2003.

[43] T. Durduran, R. Choe, W. B. Baker, and A. G. Yodh, “Diffuse optics for tissue monitoring and tomography,” *Rep. Prog. Phys*., vol. 73, no. 7, p. 076701, 2010.

[44] M. Ulrich *et al.*, “The sensitivity and specificity of optical coherence tomography for the assisted diagnosis of non pigmented basal cell carcinoma: an observational study,” *Br. J. Dermatol*., vol. 173, no. 2, pp. 428–435, 2015.

[45] B. H. Lee, “Basic principle and various applications of optical coherence tomography (OCT),” *Phys. High Technol*., vol. 26, no. 3, pp. 2–6, 2017.

[46] O. F.y *et al.*, “Supervised machine learning algorithms: Classification and comparison,” *Int. j. comput. trends technol*., vol. 48, no. 3, pp. 128–138, 2017.

[47] A. S. Lundervold and A. Lundervold, “An overview of deep learning in medical imaging focusing on MRI,” *Z. Med. Phys*., vol. 29, no. 2, pp. 102–127, 2019.

[48] G. Montavon, W. Samek, and K.-R. Müller, “Methods for interpreting and understanding deep neural networks,” *Digit. Signal Process*., vol. 73, pp. 1–15, 2018.

[49] J. Zimmermann *et al.*, “Deep neural networks for classifying complex features in diffraction images,” *Phys. Rev. E*., vol. 99, no. 6–1, p. 063309, 2019.

[50] W. Rawat and Z. Wang, “Deep convolutional neural networks for image classification: A comprehensive review,” Neural Comput., vol. 29, no. 9, pp. 2352–2449, 2017.

[51] R. Yamashita, M. Nishio, R. K. G. Do, and K. Togashi, “Convolutional neural networks: an overview and application in radiology,” *Insights Imaging*, vol. 9, no. 4, pp. 611–629, 2018.

[52] J. Dheeba, N. Albert Singh, and S. Tamil Selvi, “Computer-aided detection of breast cancer on mammograms: a swarm intelligence optimized wavelet neural network approach,” *J. Biomed. Inform*., vol. 49, pp. 45–52, 2014.

[53] A.S. Ahuja, “The impact of artificial intelligence in medicine on the future role of the physician,” *PeerJ*, vol. 7, p. e7702, 2019.

[54] J. Singh and A. S. Arora, “Automated approaches for ROIs extraction in medical thermography: a review and future directions,” *Multimed. Tools Appl.*, vol. 79, no. 21–22, pp. 15273–15296, 2020.

[55] Z. Lai and H. Deng, “Medical image classification based on deep features extracted by deep model and statistic feature fusion with multilayer perceptron,” *Comput. Intell. Neurosci*., vol. 2018, p. 2061516, 2018.

[56] C. Shorten and T. M. Khoshgoftaar, “A survey on image data augmentation for deep learning,” *J. Big Data*, vol. 6, no. 1, 2019.

[57] J. Shijie, W. Ping, J. Peiyi, and H. Siping, “Research on data augmentation for image classification based on convolution neural networks,” in *2017 Chinese Automation Congress (CAC)*, 2017.

[58] Karthika. and M. Durgadevi, “Generative Adversarial Network (GAN): a general review on different variants of GAN and applications,” in *2021 6th International Conference on Communication and Electronics Systems (ICCES)*, 2021.

[59] G. Argenziano and H. P. Soyer, “Dermoscopy of pigmented skin lesions--a valuable tool for early diagnosis of melanoma,” *Lancet Oncol*., vol. 2, no. 7, pp. 443–449, 2001.

[60] Y. LeCun, Y. Bengio, and G. Hinton, “Deep learning,” *Nature*, vol. 521, no. 7553, pp. 436–444, 2015.

[61] A. Esteva *et al.*, “Dermatologist-level classification of skin cancer with deep neural networks,” *Nature*, vol. 542, no. 7639, pp. 115–118, 2017.

[62] N. Codella, J. Cai, M. Abedini, R. Garnavi, A. Halpern, and J. R. Smith, “Deep learning, sparse coding, and SVM for melanoma recognition in dermoscopy images,” *in Machine Learning in Medical Imaging*, Cham: Springer International Publishing, 2015, pp. 118–126.

[63] K. He, X. Zhang, S. Ren, and J. Sun, “Deep residual learning for image recognition,” in *2016 IEEE Conference on Computer Vision and Pattern Recognition (CVPR)*, 2016.

[64] S. Guo and Z. Yang, “Multi-Channel-ResNet: An integration framework towards skin lesion analysis,” *Inform. Med. Unlocked*, vol. 12, pp. 67–74, 2018.

[65] A.-R. A. Ali and T. M. Deserno, “A systematic review of automated melanoma detection in dermatoscopic images and its ground truth data,” in *Medical Imaging 2012: Image Perception, Observer Performance, and Technology Assessment*, 2012.

[66] R. B. Oliveira, J. P. Papa, A. S. Pereira, and J. M. R. S. Tavares, “Computational methods for pigmented skin lesion classification in images: review and future trends,” *Neural Comput. Appl*., vol. 29, no. 3, pp. 613–636, 2018.

[67] T.J. Brinker *et al.*, “Skin cancer classification using convolutional neural networks: Systematic review,” *J. Med. Internet Res*., vol. 20, no. 10, p. e11936, 2018.

[68] E. Nasr-Esfahani *et al.*, “Melanoma detection by analysis of clinical images using convolutional neural network,” *Annu Int Conf IEEE Eng Med Biol Soc*, vol. 2016, pp. 1373–1376, 2016.

[69] D. Gutman *et al.*, "Skin lesion analysis toward melanoma detection: A challenge at the international symposium on biomedical imaging (ISBI) 2016, hosted by the international skin imaging collaboration (ISIC)," *arXiv [cs.CV]*, 2016.

[70] M. A. Marchetti *et al.*, "Results of the 2016 International Skin Imaging Collaboration International Symposium on Biomedical Imaging challenge: Comparison of the accuracy of computer algorithms to dermatologists for the diagnosis of melanoma from dermoscopic images," *J. Am. Acad. Dermatol*., vol. 78, no. 2, pp. 270-277.e1, 2018.

[71] J. Kawahara and G. Hamarneh, "Multi-resolution-tract CNN with hybrid pretrained and skin-lesion trained layers," in *Machine Learning in Medical Imaging*, Cham: Springer International Publishing, 2016, pp. 164–171.

[72] V. Pomponiu, H. Nejati, and N.-M. Cheung, "Deepmole: Deep neural networks for skin mole lesion classification," in *2016 IEEE International Conference on Image Processing (ICIP)*, 2016.

[73] A. Menegola, M. Fornaciali, R. Pires, F.V. Bittencourt, S. Avila, and E. Valle, "Knowledge transfer for melanoma screening with deep learning," in *2017 IEEE 14th International Symposium on Biomedical Imaging (ISBI 2017)*, 2017.

[74] A. Romero-Lopez, X. Giro-i-Nieto, J. Burdick, and O. Marques, "Skin lesion classification from dermoscopic images using deep learning techniques," in *Biomedical Engineering*, 2017.

[75] H. A. Haenssle *et al.*, "Man against machine: diagnostic performance of a deep learning convolutional neural network for dermoscopic melanoma recognition in comparison to 58 dermatologists," *Ann. Oncol*., vol. 29, no. 8, pp. 1836–1842, 2018.

[76] L. Bi, J. Kim, E. Ahn, and D. Feng, "Automatic skin lesion analysis using large-scale dermoscopy images and deep residual networks," *arXiv [cs.CV]*, 2017.

[77] I. Giotis, N. Molders, S. Land, M. Biehl, M. F. Jonkman, and N. Petkov, "MED-NODE: A computer-assisted melanoma diagnosis system using non-dermoscopic images," *Expert Syst. Appl.*, vol. 42, no. 19, pp. 6578–6585, 2015.

[78] I. Goodfellow *et al.*, "Generative adversarial nets," In *Advances in neural information processing systems*", pp. 2672-2680 (2014).

[79] D. Yorioka, H. Kang, and K. Iwamura, "Data augmentation for deep learning using generative adversarial networks," in *2020 IEEE 9th Global Conference on Consumer Electronics (GCCE)*, 2020.

[80] N. N. Sultana, B. Mandal, and N. B. Puhan, "Deep residual network with regularised fisher framework for detection of melanoma," *IET Comput. Vis*., vol. 12, no. 8, pp. 1096–1104, 2018.

[81] S. Demyanov, R. Chakravorty, M. Abedini, A. Halpern, and R. Garnavi, "Classification of dermoscopy patterns using deep convolutional neural networks," in *2016 IEEE 13th International Symposium on Biomedical Imaging (ISBI)*, 2016.

[82] S. S. Han, M. S. Kim, W. Lim, G. H. Park, I. Park, and S. E. Chang, "Classification of the clinical images for benign and malignant cutaneous tumors using a deep learning algorithm," *J. Invest. Dermatol.*, vol. 138, no. 7, pp. 1529–1538, 2018.

[83] *Who.int.* [Online]. Available: http://www.who.int/en/). [Accessed: 18-Apr-2022].

[84] A. Patel *et al*., "Low-dose abiraterone in metastatic prostate cancer: Is it practice changing? Facts and facets," *JCO Glob Oncol*, vol. 6, no. 6, pp. 382–386, 2020.

[85] R. K. Samala, H.-P. Chan, L. Hadjiiski, M. A. Helvie, J. Wei, and K. Cha, "Mass detection in digital breast tomosynthesis: Deep convolutional neural network with transfer learning from mammography: DBT mass detection using deep convolutional neural network," *Med. Phys.*, vol. 43, no. 12, pp. 6654–6666, 2016.

[86] S. A. Feig, "Factors contributing to mammography failure in women aged 40–49 years," *Breast Dis. Year B. Q.*, vol. 16, no. 4, pp. 323–324, 2006.

[87] G. M. Rauch, B. E. Dogan, T. B. Smith, P. Liu, and W. T. Yang, "Outcome analysis of 9-gauge MRI-guided vacuum-assisted core needle breast biopsies," *AJR Am. J. Roentgenol*., vol. 198, no. 2, pp. 292–299, 2012.

[88] C. Meeuwis *et al.*, "MR-guided breast biopsy at 3T: diagnostic yield of large core needle biopsy compared with vacuum-assisted biopsy," *Eur. Radiol.*, vol. 22, no. 2, pp. 341–349, 2012.

[89] N. Antropova, B. Q. Huynh, and M. L. Giger, "A deep feature fusion methodology for breast cancer diagnosis demonstrated on three imaging modality datasets," *Med. Phys.*, vol. 44, no. 10, pp. 5162–5171, 2017.

[90] A. A. Nahid and Y. Kong, "Histopathological breast-image classification using local and frequency domains by convolutional neural network," *Information (Basel)*, vol. 9, no. 1, p. 19, 2018.

[91] T. Araújo *et al*., "Classification of breast cancer histology images using Convolutional Neural Networks," *PLoS One*, vol. 12, no. 6, p. e0177544, 2017.

[92] B. J. Vakoc, D. Fukumura, R. K. Jain, and B. E. Bouma, "Cancer imaging by optical coherence tomography: preclinical progress and clinical potential," *Nat. Rev. Cancer*, vol. 12, no. 5, pp. 363–368, 2012.

[93] N. Singla, K. Dubey, and V. Srivastava, "Automated assessment of breast cancer margin in optical coherence tomography images via pretrained convolutional neural network," *J. Biophotonics*, vol. 12, no. 3, p. e201800255, 2019.

[94] C. L. Chen et al., “Deep learning in label-free cell classification,” *Sci. Rep.*, vol. 6, no. 1, p. 21471, 2016.

[95] H. Li, M. L. Giger, B. Q. Huynh, and N. O. Antropova, “Deep learning in breast cancer risk assessment: evaluation of convolutional neural networks on a clinical dataset of full-field digital mammograms,” *J. Med. Imaging (Bellingham)*, vol. 4, no. 4, p. 041304, 2017.

[96] A. Golatkar, D. Anand, and A. Sethi, “Classification of breast cancer histology using deep learning,” *arXiv [cs.CV]*, 2018.

[97] H. S. Salehi, N. Karimian, M. Mahdian, H. Alnajjar, and A. Tadinada, “Deep learning classifier with optical coherence tomography images for early dental caries detection,” in *Lasers in Dentistry XXIV*, 2018.

[98] T. Ching *et al.*, “Opportunities and obstacles for deep learning in biology and medicine,” *J. R. Soc. Interface*, vol. 15, no. 141, p. 20170387, 2018.

[99] A. Antoniou, A. Storkey, and H. Edwards, “Data augmentation Generative Adversarial Networks,” *arXiv [stat.ML]*, 2017.

[100] A. Krizhevsky, I. Sutskever, and G. E. Hinton, “ImageNet classification with deep convolutional neural networks,” *Commun. ACM*, vol. 60, no. 6, pp. 84–90, 2017.

[101] A. Shrivastava, T. Pfister, O. Tuzel, J. Susskind, W. Wang, and R. Webb, “Learning from simulated and unsupervised images through adversarial training,” in *2017 IEEE Conference on Computer Vision and Pattern Recognition (CVPR)*, 2017.

[102] C. Bowles *et al.*, "Gan augmentation: Augmenting training data using generative adversarial networks." *arXiv preprint arXiv:1810.10863*, 2018.

[103] P. Seebock *et al.*, “Using cyclegans for effectively reducing image variability across OCT devices and improving retinal fluid segmentation,” in *2019 IEEE 16th International Symposium on Biomedical Imaging (ISBI 2019)*, 2019.

[104] Z. Zhang, L. Yang, and Y. Zheng, “Translating and segmenting multimodal medical volumes with cycle- and shape-consistency generative adversarial network,” in *2018 IEEE/CVF Conference on Computer Vision and Pattern Recognition*, 2018.

[105] Y. Huo *et al.*, “SynSeg-Net: Synthetic segmentation without target modality ground truth,” *IEEE Trans. Med. Imaging*, vol. 38, no. 4, pp. 1016–1025, 2018.

[106] H.R. Roth *et al.*, “Improving computer-aided detection using convolutional neural networks and random view aggregation,” *IEEE Trans. Med. Imaging*, vol. 35, no. 5, pp. 1170–1181, 2016.

[107] I. Goodfellow *et al.*, "Generative adversarial nets," *Advances in neural information processing systems*, vol. 27, 2014.

[108] A. Radford, L. Metz, and S. Chintala, “Unsupervised representation learning with deep convolutional generative adversarial networks,” *arXiv [cs.LG]*, 2015.

[109] L. Alzubaidi *et al.*, “Classification of red blood cells in sickle cell anemia using deep convolutional neural network,” in *Advances in Intelligent Systems and Computing*, Cham: Springer International Publishing, 2020, pp. 550–559.

[110] S. P. K. Karri, D. Chakraborty, and J. Chatterjee, “Transfer learning based classification of optical coherence tomography images with diabetic macular edema and dry age-related macular degeneration,” *Biomed. Opt. Express*, vol. 8, no. 2, pp. 579–592, 2017.

[111] J. Bray, I. Ferlay, R. L. Soerjomataram, L. A. Siegel, and A. Torre, “CA: A Cancer J,” *CA: A Cancer J. for Clin*, vol. 68, 2018.

[112] K. D. Miller *et al.*, “Cancer treatment and survivorship statistics, 2016,” *CA Cancer J. Clin.*, vol. 66, no. 4, pp. 271–289, 2016.

[113] M. Van Goethem *et al.*, “MR mammography in the pre-operative staging of breast cancer in patients with dense breast tissue: comparison with mammography and ultrasound,” *Eur. Radiol.*, vol. 14, no. 5, pp. 809–816, 2004.

[114] J. Liu, Y. Xu, and J. Wang, “Ultrasonography, computed tomography and magnetic resonance imaging for diagnosis of ovarian carcinoma,” *Eur. J. Radiol*., vol. 62, no. 3, pp. 328–334, 2007.

[115] S. P. K. Karri, D. Chakraborty, and J. Chatterjee, “Transfer learning based classification of optical coherence tomography images with diabetic macular edema and dry age-related macular degeneration,” *Biomed. Opt. Express*, vol. 8, no. 2, pp. 579–592, 2017.

[116] W. Drexler and J. G. Fujimoto, “Springer: Berlin/Heidelberg,” 2008.

[117] N. Singla, V. Srivastava and D.S. Mehta, “In vivo classification of human skin burns using machine learning and quantitative features captured by optical coherence tomography,” Laser Phys. Lett., vol. 15, no. 2, p.025601, 2018.

[118] K. Dubey, V. Srivastava, and K. Dalal, “In vivo automated quantification of thermally damaged human tissue using polarization sensitive optical coherence tomography,” *Comput. Med. Imaging Graph.*, vol. 64, pp. 22–28, 2018.

[119] A. M. Zysk *et al.*, “Clinical feasibility of microscopically-guided breast needle biopsy using a fiber-optic probe with computer-aided detection,” *Technol. Cancer Res. Treat.*, vol. 8, no. 5, pp. 315–321, 2009.

[120] W.C. Kuo *et al.* "Real-time three-dimensional optical coherence tomography image-guided core-needle biopsy system," *Biomed. Opt. Express*, vol. 3, no. 6, pp. 1149-1161, 2012.

[121] R. A. McLaughlin *et al.*, "Imaging of breast cancer with optical coherence tomography needle probes: Feasibility and initial results," *IEEE J. Sel. Top. Quantum Electron.*, vol. 18, no. 3, pp. 1184–1191, 2012.

[122] S. J. Erickson-Bhatt *et al.*, "Real-time imaging of the resection bed using a handheld probe to reduce incidence of microscopic positive margins in cancer surgery," *Cancer Res.*, vol. 75, no. 18, pp. 3706–3712, 2015.

[123] A. M. Zysk *et al.*, "Intraoperative assessment of final margins with a handheld optical imaging probe during breast-conserving surgery may reduce the reoperation rate: Results of a multicenter study," *Ann. Surg. Oncol.*, vol. 22, no. 10, pp. 3356–3362, 2015.

[124] O. Assayag *et al.*, "Large field, high resolution full-field optical coherence tomography: a pre-clinical study of human breast tissue and cancer assessment," *Technol. Cancer Res. Treat.*, vol. 13, no. 5, pp. 455–468, 2014.

[125] V. Srivastava, S. Nandy, and D. Singh Mehta, "High-resolution full-field spatial coherence gated optical tomography using monochromatic light source," *Appl. Phys. Lett.*, vol. 103, no. 10, p. 103702, 2013.

[126] V. Srivastava, T. Anna, M. Sudan, and D. S. Mehta, "Tomographic and volumetric reconstruction of composite materials using full-field swept-source optical coherence tomography," *Meas. Sci. Technol.*, vol. 23, no. 5, p. 055203, 2012.

[127] J. Wang *et al.*, "Complementary use of polarization-sensitive and standard OCT metrics for enhanced intraoperative differentiation of breast cancer," *Biomed. Opt. Express*, vol. 9, no. 12, pp. 6519–6528, 2018.

[128] F. A. South, E. J. Chaney, M. Marjanovic, S. G. Adie, and S. A. Boppart, "Differentiation of ex vivo human breast tissue using polarization-sensitive optical coherence tomography," *Biomed. Opt. Express*, vol. 5, no. 10, pp. 3417–3426, 2014.

[129] P.L. Hsiung, D. R. Phatak, Y. Chen, A. D. Aguirre, J. G. Fujimoto, and J. L. Connolly, "Benign and malignant lesions in the human breast depicted with ultrahigh resolution and three-dimensional optical coherence tomography," *Radiology*, vol. 244, no. 3, pp. 865–874, 2007.

[130] A. M. Zysk, E. J. Chaney, and S. A. Boppart, "Refractive index of carcinogen-induced rat mammary tumours," *Phys. Med. Biol.*, vol. 51, no. 9, pp. 2165–2177, 2006.

[131] J. F. de Boer, T. E. Milner, M. J. van Gemert, and J. S. Nelson, "Two-dimensional birefringence imaging in biological tissue by polarization-sensitive optical coherence tomography," *Opt. Lett.*, vol. 22, no. 12, pp. 934–936, 1997.

[132] G. Moneron, A.C. Boccara, and A. Dubois, "Polarization-sensitive full-field optical coherence tomography," *Opt. Lett.*, vol. 32, no. 14, pp. 2058–2060, 2007.

[133] A. Dubois, “Spectroscopic polarization-sensitive full-field optical coherence tomography,” *Opt. Express*, vol. 20, no. 9, pp. 9962–9977, 2012.

[134] M. Born and E. Wolf, “Principles of optics”, *7th ed. Cambridge University Press*, Cambridge, UK, pp. 837–840, 1997.

[135] J.J. Pasquesi *et al.* "In vivo detection of exercise-induced ultrastructural changes in genetically-altered murine skeletal muscle using polarization-sensitive optical coherence tomography." *Opt. Express*, vol. 14, no. 4, pp. 1547-1556, 2006.

[136] B. D. Cameron and Y. Li, “Polarization-based diffuse reflectance imaging for non invasive measurement of glucose,” *J. Diabetes Sci. Technol.*, vol. 1, no. 6, pp. 873–878, 2007.

[137] J. Strasswimmer, M. C. Pierce, B. H. Park, V. Neel, and J. F. de Boer, “Polarization-sensitive optical coherence tomography of invasive basal cell carcinoma,” *J. Biomed. Opt.*, vol. 9, no. 2, pp. 292–298, 2004.

[138] M. Sugita *et al.*, “Analysis of optimum conditions of depolarization imaging by polarization-sensitive optical coherence tomography in the human retina,” *J. Biomed. Opt.*, vol. 20, no. 1, p. 016011, 2015.

[139] O. U. Aydın, L. Soylu, A. İ. Ercan, B. Bilezikçi, and S. Koçak, “Invasive ductal carcinoma developing from fibroadenoma,” *J. Breast Health*, vol. 11, no. 4, pp. 195–198, 2015.

[140] C. J. Lynch and C. Liston, “New machine-learning technologies for computer-aided diagnosis,” *Nat. Med.*, vol. 24, no. 9, pp. 1304–1305, 2018.

[141] S. M. McKinney *et al.*, "International evaluation of an AI system for breast cancer screening," *Nature*, vol. 577, no. 7788, pp. 89-94, 2020.

[142] M. Kowal, P. Filipczuk, A. Obuchowicz, J. Korbicz, and R. Monczak, “Computer-aided diagnosis of breast cancer based on fine needle biopsy microscopic images,” *Comput. Biol. Med.*, vol. 43, no. 10, pp. 1563–1572, 2013.

[143] H. Lu *et al.*, “Automated stent coverage analysis in intravascular OCT (IVOCT) image volumes using a support vector machine and mesh growing,” *Biomed. Opt. Express*, vol. 10, no. 6, pp. 2809–2828, 2019.

[144] N. Petrellis, “A review of image processing techniques common in human and plant disease diagnosis,” *Symmetry (Basel)*, vol. 10, no. 7, p. 270, 2018.

[145] C. Pucci, C. Martinelli, and G. Ciofani, “Innovative approaches for cancer treatment: current perspectives and new challenges,” *Ecancermedicalscience*, vol. 13, p. 961, 2019.

[146] B. P. Yakimov, E. A. Shirshin, J. Schleusener, A. S. Allenova, V. V. Fadeev, and M. E. Darvin, "Melanin distribution from the dermal-epidermal junction to the stratum corneum: non-invasive in vivo assessment by fluorescence and Raman microspectroscopy," *Sci. Rep.*, vol. 10, no. 1, p. 14374, 2020.

[147] J. Corbett and M. Woods, "UV laser radiation: Skin hazards and skin protection controls," in *International Laser Safety Conference*, 2013.

[148] M.S. Mabrouk, A. Y. Sayed, H. M. Afifi, M. A. Sheha, and A. Sharwy, "Fully automated approach for early detection of pigmented skin lesion diagnosis using ABCD," *J. Healthc. Inform. Res.*, vol. 4, no. 2, pp. 151–173, 2020.

[149] I. H. Sarker, "Machine learning: Algorithms, real-world applications and research directions," *SN Comput Sci*, vol. 2, no. 3, p. 160, 2021.

[150] A. Masood and A. Al-Jumaily, "Differential evolution based advised SVM for histopathalogical image analysis for skin cancer detection," *Annu Int Conf IEEE Eng Med Biol Soc*, vol. 2015, pp. 781–784, 2015.

[151] R. Suganya, "An automated computer aided diagnosis of skin lesions detection and classification for dermoscopy images," in *2016 International Conference on Recent Trends in Information Technology (ICRTIT)*, 2016.

[152] F. K. Nezhadian and S. Rashidi, "Melanoma skin cancer detection using color and new texture features," in *2017 Artificial Intelligence and Signal Processing Conference (AISP)*, 2017.

[153] M. Nasir, M. Attique Khan, M. Sharif, I. U. Lali, T. Saba, and T. Iqbal, "An improved strategy for skin lesion detection and classification using uniform segmentation and feature selection based approach," *Microsc. Res. Tech.*, vol. 81, no. 6, pp. 528–543, 2018.

[154] S. Mustafa, A. B. Dauda, and M. Dauda, "Image processing and SVM classification for melanoma detection," in *2017 International Conference on Computing Networking and Informatics (ICCNI)*, 2017.

[155] S. Mustafa and A. Kimura, "A SVM-based diagnosis of melanoma using only useful image features," in *2018 International Workshop on Advanced Image Technology (IWAIT)*, 2018.

[156] S. Mane and S. Shinde, "A method for melanoma skin cancer detection using dermoscopy images," in *2018 Fourth International Conference on Computing Communication Control and Automation (ICCUBEA)*, 2018.

[157] H. R. Mhaske and D. A. Phalke, “Melanoma skin cancer detection and classification based on supervised and unsupervised learning,” in *2013 International conference on Circuits, Controls and Communications (CCUBE)*, 2013.

[158] R. B. Aswin, J. A. Jaleel, and S. Salim, “Hybrid genetic algorithm - Artificial neural network classifier for skin cancer detection,” in *2014 International Conference on Control, Instrumentation, Communication and Computational Technologies (ICCICCT)*, 2014.

[159] A. Udrea and G. D. Mitra, “Generative adversarial neural networks for pigmented and non-pigmented skin lesions detection in clinical images,” in *2017 21st International Conference on Control Systems and Computer Science (CSCS)*, 2017.

[160] P. Shahi, S. Yadav, N. Singh, and N. P. Singh, “Melanoma skin cancer detection using various classifiers,” in *2018 5th IEEE Uttar Pradesh Section International Conference on Electrical, Electronics and Computer Engineering (UPCON)*, 2018.

[161] N. B. Linsangan, J. J. Adtoon, and J. L. Torres, “Geometric analysis of skin lesion for skin cancer using image processing,” in *2018 IEEE 10th International Conference on Humanoid, Nanotechnology, Information Technology,Communication and Control, Environment and Management (HNICEM)*, 2018.

[162] S. M. Jaisakthi, P. Mirunalini, and C. Aravindan, “Automated skin lesion segmentation of dermoscopic images using GrabCut and k-means algorithms,” *IET Comput. Vis.*, vol. 12, no. 8, pp. 1088–1095, 2018.

[163] P. J. Ray, S. Priya, and T. A. Kumar, “Nuclear segmentation for skin cancer diagnosis from histopathological images,” in *2015 Global Conference on Communication Technologies (GCCT)*, 2015.

[164] M. ur Rehman, S. H. Khan, S. M. Danish Rizvi, Z. Abbas, and A. Zafar, “Classification of skin lesion by interference of segmentation and convolotion neural network,” in *2018 2nd International Conference on Engineering Innovation (ICEI)*, 2018.

[165] R. Mishra and D. Ovidiu, "Deep learning for skin lesion segmentation," in *2017 IEEE International Conference on Bioinformatics and Biomedicine (BIBM)*, 2017.

[166] R. Nock F. Nielsen, “Statistical region merging,” *IEEE Transactions on pattern analysis and machine intelligence*, vol. 26, no. 11, pp. 1452–1458, 2004.

[167] N. Otsu, “A threshold selection method from gray-level histograms,” *IEEE Trans. Syst. Man Cybern.*, vol. 9, no. 1, pp. 62–66, 1979.

[168] S. Mane and S. Shinde, “A method for melanoma skin cancer detection using dermoscopy images,” in *2018 Fourth International Conference on Computing Communication Control and Automation (ICCUBEA)*, 2018.

[169] P. Ghamisi, M. S. Couceiro, J. A. Benediktsson, and N. M. F. Ferreira, "*An efficient method for segmentation of images based on fractional calculus and natural selection*," Expert Syst. Appl., vol. 39, no. 16, pp. 12407–12417, 2012.

[170] J. C. Bezdek, R. Ehrlich, and W. Full, "FCM: The fuzzy c-means clustering algorithm," *Comput. Geosci.*, vol. 10, no. 2–3, pp. 191–203, 1984.

[171] Y. Deng and B. S. Manjunath, "Unsupervised segmentation of color-texture regions in images and video," *IEEE Trans. Pattern Anal. Mach. Intell.*, vol. 23, no. 8, pp. 800–810, 2001.

[172] A. Pennisi, D. D. Bloisi, D. Nardi, A. R. Giampetruzzi, C. Mondino, and A. Facchiano, "Skin lesion image segmentation using Delaunay Triangulation for melanoma detection," *Comput. Med. Imaging Graph.*, vol. 52, pp. 89–103, 2016.

[173] A. Gupta, A. Raghav, and S. Srivastava, "Comparative study of machine learning algorithms for Portuguese bank data," in *2021 International Conference on Computing, Communication, and Intelligent Systems (ICCCIS)*, 2021.

[174] M. W. Rashad and M. Takruri, "Automatic non-invasive recognition of melanoma using Support Vector Machines," in *2016 International Conference on Bio-engineering for Smart Technologies (BioSMART)*, 2016.

[175] P. Khare and V. K. Srivastava, "A secured and robust medical image watermarking approach for protecting integrity of medical images," *Trans. emerg. telecommun. technol.*, vol. 32, no. 2, 2021.

[176] N. Hai and J. Rosen, "Phase-contrast-based holographic quantitative phase imaging by only two exposures," in *Conference on Lasers and Electro-Optics*, 2021.

[177] T. Suzuki, N. Sugawara, S. Choi, and O. Sasaki, "Acousto-optically tuned external-cavity laser diode for optical coherence tomography with continuous wavelet transform," *Opt. Eng.*, vol. 58, no. 10, p. 1, 2019.

[178] G. Barbastathis, A. Ozcan, and G. Situ, "On the use of deep learning for computational imaging," *Optica*, vol. 6, no. 8, p. 921, 2019.

LIST OF PUBLICATIONS

In Peer-Reviewed SCI Journals

1. **Shaify Kansal**, Jhilik Bhattacharya, and Vishal Srivastava, "Automated full-field polarization sensitive optical coherence tomography diagnostic systems for breast cancer", Applied Optics, (2020), DOI: 10.1364/AO.396592

2. **Shaify Kansal**, Shivani Goel, Jhilik Bhattacharya and Vishal Srivastava, "GAN-CNN based breast cancer classification using optical coherence tomographic images", Laser Physics, (2020), DOI: 10.1088/1555-6611/abb596

3. **Shaify Kansal**, Jhilik Bhattacharya, and Vishal Srivastava, "Classification of Melanoma Skin Cancer Using Deep Learning", Scientia Iranica (Under Review)

In International Conferences

1. **Shaify Kansal,** Shivani Goel, Jhilik Bhattacharya, "Inspecting the Efficiency of Deep Neural Networks for Classification of Images with Noise", IJAECS (2019)

2. **Shaify Kansal,** Jhilik Bhattacharya, Vishal Srivastava, "Diagnosis of Melanoma Skin Cancer using Machine Learning Approach for Dermoscopic Images", ICSTR (2022) (Manuscript Submitted)